An experimentally validated DEM study of powder mixing in a paddle blade mixer

Elsevier Editorial System(tm) for Powder Technology

Manuscript Draft

Manuscript Number: POWTEC-D-16-01733R1

Title: An experimentally validated DEM study of powder mixing in a paddle blade mixer

Article Type: Research Paper

Keywords: Solid mixing; cohesive powder; numerical modelling; model calibration; discrete element method; DEM.

Corresponding Author: Mr. Stefan Lyubomirov Pantaleev, MEng

Corresponding Author's Institution: University of Edinburgh

First Author: Stefan Lyubomirov Pantaleev, MEng

Order of Authors: Stefan Lyubomirov Pantaleev, MEng; Slavina S Yordanova, MEng; Alvaro Janda, PhD; Michele Marigo, EngD; Jin Y Ooi, PhD

Abstract: An investigation on the predictive capabilities of Discrete Element Method simulations of a powder mixing process in a laboratory scale paddle blade mixer is presented. The visco-elasto-plastic frictional adhesive DEM contact model of Thakur et al (2014) was used to represent the cohesive behaviour of an aluminosilicate powder in which the model parameters were determined using experimental flow energy measurements from the FT4 powder rheometer. DEM simulations of the mixing process using the contact model parameters were evaluated against the experimental measurements of the mixing rate. The results demonstrated that whilst the DEM model is capable of reproducing the FT4 flow energy of the powder to an excellent agreement, the simulations of the mixing process produced a qualitative agreement on the trend of the mixing rate in the experiments for both dry and wet powders. The mixing was under-predicted in the simulations, suggesting that flow energy measurements alone may not be sufficient for the optimization of a DEM model of powder mixing.

Cover Letter

Professor C. Wu
Department of Chemical and Process Engineering
University of Surrey
Guildford, Surrey GU2 7XH
United Kingdom

Dear Professor Wu,

Thank you very much for your time and effort in considering our manuscript. We are also grateful to the reviewers for their efforts and for providing us with detailed and constructive comments and suggestions for improving the manuscript. Please find attached the revised manuscript "An experimentally validated DEM study of powder mixing in a paddle blade mixer" which has been amended as requested. We look forward to hearing from you in due time regarding our submission and to respond to any further questions and comments you may have.

Sincerely,

Stefan Pantaleev
Institute for Infrastructure and Environment
School of Engineering
University of Edinburgh
King's Buildings, W Mains Rd, Edinburgh EH9 3JL
United Kingdom

Revised: An experimentally validated DEM study of powder mixing in a paddle blade mixer

Dear reviewers, thank you very much for taking the time to review this manuscript and for your useful questions and comments. We have revised the manuscript in accordance to your suggestions and have included clarifications which will hopefully answer your questions. Please see below our response to each point, raised in your review.

Comments from Reviewer #1:

1) *Equation # 3 is wrong in units as there is a mismatch in units in left and right sides of the equation.*

Revisit equation 2 and 3 and do the needful revision.

We thank the reviewer and have corrected the equation. Now both sides of the equation are in units of energy.

2) *Fig 3 should have been drawn with opposite direction in change of the variable in the abscissa.*

While the reviewer's suggestion might make the graph easier to read, this is the standard way of presenting results for the FT4 Basic Flow Energy (BFE) test already adopted in the literature [1][2] and we have maintained the graph in that standard form.

3) *Fig 3 why there are so many 100s is the label of abscissa?*

The abscissa shows the blade tip speed corresponding to each flow energy measurement. The standard test procedure for the FT4 BFE test consists of 8 consecutive tests at 100 mm/s blade tips speed and a further 3 at 70, 40 and 10 mm/s. The first 8 tests at the same blade tip speed (100mm/s) are recommended to assess the repeatability of the measurement [1]. We have added this clarification in the manuscript (page 6).

4) *Why does the blue coloured powder show an initial rise whereas other powders are mostly showing a drop in total energy? Explain.*

A potential explanation for the observed difference between the pink and blue coloured powders is the different method of preparation. The blue powder was wetted with dye until the desired moisture content was achieved. For the pink powder a single batch with a high moisture content (the P_32) was produced and then lower moisture content batches were prepared by oven drying that high moisture content batch at 200 degrees Celsius. This was done to use the powder material more efficiently. The drying of the powder at this temperature could have affected the mechanical and chemical properties of the powder particles and agglomerates of particles leading to the observed difference in behaviour. Indeed, it can be seen that the trend for the B_30 and P_32 samples, which were not oven dried, is not too dissimilar in that there is an initial increase in flow energy between the 70 mm/s and 100 mm/s test, whereas the flow energy of the oven dried samples (P_19, P_14) continues to decrease. We have clarified this point in the manuscript on page 6.

5) *Figure 11 Authors should add time stamps in the figure or specify the same in the text of the revised manuscript.*

We thank the reviewer for the suggestion and have added time stamps to the figure.

Comments from Reviewer #3:

1) *The authors mentioned that: "the resultant materials and their properties are listed in Table 2 and plotted in Fig.2 (page 4)". However, the values presented in Table 2 are not corresponding to Figure 2. Please check the values in Table 2 and Figure 2.*

We thank the reviewer for the comment and have corrected the values in the table.

2) *Authors mentioned that "The flow energy increases with increasing moisture content (page 20 also page 6), but based on Figure 3, P_14 has higher total energy than P_19? Please clarify why this trend was observed?*

While the flow energy does increase markedly between the two moisture content extremes, you are correct in pointing out that this is not the case for the powders at intermediate moisture contents. On the basis of these results, it seems that the relationship between moisture content and flow energy is more complex and we have modified our statements on pages 6 and 20 accordingly. We do not have an explanation for the observed behaviour at the intermediate moisture contents and are not aware of any study exploring the effect of moistue content on the flow energy.

3) *Please add explanation regarding the modelling of rolling friction and the chosen (calibrated) value for the coefficient of rolling friction.*

We thank the reviewer and have added an explanation on page 14 of the manuscript.

4) *The contact parameters between two types of powder …… (page 15) " Why did not authors try to perform the FT4 experiments for a mixture of powders and then calibrate the simulation of the FT4 results for a mixture instead of using the averaged optimized parameter values stated in page 15? The authors should explain to what extent using the average values can lead to the observed discrepancies between the simulation and experimental results?*

We thank the reviewer for his/her suggestion. Certainly, the use of average values for the contact model parameters in the case of interaction of particles of different type may contribute to the observed discrepancies. Following his/her suggestion we have added further discussion on this on pages 18 and 20 of the manuscript. Concerning, the suggestion of using a mixture of the two powders to calibrate the model parameters, it is an excellent idea and definitely something to be explored in future investigations. In this case, it would be important to investigate whether a single set of model parameters for these contacts can capture the flow energy of the powder mix at different mass fractions of the two powders. Note that during the mixing process, the mass fraction of the two powders that are in contact significantly varies with time and location in the mixer. Therefore, it might be also necessary to adopt a more complex approach where the mass fraction of each powder is also considered during the optimization of the values of the contact parameters. A further discussion about these points has been added in the manuscript.

5) Please add references if other papers have used kinetic pressure to analyse the dynamic of the system (Equation 23). More explanation regarding this equation can help the reader.

We thank the reviewer for the suggestion. A more detailed explanation about the calculation of the kinetic pressure together with references for its theoretical calculation have been added. Moreover, we have added references where a similar metric was used to investigate the performance of mixing in granular systems.

References

[1] R. Freeman, Measuring the flow properties of consolidated, conditioned and aerated powders - A comparative study using a powder rheometer and a rotational shear cell, Powder Technol. 174 (2007) 25–33. doi:10.1016/j.powtec.2006.10.016.

[2] M. Leturia, M. Benali, S. Lagarde, I. Ronga, K. Saleh, Characterization of flow properties of cohesive powders: A comparative study of traditional and new testing methods, Powder Technol. 253 (2014) 406–423. doi:10.1016/j.powtec.2013.11.045.

***Graphical Abstract (for review)**

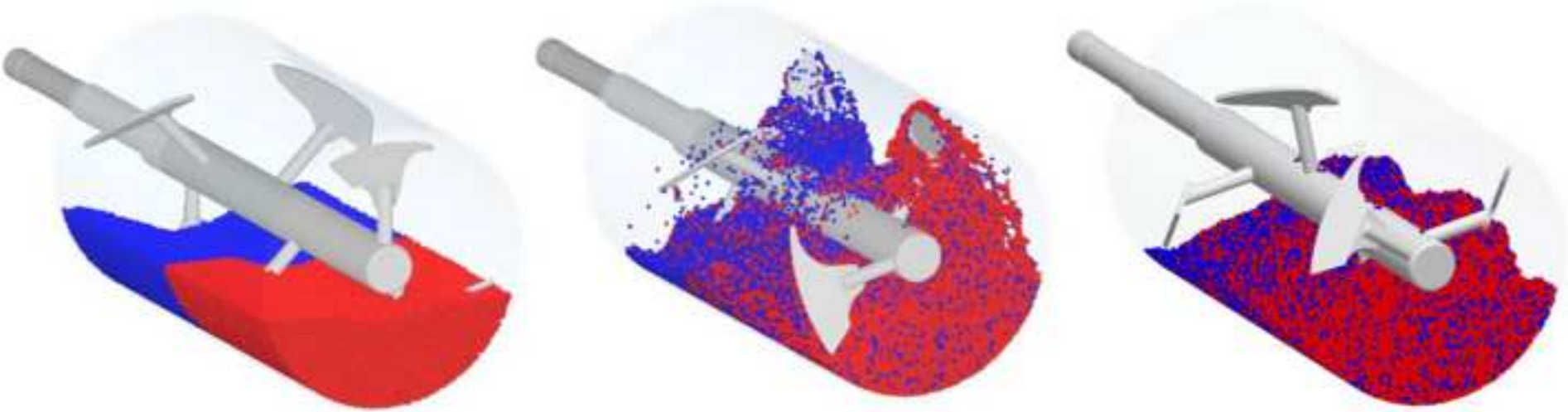

***Abstract**

An investigation on the predictive capabilities of Discrete Element Method simulations of a powder mixing process in a laboratory scale paddle blade mixer is presented. The visco-elasto-plastic frictional adhesive DEM contact model of Thakur et al (2014) was used to represent the cohesive behaviour of an aluminosilicate powder in which the model parameters were determined using experimental flow energy measurements from the FT4 powder rheometer. DEM simulations of the mixing process using the contact model parameters were evaluated against the experimental measurements of the mixing rate. The results demonstrated that whilst the DEM model is capable of reproducing the FT4 flow energy of the powder to an excellent agreement, the simulations of the mixing process produced a qualitative agreement on the trend of the mixing rate in the experiments for both dry and wet powders. The mixing was under-predicted in the simulations, suggesting that flow energy measurements alone may not be sufficient for the optimization of a DEM model of powder mixing.

An experimentally validated DEM study of powder mixing in a paddle blade mixer

Stefan Pantaleev [a], Slavina Yordanova [b], Alvaro Janda[c], Michele Marigo[d], Jin Y. Ooi[a]

Corresponding author:
Stefan Pantaleev
e-mail: s.pantaleev@ed.ac.uk
tel: 131 650 5790

[a]Institute of Infrastructure and Environment, School of Engineering, University of Edinburgh, Edinburgh, EH9 3JY, Scotland, UK

[b]Arup Group Ltd, Scotstoun House, South Queensferry, Edinburgh, EH30 9SE, Scotland, UK

[c] Particle Analytics Ltd, Alrick Building, Max Born Crescent, The King's Buildings , Edinburgh, EH9 3BF, UK

[d]Johnson Matthey Technology Centre, PO Box 1, Belasis Avenue, Billingham TS23 1LB, UK

Abstract

An investigation on the predictive capabilities of Discrete Element Method simulations of a powder mixing process in a laboratory scale paddle blade mixer is presented. The visco-elasto-plastic frictional adhesive DEM contact model of Thakur et al (2014) was used to represent the cohesive behaviour of an aluminosilicate powder in which the model parameters were determined using experimental flow energy measurements from the FT4 powder rheometer. DEM simulations of the mixing process using the contact model parameters were evaluated against the experimental measurements of the mixing rate. The results demonstrated that whilst the DEM model is capable of reproducing the FT4 flow energy of the powder to an excellent agreement, the simulations of the mixing process produced a qualitative agreement on the trend of the mixing rate in the experiments for both dry and wet powders. The mixing was under-predicted in the simulations, suggesting that flow energy measurements alone may not be sufficient for the optimization of a DEM model of powder mixing.

Keywords

Solid mixing, cohesive powder, numerical modelling, model calibration, discrete element method, DEM.

1. Introduction

Particulate materials are important in a wide range of industries including the pharmaceutical, chemical, metallurgical, food and others. Within these industrial mixing and blending of materials are some of the most demanding unit operations. Successful manufacturing of a variety of products is heavily dependent on the efficiency of this process, because the final product quality is inherently dependent on the quality of the obtained mixture. Inefficient mixing resulting in a non-homogenous product (typical detrimental effects can include segregation, particle breakage, unwanted agglomeration) can lead to products that might not meet the required quality in terms of chemical composition, colour, texture, flavour, reactivity, or particle size.

A variety of solid mixers are available in industry; these can be divided into two categories: mixers with rotating vessels (rotating drum, double cone blender, V-blenders, octagonal blender) and mixers with fixed vessels and rotating components (ribbon blender, paddle blender, plough mixer, double paddle mixer). Mixers can also be grouped depending on the predominant mixing mechanism that is driving the material such as convection, dispersion and shear [1].

A large amount of experimental and modelling work has been carried out on the mixing of powders in a variety of mixers, but the scientific understanding of the process remains limited. As a consequence the design and selection of appropriate mixing equipment is not straight forward and the common problems related to scale up and operation of mixing processes remain unsolved.

The experimental and numerical tools for the study of mixing in particulate systems are briefly reviewed below and the current developments have been reported extensively in the literature [e.g. 2]. Non-invasive experimental techniques such as positron emission tomography (PET) [3], positron emission particle tracking (PEPT) [4-8], X-ray tomography [9,10] and magnetic resonance imaging (MRI)[11,12] have been applied to look at the material flow, mixing and segregation within a variety of mixing unit operations. Although these techniques can give insightful information regarding the material behaviour within a particular system, they are costly and relatively difficult to access. A cheaper and easily accessible technique is to look at the material flow by optical imaging and post processing methods such particle image velocimetry [12–14]. However, these are limited to a 2D field of views or applied only at the free surface boundaries, which makes it challenging to apply to a plough or paddle type mixer.

Particulate material mixing and segregation in blenders have also been extensively studied numerically using the discrete element method (DEM). Various blender designs and the effect of operating variables (e.g. fill level, operating speed, and material type) have been investigated [15–17]. The motion of individual particles can be tracked in DEM simulations and therefore insight can be obtained into the mechanisms governing particles flow in a variety of mixing processes. The obtained information can then be used to inform the design, selection and operation of powder mixing equipment, reducing the need for pilot studies and speeding up the design optimization process.

Although DEM has been widely used to study a variety of processes, the experimental quantitative validation of the simulation results is rarely reported in the literature [18]. Furthermore, the appropriate methodology to determine DEM input parameters for a given application is often unclear [19]. This is especially true in the case of fine powders which are abundant in industry. Additionally, the computational cost to model a large number of particles of small sizes that constitute fine powders poses a significant challenge for the DEM modelling of these materials.

Often in the literature, the values of the DEM parameters are optimized with a global fitting between DEM simulation and an actual small scale experiment [20]. Extensive work has also been carried out to develop a multi-level parametric sensitivity method to understand the impact of the DEM input parameters on the bulk responses for a given simple system [19], [21]. The proposed approach provides a systematic method that can be used to show the importance of specific input parameters for a given system and then potentially facilitates their selection. Moreover particle scale methodologies have been developed to scale-up particles in a DEM model to capture a material bulk response similar to systems comprised of much smaller particles [22,23]. Considering these recent developments, DEM has become a promising simulation method for fine powders.

DEM simulations of the mixing of non-cohesive bulk solids have demonstrated a measure of quantitative accuracy when appropriate values of the model parameters were used [24]. Therefore, it would be of interest to determine if a quantitatively accurate model for cohesive powder mixing can be produced when its input parameters are appropriately optimized..

This study evaluates the predictive capabilities of a visco-elasto-plastic frictional adhesive DEM model [25] for the simulation of aluminosilicate powder mixing in a laboratory scale mixer. The mixer of choice was the MLH12 (WAM Group) paddle blade mixer, which is a laboratory scale mixer with a capacity of 12 litres. The FT4 powder rheometer was used to characterize the mechanical properties of the powder at a wide range of moisture contents. The test was replicated in DEM simulations and the contact model parameters were optimized to reproduce the experimental total flow energy measurements in the FT4 rheometer. A simple Plackett-Burman design of experiments was used to produce a set of simulations with systematically varied parameter values and a linear response model was fitted to the simulated total flow energy. The response model was then used to determine the input parameters, which produced the closest match to the experimental flow energy measurements. DEM simulations of the mixing process were performed using the optimized model parameters and the mixing rate in the simulations was calculated from the statistical distribution of particle concentrations. Finally, the simulation results were compared against experimental measurements of the mixing rate to assess the predictive capability of the DEM model.

2. Physical and mechanical properties of the test material

Synthetic zeolite powder was used as the test material for this study. It is a fine aluminosilicate powder representative of cohesive powders with challenging behaviour in industrial mixing applications.

The particle size distribution of the powder (Table 1) was measured using a Malvern Mastersizer 2000

particle size analyser [26]. Measurements were made using both a dry and wet dispersal and using two levels of ultrasonication power for the wet dispersal. The mean particle size of the powder (D50) was higher under wet dispersal conditions, demonstrating the ability of the particles to form stable agglomerates even in a water suspension. The mean particle size decreased with the increase in ultrasonication power due to the breakup of these agglomerates by the ultrasonic waves passing through the suspension. A Scanning Electron Microscopy (SEM) image of a powder sample (Figure 1) shows the tendency of the particles to agglomerate together due to van der Waals and liquid bridge type forces. On the bulk scale the powder was also observed to form stable agglomerates of millimeters in size, especially at higher moisture contents. Moreover, the non-spherical nature of the individual particles is evident from the SEM images suggesting that particle interlocking might have a significant effect on the bulk strength and flowability of the material.

The physical and mechanical properties of the zeolite powder were determined at several moisture contents in order to capture the wide range of its flow behaviour and to encompass a variety of operational conditions, found in industrial powder mixing applications. Batches of pink or blue coloured powder with different moisture contents were prepared. The powders were coloured, because the subsequent mixing experiments relied on colour measurement to quantify the rate of mixing. The highest moisture content powders of each colour were prepared by adding distilled water and dye to the powder and mixed to homogeneity in the MLH12 mixer. Powders at lower levels of moisture content were made by oven drying the high moisture content powders at 200^0C. A halogen moisture balance was used to determine the total moisture content of all batches, making three measurements for each. The instrument uses a halogen lamp to heat a sample to 110^0C and measure the change in its mass. The moisture content is then calculated from Eq. 1.

$$w_t = M_w/M_t \quad (1)$$

where M_w is the mass of water and M_t is the total mass of the sample.

Additionally, the bulk density of the powders was determined by filling the 160 ml glass cylinder of the FT4 powder rheometer with powder and measuring its mass. The resultant materials and their properties are listed in Table 2 and plotted in Fig. 2. The notation for each powder consists of a letter and a number. The letter indicates the colour of the powder – P for pink, B for blue and W for white (no dye added), while the number indicates the moisture content of the powder to the nearest integer.

Figure 2 shows the bulk density as a function of the moisture content of the different tested materials. The addition of a chemical dye to the powder could alter the chemical and mechanical properties of the particles and hence, the bulk properties of the material as a whole. It could, for example, affect the van der Waals forces and therefore particle agglomeration. Therefore only the properties of powders of the same colour can be rigorously compared. The effect of moisture content on the bulk density was assessed for the pink coloured powders as shown by the dashed line in Figure 2. The bulk density initially decreases with increasing moisture content resulting in an increase in porosity caused by the formation of liquid bridges between the particles which keep them slightly apart. As moisture content increases towards saturation, the bulk density reaches a minimum before increasing again due to the mass of the added water and a reduction of porosity with the disappearance of liquid bridging between particles.

The FT4 powder rheometer is increasingly used for characterization of powder flowability both in academia and industry [27]. It can measure some of the mechanical properties traditionally employed for the evaluation of powder flow behaviour, such as shear strength, compressibility and permeability. Furthermore, a common methodology for characterizing powder flowability with this instrument is the measurement of flow energy, which is the energy needed to drive an impeller blade through a bed of powder. The flow energy has been reported to correlate well with traditional flowability characterization techniques [27,28]. Using this methodology, the powder flowability is characterized in a dynamic flow

regime and under free surface conditions [28]. This is in contrast with the traditional methodologies which characterize the flowability in a quasi-static regime. Powder mixing in paddle-blade mixers, which is the process targeted in the current study, also occurs under dynamic flow and free surface conditions. This apparent correspondence between the flow conditions in the characterization experiment and the process under investigation suggests that the flow energy could be a relevant measurement of powder flowability for this study.

The Basic Flow Energy (BFE) test of the FT4 Powder rheometer, used for the determination of the flow energy, is described in full detail elsewhere [28]. In this test an impeller blade moves through a bed of powder. The movement of the impeller is defined by the helix velocity of the blade termed the blade tip speed. The incremental flow energy as the blade ploughs through an increment depth dz is calculated from the translational and rotational work of the blade using Eq. 2.

$$E_f = \left(F + \frac{T}{R\tan(\alpha)}\right) dz \quad (2)$$

where F and T are the instantaneous vertical force on the bottom of the vessel and the instantaneous torque on the shaft of the blade respectively, R is the radius of the impeller and α is the helix angle of the blade path.

The cumulative flow energy required for the blade to penetrate the sample to a depth z is then:

$$E_c = \int_0^z E_f dz \quad (3)$$

and the total flow energy at the end of the test E_T is the cumulative energy at the maximum penetration depth of 70 mm.

While the evolution of the cumulative energy with depth can be obtained from the test, only the total flow energy is commonly used to characterize the powder flowability. In general, higher total flow energy corresponds to lower flowability and vice versa.

All test powders were characterized using the BFE test procedure in which the 48 mm impeller blade was used. Initially a conditioning cycle was performed in which the blade slowly moved upwards clockwise through the sample at a helix angle of 5° and a blade tip speed of 60mm/s to create a reproducible loose packing state. The glass cylinder containing the sample was then split at the top to level off excess material, which resulted in a cylindrical powder bed, 80mm high and 50mm in diameter. Finally the impeller was driven anti-clockwise from the top to the bottom of the bed at a given blade tip speed to measure the flow energy.

The full set of measurements consisted of 11 test runs on the same sample at different blade tip speeds. The previously described conditioning cycle was performed before each run to erase the stress history effect of the previous run. The results of the total flow energy as a function of the blade tip speed are shown in Figure 3. The measurements were repeated three times for each test condition, i.e. material and blade tip speed, and the average value and coefficient of variation was computed. An average value of the coefficient of variation for each test set is indicated in square brackets and demonstrates the good repeatability of the measurements.

The total flow energy measurements for the pink powders clearly differentiate between the two moisture content extremes and show that increasing the moisture content of the powder decreases its flowability. This can be explained by higher inter-particle adhesion caused by the increased moisture content. The

results for the blue and white powders (B_30 and W_6) seem to be inconsistent with this trend but as discussed before, results for different coloured powders are not directly comparable.

It is interesting to note that at low moisture contents, the total flow energy increases markedly when the blade tip speed decreases. This behaviour has been observed before [27,28], but an adequate explanation has not been proposed. Only the results at the 100 mm/s blade tip speed were used for the calibration of the DEM model in this study.

3. Modelling methodology

The discrete element method (DEM) has been shown to be a powerful numerical method for modelling granular materials. DEM which was initially proposed by Cundall and Strack in 1979 [29] uses discrete particles that are allowed to overlap to mimic the particle contact deformation. The particles interact through contact forces that are calculated based on the magnitude of the overlap or interpenetration distance. Based on Newton's second law of motion, the position and velocity of the particles is calculated by integrating the total force on each particle with respect to time. The discrete representation of the material makes this method suitable for modelling particulate solids and processes where large discontinuous deformations take place in the material.

One of the crucial aspects for the successful application of DEM is to formulate contact force models capable of reproducing the mechanical behaviour of the real material. In the case of cohesive powders, this becomes very challenging since adhesive forces can have different physical origins including liquid bridges, electrostatic and van der Waals forces. Several DEM contact models have been proposed in literature to model the different types of adhesive forces between individual particles [30–34] and have been shown to be able to reproduce the behaviour of these forces. However they require the DEM particles to be of the size of the real powder particles. This approach becomes impractical because of the prohibitive computational time required to simulate the huge number of particles in an industrial system. For instance, a small powder specimen of $1cm^3$ can contain more than 10^9 micro-sized powder particles and one second of the simulation would take several years on a 12-core workstation. Furthermore, these adhesive contact models are only valid for the very simple cases of 2D disks or 3D spheres whereas in reality, the powder particles have complex shapes and the surfaces present asperities that render these models unsuitable for modelling real powders accurately in the current state of the art of DEM simulations.

In this study, the behavior of cohesive powders was modelled by means of a visco-elasto-plastic frictional adhesive contact model recently proposed by Thakur et al. [25]. The contact model does not attempt to model the source of each adhesive force precisely. Instead it is based on modelling the experimentally observed phenomena that when two particles or agglomerates are pressed together, they undergo elastic and plastic deformations, and that the pull-off (adhesive) strength increases with an increase of the plastic contact area. The target is therefore to use this phenomenological based model to capture the macroscopic mechanical behaviour observed in typical bulk characterization experiments. The model has been shown to be capable of providing good quantitative predictions of the behaviour of cohesive materials under different loading conditions including compression and shear failure [23,35].

The contact model comprises of a hysteretic spring for the normal force to capture the effect of the plastic deformation on the contact surface of the particles during compression. The loading and unloading/reloading branches of the hysteretic spring are defined by the stiffness parameters k_1, k_2 respectively and an exponent n that allows for non-linearity in the contact stiffness. The contact model also has a load dependent adhesive branch that captures the increase of the adhesive pull-off force with the increase of the contact surface due to plastic deformation. This branch is defined by the adhesive stiffness parameter k_{adh} and the exponent x that takes into account the non-linear reduction of the

attractive force when two particles are separating [36]. The maximum adhesive normal force is defined by $f_{min} = \frac{3}{2}\pi\Delta\gamma a$ where $\Delta\gamma$ represents an adhesion surface energy that is an input parameter of the simulation and a is the contact patch radius. Note that this limiting force has a similar form to that found in JKR [37] and DMT [38] theory for adhesive contacts. Finally, a constant pull-off force f_o is also included to mimic any van der Waals type adhesive forces. A schematic representation of the hysteretic spring normal force as a function of the contact normal overlap is shown in Figure 4.

The total normal contact force f_n is calculated as the sum of the hysteretic spring force f_{hys} and the normal viscous damping force f_{nd}:

$$f_n = f_{hys} + f_{nd} \quad (4)$$

The hysteretic spring force is mathematically expressed by:

$$f_{hys} = \begin{cases} f_0 + k_1\delta^n & if\ k_2(\delta^n - \delta_p^n) \geq k_1\delta^n \\ f_0 + k_2(\delta^n - \delta_n^p) & if\ k_1\delta^n > k_2(\delta^n - \delta_p^n) > -k_{adh}\delta^n \\ f_0 - k_{adh}\delta^n & if - k_{adh}\delta^n \geq k_2(\delta^n - \delta_p^n) \end{cases} \quad (5)$$

The normal damping force f_{nd} is computed as:

$$f_{nd} = \beta_n v_n \quad (6)$$

where v_n is the magnitude of the relative normal velocity of the pair of particles in contact and β_n is the dashpot coefficient calculated as:

$$\beta_n = \sqrt{\frac{4m^* k_1}{1 + \left(\frac{\pi}{\ln e}\right)^2}} \quad (7)$$

with the coefficient of restitution e, the equivalent mass of the particle m^* defined as $m_i m_j/(m_i + m_j)$ where $m_{i,}$ *and* m_j are the masses of the two particles in contact.

Similar to the normal force, the total tangential force f_t is the sum of the tangential spring force f_{ts} and the tangential viscous damping force f_{td}:

$$f_t = f_{ts} + f_{td} \quad (8)$$

The tangential spring force is computed in an incremental way as:

$$f_{ts} = f_{ts(n-1)} + \Delta f_{ts} \quad (9)$$

where $f_{ts(n-1)}$ is the tangential force spring force in the previous time-step and Δf_{ts} is the increment of the tangential force given by:

$$\Delta f_{ts} = -K_{tm} k_1 \delta_t \quad (10)$$

where K_{tm} is the tangential stiffness factor and δ_t is the increment of the tangential overlap. The tangential damping force f_{td} is defined by the tangential dashpot coefficient β_t and the relative tangential velocity as:

$$f_{td} = -\beta_t v_t \quad (11)$$

The tangential dashpot coefficient is expressed:

$$\beta_t = \sqrt{\frac{4m^* K_{tm} k_1}{1 + \left(\frac{\pi}{\ln e}\right)^2}} \quad (12)$$

The limiting tangential friction f_{ct} is calculated using the Coulomb friction criterion including the additive terms f_0 and $k_{adh}\delta^x$:

$$f_{ct} \leq \mu(f_n + k_{adh}\delta^x - f_0) \quad (13)$$

where f_n is the contact normal spring force and μ is the friction coefficient.

In the current investigation, an exponent $n = 3/2$ was used for the loading and unloading/reloading branches of the contact model. In this case, it is worth to note that the loading branch becomes equivalent to the standard Hertz theory. Therefore, a similar approach based on the equivalent Young's modulus E^* and the equivalent radius of the particles involved in each contact R^* has been followed to calculate the value of the loading stiffness parameter k_1:

$$k_1 = \frac{4}{3}\sqrt{r^*}E^* \quad (14)$$

where E^* is defined as $1/E^* = (1-\nu_i)/E_i + \left(1-\nu_j\right)/E_j$ and $r^* = r_i r_j/(r_i + r_j)$ with $E_{i,j}$, , $\nu_{I,j}$ and $r_{i,j}$ being the Young's modulus, Poisson ratio and radius of each particle in contact. Moreover, the Young modulus of the particles is calculated as $E_{i,j} = 2G_{i,j}(1 + \nu_{i,j})$ where $G_{i,j}$ is the shear modulus of the particles.

The unloading/reloading stiffness is expressed as a function of the loading stiffness k_1 with a contact plasticity parameter λ_p as follows:

$$k_2 = \frac{k_1}{1-\lambda_p} \quad (15)$$

Note that the contact becomes purely elastic when $\lambda_p = 0$ with contact plasticity approaching rigid-plastic as the value of λ_p tends to one.

4. DEM representation of the physical system

In DEM, the bulk material is represented by discrete spherical or multi-spherical particles. The shape and size of these particles affects the mechanical behaviour of the model and their representation is an important aspect of DEM simulations.

The non-spherical shape of the powder particles can be seen in the SEM images in Figure 1. Mechanical interlocking of non-spherical particles could be a significant source of bulk shear strength of a granular material and therefore can affect its flowability. Hartl and Ooi [39] have shown that the geometric interlocking from non-spherical particle interaction has a significant effect on the bulk internal friction of a granular material and should be introduced in DEM simulations to capture the bulk shear strength of the

material. The same study demonstrated that the exact shape of the particles does not need to be replicated and a two sphere paired particle with an aspect ratio larger than one can provide a satisfactory quantitative prediction. Bharadvaj et al. [40] studied the effect of particle aspect ratio on the simulated flow energy in the FT4 powder rheometer using paired particles of various aspect ratios. The authors established that introducing a particle aspect ratio of 1.25 caused a significant increase in the predicted flow energy but increasing the aspect ratio further up to 2 did not make any further difference. Therefore the non-spherical paired particle with an aspect ratio of 1.25 shown in Figure 5 was used in the simulations.

As discussed before, bulk materials consist of very large numbers of particles per unit volume and simulating industrial processes using the physical particle size becomes extremely computationally expensive in DEM simulations. This is especially true for powders which have a mean particle size in the micro scale. Some level of particle upscaling is therefore needed to make DEM simulations practical. In this study, the particle size was upscaled two orders of magnitude to achieve practical computational times. Studies have shown that the contact-model, outlined above, is capable of quantitatively capturing the bulk mechanical behaviour of powders at similar levels of particle upscaling as long as the scaling laws are applied correctly [22,23,25]. Concerning the particle size distribution, the study by Bharadvaj et al. [40] suggests that it has no significant effect on the simulated flow energy in the FT4 rheometer at this level of particle upscaling. Therefore, mono-dispersed particles were adopted in the simulations presented in this paper. This decision can be further justified by the narrow particle size distribution of the zeolite powder.

The Basic Flowability Energy test of the FT4 powder rheometer was replicated in EDEM, which is a widely used commercial DEM code, previously verified against a set of benchmark tests by Chung and Ooi [41].

The contact model described in section 3 was used for the particle-particle interaction in order to capture the elasto-plasticity and stress dependent cohesive strength of the zeolite powder. The powder particles were not observed to adhere to the surface of the glass vessel or the blade of the instrument during the tests, despite their small mass. This suggests that the adhesion forces between the particle and these surfaces are negligible. Therefore, the purely elastic non-adhesive Hertz-Mindlin contact model with a tangential frictional slider [42] was used for the particle-geometry interaction.

The DEM material parameters used in the simulations are given in Table 3. Experimentally measured values were directly assigned for the parameters of the vessel and the blade [43]. However, assigning such values to the particle material is less meaningful due to the adopted mesoscopic modelling approach. This will be explained in more detail in section 5.

One parameter of special significance is the particle shear modulus. It is the determining parameter with respect to the overall stiffness of the system and hence the critical time-step for numerical stability [44]. A higher particle shear modulus leads to a lower critical time-step and longer computational times. The particle shear modulus was therefore chosen low enough to produce practical computational times but high enough to avoid excessive normal particle overlaps. From a physical point of view, the adopted low value is not unreasonable considering that each particle in the simulation represents a powder agglomerate, which is quite soft in reality.

The standard test procedure of the BFE test, described in section 2, was reproduced in the simulations. The particles were generated using a random particle factory in EDEM and were allowed to fall and settle into the vessel under gravity, to mimic the experimental filling procedure as close as possible. The system was kept at rest until the total kinetic energy reached values below 10^{-5} J to ensure static conditions were attained.

As Bharadwaj et al. [40] has established that the conditioning cycle of the test has no effect on the flow energy in DEM simulation, the conditioning cycle was omitted in this study to reduce the required computational time. After filling, the splitting of the sample was achieved by accelerating the upper cylinder in the horizontal direction to a velocity of 0.05 m/s in 1 second and then reversing the motion. In the final step the blade was moved into the bed at a 100mm/s blade tip speed and a helix angle of 5°, which correspond to the highest blade tip speed test. Images of the simulation during the different stages of the test are shown in Figure 6.

The instantaneous vertical force and torque on the shaft of the blade were exported from the simulations with a sampling frequency of 20 Hz, which corresponds to the sampling frequency of the physical experiments. The evolution of the cumulative flow energy with penetration depth was then calculated from the instantaneous measurements using Eq. 2 and 3. An example of the simulation results can be seen in Figure 7.

The importance of selecting an appropriate value for the time-step in DEM simulation has been discussed before [44]. The effect of the time-step on the simulation results was explored by running identical simulations with the values of 0.2× T_R and 0.05× T_R, where T_R is the Rayleigh time-step value calculated from Eq. 16.

$$T_R = \left(\frac{\pi r}{0.163\nu + 0.8766}\right)\sqrt{\frac{\rho}{G}} \quad (16)$$

where r is the radius of the particles, ν is the Poisson ratio, ρ is the particle solid density and G is the shear modulus.
The results are plotted in Figure 7 and show that the size of the time-step has no effect on the flow energy within this range of values. Therefore a value of 0.2× T_r was chosen for all simulations, to minimize the required computational time.

5. Determination of the DEM contact model parameters

The determination of appropriate values of the DEM contact model parameters is essential in order to get accurate quantitative predictions of the behaviour of the material in a physical process. Two broad approaches can be found in the literature. The first one consists of determining the properties of the individual particles that are related to the parameters of the DEM contact model [45,46]. This approach usually requires time-consuming and expensive experimental techniques which make it not feasible for industrial cases. Moreover, even if the properties of the individual particles can be measured, the predictions obtained by means of the DEM simulations may not be in good agreement with the experiments because the DEM particle is often a drastic simplification of the real particle. The second approach consists of determining the value of the DEM contact model parameters so that the simulations are able to reproduce the mechanical response of the material observed in selected bulk experiments [20,45,47,48]. For this approach, it is of vital importance that the bulk experiments and responses obtained from them are representative of the loading regimes that the material experiences in the process under investigation.

In this study, the second approach based on matching the experimental and numerical responses from a bulk test was followed. As discussed in section 2 the FT4 rheometer has been chosen as a suitable test for characterising the rheological behaviour of the powders [28]. Furthermore, its total flow energy measurement is correlated well with the flowability of bulk materials, which is expected to be an important property with respect to powder mixing. Thus, the determination of the model parameters is based on reproducing the total flow energy of the powder material in the FT4 test at a tip speed of 100

mm/s. This is the highest tip speed test that can be performed with the FT4 rheometer and was chosen as the most representative of the loading regime that the material experiences during the mixing process, where blade velocities are even higher.

The determination of the values of DEM contact model parameters is usually achieved by trial and error. However, this approach becomes very time consuming since many different combinations of the values of the contact model parameters need to be tested until the DEM simulation matches the experimental response selected for parameter optimization. Moreover, this process would need to be repeated from scratch for materials with different values of the bulk response.

An alternative approach is to take advantage of Design of Experiments (DoE) [21,49] to reduce the number of simulations that need to be conducted. The results from the simulations in a DoE can be used to establish a response function that relates the values of the DEM model parameter with the bulk responses.

In this investigation a Plackett-Burman design of experiments [50] was selected to speed-up the determination of the contact model parameters. This kind of design of experiments is suitable for screening of parameters and determining principal effects of the different parameters on the bulk response. Its main advantage is that the number of points needed is low and as a consequence the number of simulations to be run is reasonable. Nevertheless, this kind of DoE does not provide information on any interaction effects between the parameters or any non-linear effects in the responses.

The Plackett-Burman design was applied for the DEM model parameters listed in Table 4a. For each contact model parameter low and high values were defined so that a spectrum of total flow energies can be reproduced. In the case of the particle-cylinder static friction $\mu_{sp\text{-}g}$ and particle-blade static friction $\mu_{sp\text{-}b}$, their values were always lower than or equal to the particle-particle static friction $\mu_{sp\text{-}p}$. This was achieved by defining the particle-cylinder relative static friction $\chi = \mu_{sp-g}/\mu_{sp-p}$ and particle-blade relative static friction $\psi = \mu_{sp-b}/\mu_{sp-p}$ that was constrained to a high value equal to one.

The resulting design consisted of a set of 12 different simulations with the combinations of the high and low values specified for the DEM parameters. Simulation of the FT4 basic flowability energy test was run for each of these combinations. From each simulation, the total flow energy was calculated from the force and torque on the blade geometry as described in Eq. 2 and Eq. 3.

In order to establish an empirical correlation between the values of the DEM contact model parameters and the total flow energy E_t, the data obtained from the simulations of the DoE were fitted by the following linear response model:

$$E_t = c_0 + c_1 e + c_2 \mu_{sp-p} + c_3 \chi + c_4 \psi + c_5 f_0 + c_6 \Delta\gamma + c_7 \rho_s \quad (17)$$

where the c_n are the coefficients to be determined by fitting the simulation data.

The goodness of fit of Eq. 17 was evaluated by plotting the values of total flow energy measured in the simulations as a function of the values of the total flow energy predicted by the linear response model (Figure 8). The results show that the linear model is able to capture the overall trend of the total flow energy within the explored range of values of the DEM contact model parameters. Nevertheless, they also show some discrepancies, especially for low values of the total flow energy where the model predictions are not so accurate. This fact could be due to the simplicity of the linear model which is not able to capture non-linear effects of the contact model parameters or interactions between them. A potential improvement of the predictions could be achieved by means of a more sophisticated model including

quadratic and interaction terms. For this purpose, a three level DoE such as Box-Behnken or Central Composite Designs would be needed [49]. This would imply a larger number of simulations and is out of the scope of the current investigation.

The linear response model fitted to the results of the DoE was used to optimize the contact model parameters in order to reproduce the experimental total flow energy of the test materials. This range of materials includes both low and high moisture contents in the powders (see section 2). The optimization was conducted by means of the function *fmincon* of Matlab® [51]. The objective function *f* to minimize during the optimization process was defined as the absolute value of the relative error between the experimental total flow energy E_t^{exp} and the value predicted by the linear response model E_t^{LM} obtained in section 5:

$$f = \left| \frac{E_t^{exp} - E_t^{LM}}{E_t^{exp}} \right| \quad (18)$$

The optimization of the parameters was conducted separately for each of the powder materials. In all cases the final value of the objective function was lower than 0.03, which corresponds to a relative error lower than ±3%. The values obtained for the DEM contact model parameters for each tested material are shown in Table 4b.

In order to check the results obtained from the optimization using the linear model, the values of the contact model parameters were used to simulate the FT4 BFE test. For each simulation the evolution of the cumulative flow energy E_c with the penetration depth was computed (see Eq. 2 and 3) and compared with their corresponding experimental curves. The numerical and experimental curves for the four different materials are shown in Figure 9. In the case of the powders with high moisture content (B_30 and P_32), the experimental and numerical curves are in good agreement. However, larger discrepancies are observed for the powders with low moisture content (P_5 and W_6). This is attributed to the capability of the linear response model to reproduce the relationship between the DEM contact model parameters and the total flow energy in the simulations. As discussed before, the accuracy of the linear model is biased towards high values of the total flow energy observed in powders B_30 and P_32 and as a consequence, the results of the optimization for these cases are in agreement with the experimental values. However the predictions of the linear model show significant discrepancies for low values of total flow energy and as a result, the simulated curves obtained with the optimized parameters for P_5 and W_6 deviate significantly from the experimental ones. As stated previously, this problem could be solved by augmenting the DoE so that a more complex response model could be used to reproduce more accurately the relationship of the DEM contact model parameters and the total flow energy.

A further optimization of the parameters was conducted for the powders in order to get closer agreement between the numerical and experimental flow energy curves. This was performed by further tuning the parameter estimates obtained from the optimization of the linear model. The results of this further optimization of parameters are shown in Figure 10 and Table 4c. An excellent agreement between the numerical and experimental curves can be observed for all powders. These further optimized values of the DEM contact model parameters will be used in the next section for simulating the mixing process with the aim of evaluating the predictive capabilities of the DEM simulations against mixing experiments.

The model parameters, not included in the design of experiments, were assigned the fixed values shown in Table 5. The value adopted for the particle shear modulus was discussed in the previous section. The contact plasticity was set to $\lambda = 0.9$ to take into account the high plasticity of the powder material. In the case of the tangential stiffness multiplier, its value was set to 2/7 as suggested in previous studies in the literature for a hysteretic spring contact model [52]. Finally, the exponent *n* for the loading and

unloading/reloading branches was set to 3/2 and the exponent of the adhesion branch was set to $x = 5$ to include non-linearity of the load dependent adhesion branch as observed in experimental AFM measurement for silica particles [36].

6. Assessing the predictive capabilities of the optimized DEM models for powder mixing

6.1 Mixing simulations

DEM simulations of powder mixing in the MLH12 [53] laboratory scale paddle blade mixer were performed. The mixer consists of a cylindrical vessel with a rotating shaft, passing through its centre. The vessel is 220 mm in diameter, 350 mm long and with a capacity of approximately 12 litres. The geometry of the mixer was replicated in the simulations. The shaft and vessel of the mixer are entirely made of stainless steel and were assigned the relevant material properties (shear modulus, Poisson's ratio and density) as listed in Table 3.

The mixing of the lowest and the highest moisture content powders was studied to provide the two extreme cases for the comparison between simulations and experiments. The test configurations are listed in Table 6.

The powder material was represented with the same DEM particle shape and size used in the previous simulation of the FT4 powder rheometer (see section 4) in order to remain consistent with the conducted optimization of the contact model parameters. The further optimized contact model parameters listed in Table 5 were used. However, the contact parameters between two types of powders in each simulation have not been measured. A simple approach of using the averaged optimized parameter values for the contact between particles representing different powders was adopted in this study.

The initial state of the mixing simulations was a completely segregated lateral fill (see figure 11a) which replicated the experimental conditions. This was achieved by generating 600 grams of particles representing each of the two materials using the random rainfall method. The resultant level of filling was approximately 12% and 25% for the simulations with high and low moisture content powders respectively. The experimental mixing process was replicated in the simulations. The experiments included stopping the mixer for sampling at specific time intervals and this was also included in the simulations. At each stop in the simulation the system was kept at rest until the total kinetic energy of the particles was lower than 10^{-5} J. Images of the simulations at different stages can be seen in Figure 11. The mixing rates in the simulations were calculated to compare against the experimental measurements. The mixing rate was characterized by the temporal evolution of the homogeneity of the mix. The mix homogeneity at a given time can be quantified in DEM simulations using a variety of statistical methods [54]. One such method, which has been successfully used before, is the calculation of the relative standard deviation of particle concentrations in a number of samples within the mixer volume[17,55]. This simple but effective approach was adopted in the present study. The relative standard deviation (RSD) of the concentration of particles of one of the powder materials in the samples was calculated using Eq. 19:

$$\mathrm{RSD} = \frac{\sigma}{\bar{x}}, \qquad \sigma = \sqrt{\sum_{i=1}^{n} \frac{(\bar{x} - x_i)^2}{n-1}} \quad (19)$$

where x_i is the concentration of particles of one of the power materials in sample i, $\bar{x}$ is the mean concentration over all samples and n is the total number of samples. A value of RSD equal to 1

corresponds to a completely segregated state and a value close to 0 to a perfectly random mix. To avoid the disproportional effect of samples with a small number of particles, the average number of particles in each sample was computed and only those containing more particles than the average were included in the calculation [16].

The sample procedure was implemented by discretizing the volume of the mixer using the lattice shown in Figure 12. In the experiments, the sampling was done at the surface of the powder bed only. This procedure was mimicked in the simulations by exporting the particle coordinates and detecting the particle with the largest positive y-coordinate in each cell during each stop. In the case where there were particles resting on top of the mixer shaft, those particles were ignored for the detection. The particles which were at a given depth below the maximum detected y-coordinate were then included in the sample for the calculation of the RSD values. A depth of 20 mm was used as an estimate of the sampling depth in the experiment. This procedure ensured that the state of the mix was evaluated on the surface of the powder bed in both the simulations and the experiments.
Using a lattice with a small number of samples can lead to an underestimation of the RSD values and therefore the effect of the lattice density was explored. The 28 by 28 lattice (Figure 12) was found to be sufficiently dense as increasing the number of samples further did not affect the results.

6.2 Mixing experiments

Mixing experiments corresponding to the test configurations in Table 6 were performed in order to provide experimental data for the validation of the DEM model. A completely segregated lateral fill was created in the MLH12 laboratory mixer, by adding 600 grams each of two powders of different colours. This resulted in a level of fill of approximately 16% and 20% for the high and low moisture content experiments respectively.

Colour measurement has been used in a number of studies for the evaluation of different mixers and mixing conditions [56–58]. Barling et.al. (2014) successfully used colour measurement to study different technologies and process conditions for mixing of lactose powders (white colour) with iron oxide tracer (red colour) in order to identify their effect on the mixing behaviour and mixture quality.

In this study, the performance of the mixing process was characterized by measuring the colour of powder samples taken from eight different locations in the mixer (see figure 13). To this end, the mixer was periodically stopped and material was scooped only from the surface of the settled powder bed to minimize disturbance to the mixture. For the sampling points in the region of the shaft of the mixer, the samples were taken from the surface underneath the shaft and not from the powder resting on top of it. The material was scooped to a depth of approximately 20 mm to provide a large enough sample for colour measurement and the sample was then returned to the same location after the measurement.

The bulk colour of each sample was analysed using the Konica Minolta Chroma Meter colorimeter [59]. The colour was characterized in the CIELAB colour space in terms of a lightness channel L* and two colour channels – a* and b*. The compound colour of each sample was quantified by the chroma, calculated from Eq. 20.

$$C^* = \sqrt{(a^{*2} + b^{*2})} \quad (20)$$

The homogeneity of the mix was quantified by the relative standard deviation of the chroma measurement over the eight sampling points, calculated from Eq. 21. This allowed the experimental and simulation results to be compared against the same measure.

$$\mathrm{RSD} = \frac{\sigma}{\overline{C^*}}, \qquad \sigma = \sqrt{\sum_{i=1}^{n} \frac{(\overline{C^*} - C_i^*)^2}{n}} \quad (21)$$

where C^* is the chroma value defined in Equation 20, C_i^* is the chroma value in sample i, $\overline{C}^*$ is the average chroma value and n is the number of sampling points.

The L* measurements, which indicate lightness, were found to be nearly constant for all samples and were not used in the study.

6.3 Comparison between simulations and experiments

Here the simulations are compared against experimental measurements to assess the accuracy of the model. Only limited information is available from the experiments and therefore the validation process was based only on the rate of mixing, which is often the parameter of interest in industrial mixing applications. As discussed before, the relative standard deviation (RSD) of particle concentrations in the simulations and chroma measurements in the experiments were used to characterize the homogeneity of the mixture at a given time. The temporal evolution of the RSD can then be used as an indication of the mixing rate.

A comparison between the experimental and simulation results for the high and the low moisture content powders can be seen in figure 14 and figure 15 respectively. Despite the optimization, the DEM simulations overpredicted the experimental RSD values (i.e. underpredicted the degree of mixing). However, the agreement between the simulation and the experiments improves when examining only the results for the sampling points away from the end boundaries of the mixer (points 3 to 6 in Figure 13) with the corresponding region in the simulations as shown in Figure 16. The results for these cases are shown in figures 17 and 18. Notably, the DEM modelling appears to give a satisfactory prediction of the trend for the RSD for both moisture content extremes. However significant quantitative differences still exist in the RSD values from simulation and experiment which are further explored with the following explanations.

Firstly, the relationship between the chroma of a sample and the concentration of the two coloured powders in it may not be directly comparable. Indeed, previous studies have shown that this relationship can be complex and non-linear [68]. Therefore the direct quantitative comparison of the two RSD values as presented above becomes questionable. This issue could be addressed if an experimental calibration of the chroma measurements with respect to the concentration of the two coloured powders in a sample is carried out.

Secondly, the adopted large DEM particle size could have an effect on the RSD calculation in the simulations. Examining equation 19 it is clear that the value of the RSD is dependent both on the number of cells in the lattice used for the calculation and the concentration of particle types in each cell. Statistically, a small number of cells leads to an underestimation of the RSD value, so a sufficiently dense lattice is needed [54]. The result is a limited number of DEM particles in each cell, which reduces the resolution of the calculated particle concentration. Therefore the direct quantitative comparison of the RSD measurements requires both a sufficiently dense mesh and small enough particle size. This has been confirmed by a previous study of a similar mixing process which established that both the lattice density and the particle size have an effect on the RSD in the simulation [17].

Lastly it is possible that the FT4 basic flow energy is not a sufficient response for the optimization of a DEM model for powder mixing and that the model needs to be calibrated against different or additional

experimental measurements to fully capture the mechanics of mixing.

The larger discrepancy of the results when the ends of the mixer are included could be explained by an enhanced boundary effect due to the DEM particle size. In the following section (6.4) we present further analysis of the simulation results to explore this hypothesis.

The homogeneity of the mix was evaluated only at the free surface in both the simulations and the experiments. Therefore there is the question of how representative the free surface is of the entire mixer volume. The simulation results can be used to give an indication of this. In figures 19 and 20 we show the effect of the sampling depth on the RSD. We limit the investigation to the central part of the mixer only, where the simulations provide a better agreement with the experiments. The depth of 20 mm is representative of the depth of the sampling in the experiments and the sampling depth of 110 mm means the entire bed is sampled underneath each cell. The experimental results have been added to the graphs for comparison.

The results show that the homogeneity of the mix was lower on the surface than it was for the full depth and suggest that the state at the free surface is not representative of the full volume of the bed at least for the simulations presented here. However, it is also possible that the differences arise from the increased number of particles in the now taller cells of the lattice in the simulations as discussed before. To improve the confidence in the model validation, more sophisticated experimental techniques such as positron emission tomography (PET) [3], positron emission particle tracking (PEPT) [4-8], X-ray tomography [9, 10] or magnetic resonance imaging (MRI)[11, 12] should be used as these provide information about the internal flow of the powder during mixing.

6.4 Further analysis of the mixing performance

In this section we employ the spatial and temporal coarse-graining method [61] to analyze the performance of the mixer on the basis of the DEM simulations. This method allows the calculation of local macroscopic variables (e.g. stress, solid fraction) from the discrete particle data in DEM simulations. The analysis was performed using the commercial software developed by Particle Analytics Limited [62].

Using this coarse graining technique, it is possible to examine the evolution of mixing by directly visualizing the relative concentration of particles of one type in the simulations. Figure 21 shows the particle concentration at the end of mixing at different positions along the axis of the mixer. The cut planes are normal to the shaft axis and are located at the centerlines of the blades. The values of 1 and 0 correspond to zones fully saturated with opposite particle types and a value of 0.5 corresponds to an ideal mix of the two types. It is also possible to spatially average the results over all planes normal to the shaft axis. This reduces the results to a single value at each point on the shaft axis. Plotting these values against time leads to the 2D plot in Figure 22 that shows the evolution of the particle concentration with time along the shaft axial direction of the mixer.

It can be seen from Figure 22 that initially the particles are completely segregated in the axial direction except for a small mixed region in the center of the mixer where the two powder beds interface. As time progresses the mixed zone spreads axially from the center to the ends of the mixer but never reaches the mixer end-walls. Instead there are clearly visible dead zones where mixing has not occurred for both the wet and dry mixing simulations. These are also visible in Figure 21 on the planes at the ends of the mixer. Whilst dead zones were observed in the experiments, they were not to the extent seen in the simulations and, as discussed before, this could be the cause of the quantitative discrepancy between the simulation and experimental results when the entire mixer volume is considered. The over-prediction of these dead zones could be the result of the particle size used in the simulations.

To investigate the cause of the different efficiency of mixing at high and low moisture contents we analysed the dynamics of the system in terms of the kinetic pressure calculated from Eq. 23.

$$P_k = \frac{tr(\sigma_k)}{3} \quad (23)$$

where σ_k is the kinetic stress,

$$\sigma_k = \sum_{i=1}^{N} m_i V_i^{'} V_i^{'} W(r - r_i) \quad (24)$$

V_i' is the particle velocity fluctuation given by

$$V_i^{'} = V - V_i \quad (25)$$

m_i is the particle mass, V_i the individual particle velocity and V is the mean particle velocity.

The time averaged kinetic pressure distribution along the shaft axis of the mixer is shown in Figure 23. The wet mixing simulation has significantly higher values of the kinetic pressure, suggesting that it is in higher dynamic regime than the dry mixing one. This could be the explanation of the higher mixing rate both predicted and observed for the wet powders. The higher kinetic pressure during wet mixing could be explained by the lower level of fill, because a shallower powder bed poses less resistance and provides more space for particle movement in the mixer volume.

Figures 24 show the time-averaged kinetic pressure results at the locations of the mixer paddles for both the wet and dry mixing simulations. It can be seen that the values are similar for the central four blades but are significantly lower for the two blades at the axial ends of the mixer. This suggests that these two blades are less effective and their performance could be improved by changing their geometry. The low efficiency of these blades could also explain the predicted dead zones at the ends of the mixer.

7 Conclusions

The predictive capabilities of a visco-elasto-plastic frictional adhesive DEM contact model for simulating the mixing process of zeolite powder with different moisture contents were assessed in this study. To this end, a methodology for the optimization of the DEM model parameters against experimental flow energy measurements from the FT4 powder rheometer was used. The methodology takes advantage of a statistical design of experiments approach in order to reduce the number of simulations required for the optimization. The powder mixing in the MLH12 paddle blade mixer at two extremes of moisture content was simulated and compared to experimental measurements of the homogeneity of the mix in order to validate the model. The following conclusions can be drawn from the work.

The flow energy measurement in the FT4 rheometer increases with increasing moisture content, suggesting that the contribution of inter-particle adhesive forces to the shear resistance of zeolite powder is significant. Overall the moisture content appears to be a major factor in the flow energy measurement for the powder with a fourfold increase in flow energy between the low and high moisture content extremes studied.

The DEM simulations using the final optimized contact model parameters were able to reproduce the measured flow energies for low and high moisture contents with an excellent agreement both in terms of the total flow energy and the evolution of the cumulative energy with time.

With regards to the optimization methodology of the model parameters, the results show that whilst a simple Plackett-Burman Design of Experiments with a linear response model is able to reproduce the total flow energy measurements in FT4, some discrepancies did exist for low values of the total flow energy which suggests a more complex response model, which captures the non-linear terms and the interaction between the model parameters, may be needed. It can be expected that a non-linear response model produced with a higher order DoE would result in a more accurate optimization.

Using the optimized DEM model parameters, the simulations of the mixing process showed a good agreement of the evolution of mixing over time with the experiments but significantly overpredicted the RSD values i.e. predicted a poorer rate of mixing than the experiments. The prediction of mixing rate improved significantly when considering only the central region of the mixer. The poorer prediction for the regions adjacent to the mixer ends can be attributed to the large DEM particle size used or the fact that the DEM model was not optimized against an experimental response involving a powder-steel interaction and therefore may not capture adequately the stress and flow regimes near the mixer end walls. It is also plausible that the total flow energy measurement from FT4 rheometer is not sufficient as a single response for the optimization of the DEM model parameters. Additional powder characterization measurements to better calibrate the model optimization process should improve the predictive capabilities of the DEM model.

The quantitative discrepancies between the simulations and the experiments could also be caused by a non-linear relationship between the colour of the samples and the concentration of each powder in them. Therefore, establishing this relationship experimentally is vital if colorimetry is to be used for the validation of DEM models in powder mixing.

A further source of error could be the effect of the large DEM particle size on the calculation of the RSD in the simulations.

In addition, the simulation results suggest that the mixing state at the free surface of the powder bed is not representative of the entire volume of the powder bed and therefore the adopted strategy of sampling at the superficial region only may be inadequate. More advanced non-invasive experimental techniques should be used to provide information about the internal flow of the powder during mixing.

Acknowledgements

The financial support of Johnson Matthey Plc is gratefully acknowledged.

Funding sources

This research did not receive any specific grant from funding agencies in the public, commercial, or not-for-profit sectors.

References

[1] N. Harnby, M.F. Edwards, A.W. Nienow, Mixing in the process industries, second ed., Oxford, 2001.

[2] A.-N. Huang, H.-P. Kuo, Developments in the tools for the investigation of mixing in particulate systems – A review, Adv. Powder Technol. 25 (2014) 163–173. doi:10.1016/j.apt.2013.10.007.

[3] E. Barrett, The study of pharmaceutical powder mixing through improved flow property characterization and tomographic imaging of blend content uniformity, Birmingham University, 2011.

[4] S.Y. Lim, J.F. Davidson, R.N. Forster, D.J. Parker, D.M. Scott, J.P.K. Seville, Avalanching of granular material in a horizontal slowly rotating cylinder: PEPT studies, Powder Technol. 138 (2003) 25–30. doi:10.1016/j.powtec.2003.08.038.
[5] H.P. Kuo, P.C. Knight, D.J. Parker, J.P.K. Seville, Solids circulation and axial dispersion of cohesionless particles in a V-mixer, Powder Technol. 152 (2005) 133–140. doi:10.1016/j.powtec.2004.12.003.
[6] P.M. Portillo, A.U. Vanarase, A. Ingram, J.K. Seville, M.G. Ierapetritou, F.J. Muzzio, Investigation of the effect of impeller rotation rate, powder flow rate, and cohesion on powder flow behavior in a continuous blender using PEPT, Chem. Eng. Sci. 65 (2010) 5658–5668. doi:10.1016/j.ces.2010.06.036.
[7] B.F.C. Laurent, P.W. Cleary, Comparative study by PEPT and DEM for flow and mixing in a ploughshare mixer, Powder Technol. 228 (2012) 171–186. doi:10.1016/j.powtec.2012.05.013.
[8] M. Marigo, M. Davies, T. Leadbeater, D.L. Cairns, a. Ingram, E.H. Stitt, Application of positron emission particle tracking (PEPT) to validate a discrete element method (DEM) model of granular flow and mixing in the Turbula mixer, Int. J. Pharm. 446 (2013) 46–58. doi:10.1016/j.ijpharm.2013.01.030.
[9] C.-Y. Yang, X.-Y. Fu, Development and validation of a material-labeling method for powder process characterization using X-ray computed tomography, Powder Technol. 146 (2004) 10–19. doi:10.1016/j.powtec.2004.06.011.
[10] R. Liu, X. Yin, H. Li, Q. Shao, P. York, Y. He, T. Xiao, J. Zhang, Visualization and quantitative profiling of mixing and segregation of granules using synchrotron radiation X-ray microtomography and three dimensional reconstruction, Int. J. Pharm. 445 (2013) 125–133. doi:10.1016/j.ijpharm.2013.02.010.
[11] N. Sommier, P. Porion, P. Evesque, B. Leclerc, P. Tchoreloff, G. Couarraze, Magnetic resonance imaging investigation of the mixing-segregation process in a pharmaceutical blender, Int. J. Pharm. 222 (2001) 243–258. doi:10.1016/S0378-5173(01)00718-9.
[12] C. Wightman, F.J. Muzzio, J. Wilder, A quantitative image analysis method for characterizing mixtures of granular materials, Powder Technol. 89 (1996) 165–176. doi:10.1016/S0032-5910(96)03178-6.
[13] X. Liu, C. Zhang, J. Zhan, Quantitative comparison of image analysis methods for particle mixing in rotary drums, Powder Technol. 282 (2014) 32–36. doi:10.1016/j.powtec.2014.08.076.
[14] S.L. Conway, A. Lekhal, J.G. Khinast, B.J. Glasser, Granular flow and segregation in a four-bladed mixer, Chem. Eng. Sci. 60 (2005) 7091–7107. doi:10.1016/j.ces.2005.03.008.
[15] M. Lemieux, G. Léonard, J. Doucet, L. a. Leclaire, F. Viens, J. Chaouki, F. Bertrand, Large-scale numerical investigation of solids mixing in a V-blender using the discrete element method, Powder Technol. 181 (2008) 205–216. doi:10.1016/j.powtec.2006.12.009.
[16] P.W. Cleary, M.D. Sinnott, Assessing mixing characteristics of particle-mixing and granulation devices, Particuology. 6 (2008) 419–444. doi:10.1016/j.partic.2008.07.014.
[17] M. Alian, F. Ein-Mozaffari, S.R. Upreti, Analysis of the mixing of solid particles in a plowshare mixer via discrete element method (DEM), Powder Technol. 274 (2015) 77–87. doi:10.1016/j.powtec.2015.01.012.
[18] Y.C. Chung, J.Y. Ooi, A study of influence of gravity on bulk behaviour of particulate solid, Particuology. 6 (2008) 467–474. doi:10.1016/j.partic.2008.07.017.
[19] Z. Yan, S.K. Wilkinson, E.H. Stitt, M. Marigo, Discrete element modelling (DEM) input parameters: understanding their impact on model predictions using statistical analysis, Comput. Part. Mech. (2015). doi:10.1007/s40571-015-0056-5.
[20] M.W. Johnstone, Calibration of DEM models for granular materials using bulk physical tests The University of Edinburgh, (2010).
[21] M.M. Z. Yan*, S.K. Wilkinson, S.A. Turnbull, E.H. Stitt, Parametric evaluation for powder flowability using a Freeman rheometer: a discrete element method study, in: Crossroads Part. Sci. Technol., 2015.

[22] S.C. Thakur, J.Y. Ooi, H. Ahmadian, Scaling of discrete element model parameters for cohesionless and cohesive solid, Powder Technol. (2015). doi:10.1016/j.powtec.2015.05.051.
[23] A. Janda, J.Y. Ooi, DEM modelling of cone penetration and unconfined compression in cohesive solids, Powder Technol. (2015). doi:10.1016/j.powtec.2015.05.034.
[24] R.L. Stewart, J. Bridgwater, Y.C. Zhou, A.B. Yu, Simulated and measured ow of granules in a bladed mixer — a detailed comparison, 56 (2001) 5457–5471.
[25] S.C. Thakur, J.P. Morrissey, J. Sun, J.F. Chen, J.Y. Ooi, Micromechanical analysis of cohesive granular materials using the discrete element method with an adhesive elasto-plastic contact model, Granul. Matter. 16 (2014) 383–400. doi:10.1007/s10035-014-0506-4.
[26] Malvern Instruments, Malvern.com, (2015). http://www.malvern.com/en/products/product-range/mastersizer-range/mastersizer-2000/ (accessed April 10, 2015).
[27] M. Leturia, M. Benali, S. Lagarde, I. Ronga, K. Saleh, Characterization of flow properties of cohesive powders: A comparative study of traditional and new testing methods, Powder Technol. 253 (2014) 406–423. doi:10.1016/j.powtec.2013.11.045.
[28] R. Freeman, Measuring the flow properties of consolidated, conditioned and aerated powders - A comparative study using a powder rheometer and a rotational shear cell, Powder Technol. 174 (2007) 25–33. doi:10.1016/j.powtec.2006.10.016.
[29] P.A. Cundall, O.D.L. Strack, A discrete numerical model for granular assemblies, Géotechnique. 29 (1979) 47–65. doi:10.1680/geot.1979.29.1.47.
[30] J. Tomas, Assessment of Mechanical Properties of Cohesive Particulate Solids. Part 1: Particle Contact Constitutive Model, Part. Sci. Technol. 19 (2001) 95–110. doi:10.1080/02726350152772056.
[31] V. Richefeu, M.S. El Youssoufi, R. Peyroux, F. Radjaï, A model of capillary cohesion for numerical simulations of 3D polydisperse granular media, Int. J. Numer. Anal. Methods Geomech. 32 (2008) 1365–1383. doi:10.1002/nag.674.
[32] Y. Muguruma, T. Tanaka, Y. Tsuji, Numerical simulation of particulate flow with liquid bridge between particles (simulation of centrifugal tumbling granulator), Powder Technol. 109 (2000) 49–57. doi:10.1016/S0032-5910(99)00226-0.
[33] F. Soulié, F. Cherblanc, M.S. El Youssoufi, C. Saix, Influence of liquid bridges on the mechanical behaviour of polydisperse granular materials, Int. J. Numer. Anal. Methods Geomech. 30 (2006) 213–228. doi:10.1002/nag.476.
[34] T. Gröger, U. Tüzün, D.M. Heyes, Modelling and measuring of cohesion in wet granular materials, Powder Technol. 133 (2003) 203–215. doi:10.1016/S0032-5910(03)00093-7.
[35] S.C. Thakur, H. Ahmadian, J. Sun, J.Y. Ooi, An experimental and numerical study of packing, compression, and caking behaviour of detergent powders, Particuology. 12 (2014) 2–12. doi:10.1016/j.partic.2013.06.009.
[36] R. Jones, H.M. Pollock, D. Geldart, a. Verlinden, Inter-particle forces in cohesive powders studied by AFM: Effects of relative humidity, particle size and wall adhesion, Powder Technol. 132 (2003) 196–210. doi:10.1016/S0032-5910(03)00072-X.
[37] K.L. Johnson, K. Kendall, A.D. Roberts, Surface Energy and the Contact of Elastic Solids, Proc. R. Soc. A Math. Phys. Eng. Sci. 324 (1971) 301–313. doi:10.1098/rspa.1971.0141.
[38] B.V. Derjaguin, V.M. Muller, Y.P. Toporov, Effect of contact deformations on the adhesion of particles, Prog. Surf. Sci. 45 (1994) 131–143. doi:10.1016/0079-6816(94)90044-2.
[39] J. Härtl, J.Y. Ooi, Numerical investigation of particle shape and particle friction on limiting bulk friction in direct shear tests and comparison with experiments, Powder Technol. 212 (2011) 231–239. doi:10.1016/j.powtec.2011.05.022.
[40] R. Bharadwaj, W.R. Ketterhagen, B.C. Hancock, Discrete element simulation study of a Freeman powder rheometer, Chem. Eng. Sci. 65 (2010) 5747–5756. doi:10.1016/j.ces.2010.04.002.
[41] Y.C. Chung, J.Y. Ooi, Benchmark tests for verifying discrete element modelling codes at particle impact level, Granul. Matter. 13 (2011) 643–656. doi:10.1007/s10035-011-0277-0.
[42] DEM Solutions, EDEM 2.6 Theory Reference Guide, Edinburgh, 2014. http://www.dem-

solutions.com/forum/viewtopic.php?f=17&t=653&sid=19b09cd9bcfb2d3c91734e34c2ca128c.
[43] E.Z. Grigoriev, I.S., Meilikhov, Handbook of physical quantities, CRC Press, LLC, 1997.
[44] O. Sullivan, D. Jonathan, Selecting a suitable time step for discrete element simulations that use the central difference time integration scheme, Eng. Comput. 21 (2004) 2–4.
[45] C. González-Montellano, Á. Ramírez, E. Gallego, F. Ayuga, Validation and experimental calibration of 3D discrete element models for the simulation of the discharge flow in silos, Chem. Eng. Sci. 66 (2011) 5116–5126. http://linkinghub.elsevier.com/retrieve/pii/S0009250911004696.
[46] F. Alonso-Marroquín, Á. Ramírez-Gómez, C. González-Montellano, N. Balaam, D.A.H. Hanaor, E.A. Flores-Johnson, Y. Gan, S. Chen, L. Shen, Experimental and numerical determination of mechanical properties of polygonal wood particles and their flow analysis in silos, Granul. Matter. 15 (2013) 811–826. doi:10.1007/s10035-013-0443-7.
[47] M. Marigo, E.H. Stitt, Discrete Element Method (DEM) for Industrial Applications: Comments on Calibration and Validation for the Modelling of Cylindrical Pellets, KONA Powder Part. J. 32 (2015) 236–252. doi:10.14356/kona.2015016.
[48] C.J. Coetzee, D.N.J. Els, Calibration of discrete element parameters and the modelling of silo discharge and bucket filling, Comput. Electron. Agric. 65 (2009) 198–212. http://linkinghub.elsevier.com/retrieve/pii/S0168169908002184.
[49] J.P.C. Kleijnen, Design and analysis of simulation experiments, Springer, Verlag, 2008.
[50] J.P. Plackett, R. L., Burman, The Design of Optimum Multifactorial Experiments, Biometrika. 33 (1946) 305–325.
[51] Matlab, version 8.3.0 (R2014a), (2014).
[52] O.R. Walton, Viscosity, granular-temperature, and stress calculations for shearing assemblies of inelastic, frictional disks, J. Rheol. (N. Y. N. Y). 30 (1986) 949. doi:10.1122/1.549893.
[53] WAM Group, A laboratory mixer, (2015). http://pdf.directindustry.com/pdf/wamgroup-spa/laboratory-mixer-mlh-12-brochure/29492-172485.html.
[54] Z. Gu, J.J.J. Chen, A probabilistic analysis of some selected mixing indices, Chem. Eng. Res. Des. 93 (2015) 293–303. doi:10.1016/j.cherd.2014.04.014.
[55] L. Pezo, A. Jovanović, M. Pezo, R. Čolović, B. Lončar, Modified screw conveyor-mixers – Discrete element modeling approach, Adv. Powder Technol. (2015). doi:10.1016/j.apt.2015.07.016.
[56] M. Satoh, T. Yoshida, T. Yanagida, T. Iwasaki, H. Kimura, Evaluation of the mixing process based on a disintegrating rate model of the powder agglomerates, Adv. Powder Technol. 9 (1998) 377–390. doi:10.1016/S0921-8831(08)60567-1.
[57] T. Iwasaki, M. Satoh, Characterization of powder mixers based on mechanical energy using soft dye granules, Adv. Powder Technol. 13 (2002) 395–409. doi:10.1163/156855202320536034.
[58] D. Barling, D. a V Morton, K. Hapgood, Pharmaceutical dry powder blending and scale-up: Maintaining equivalent mixing conditions using a coloured tracer powder, Powder Technol. 270 (2014) 461–469. doi:10.1016/j.powtec.2014.04.069.
[59] Konica-Minolta, Konica-Minolta, (2015). http://www.konicaminolta.eu/en/measuring-instruments/products/colour-measurement/chroma-meters/cr-400-410/introduction.html.
[60] J. Matsuda, Y., Shiromoto, S., Takeda, Y., Hayashi, S.-I., Okada, Mixing of Pharmaceutical Powders examined by Use of Colored Particles: Discussions on Coloration Difference, Chem. Pharm. Bull. 22 (1975) 2803–2811.
[61] C. Labra, J.Y. Ooi, J. Sun, Spatial and temporal coarse-graining for DEM analysis, in: AIP Conf. Proc., 2013: pp. 1258–1261. doi:10.1063/1.4812167.
[62] Particle Analytics, (2016). http://particle-analytics.com/ (accessed June 21, 2016).

Figure captions

Figure 1 Scanning Electron Microscopy image of a virgin zeolite powder sample at x3000 magnification.

Figure 2: Bulk density as a function of moisture content for all zeolite powders. The error bars correspond to the coefficient of variation of the measurements. The dashed line represents the trend for the pink samples as explained in the main text.

Figure 3 FT4 Powder rheometer BFE test measurements: Total Flow Energy vs. Blade Tip Speed.

Figure 4 Normal contact force – normal overlap relationship of the elasto-plastic frictional adhesive contact model [25].

Figure 5 Size and shape of the DEM particles used in the simulations.

Figure 6 DEM simulation of the FT4 powder rheometer (cut through centre of the blade).

Figure 7 Effect of timestep for integration on the cumulative flow energy in FT4 test simulations.

Figure 8 Goodness of the linear model fitted to the DoE results: DEM simulation results vs values predicted by the model. The solid line represents where the points should locate for a perfect fitting.

Figure 9 Comparison of the cumulative flow energy in experiments and DEM simulations, optimized using the linear response model.

Figure 10 Comparison of the cumulative flow energy in experiments with the further optimized DEM simulations.

Figure 11 DEM mixing simulations a) before mixing b) during mixing c) during a stop for sampling

Figure 12 Cell lattice for the calculation of the RSD in the DEM simulations

Figure 14 Temporal evolution of the RSD for low moisture content powders.

Figure 15 Temporal evolution of the RSD for high moisture content powders.

Figure 16 Portion of the cell lattice used for the calculation of the RSD in the center of the mixer.

Figure 17 Temporal evolution of the RSD for low moisture content powders – results for central part of mixer only.

Figure 18 Temporal evolution of the RSD for high moisture content powders – results for central part of mixer only.

Figure 19 Temporal evolution of the RSD for low moisture content powders – effect of sampling depth in the central part of the mixer only.

Figure 20 Temporal evolution of the RSD for high moisture content powders – effect of sampling depth in the central part of the mixer only.

Figure 21 Final state of mix at different locations along the shaft axis at the end of the simulations for both wet and dry powders. The cut planes are normal to the shaft axis.

Figure 22 Temporal evolution of mixing along the axial direction of the mixer for the high and low moisture content powders. The results are spatially averaged over the planes normal to the shaft axis.

Figure 23 Time-averaged kinetic pressure distribution along the shaft axial direction for both wet and dry mixing simulations.

Figure 24 Time-averaged kinetic pressure on planes normal to the shaft axis for both wet and dry mixing simulations.

Tables

Table 1 Particle size distribution of zeolite 4A powder

D10 (μm)	D50 (μm)	D90 (μm)	Dispersal	Ultrasonication power	Relative Error
1.7	3.5	6.2	Wet	85 %	2 %
2	4.1	7.3	Wet	0 %	2 %
1.1	2.9	5.5	Dry	2 %	2 %

Table 2 Moisture content and bulk density measurements of the zeolite powders. The values correspond to the arithmetic average of the measurements for each material.

Notation	Moisture Content (%)	Bulk Density (kg/m3)
P_32	32.4	380
P_19	19.2	455
P_14	13.7	489
P_5	4.5	612
B_30	30.2	566
W_6	6.3	530

Table 3 Shear moduli, Poisson's ratios and solid densities used in the simulations.

Zeolite			
Poisson ratio	v	0.25	
Shear modulus	G	5.00E+06	Pa
Solid density	ρ	Variable	kg/m3
Stainless steel			
Poisson ratio	v	0.3	
Shear modulus	G	7.30E+10	Pa
Solid density	ρ	7800	kg/m3
Borosilicate glass			
Poisson ratio	v	0.3	
Shear modulus	G	2.40E+07	Pa
Solid density	ρ	2500	kg/m3

Table 4 Values of the DEM contact model parameters explored in the optimization phase.

a)

DoE Parameters	**Notation**	**Low**	**High**
Restitution coefficient	e	0.2	0.6
Particle-Particle Static Friction	μ_{sp-p}	0.1	0.7
Particle - Cylinder Relative Static Friction	$\chi = \mu_{sp-g}/\mu_{sp-p}$	0.1	1
Particle - Blade Relative Static Friction	$\psi = \mu_{sp-b}/\mu_{sp-p}$	0.1	1
Const. Pull-off force (N)	f_0	-1E-2	-1E-05
Surface Energy (J/m2)	$\Delta\gamma$	0.01	5
Particle solid density (kg/m3)	ρ_s	600	1400

b)

Linear Response Model Optimization							
Notation	**ρ_s**	**μ_{sp-p}**	**χ**	**ψ**	***f_0***	**$\Delta\gamma$**	**e**
W_6 LM	600	0.24	0.08	0.11	-0.0045	2.68	0.35
P_5 LM	600	0.35	0.17	0.19	-0.005	2.56	0.39
B_30 LM	1400	0.7	0.7	0.7	-0.008	1.4	0.6
P_32 LM	1400	0.7	0.7	0.7	-0.01	0.01	0.6

c)

Further Optimization							
Notation	**ρ_s**	**μ_{sp-p}**	**χ**	**Ψ**	***f_0***	**$\Delta\gamma$**	**e**
W_6 FO	600	0.3	0.3	0.4	-1.0E-05	0.01	0.4
P_5 FO	600	0.69	0.69	0.25	-0.0005	2.06	0.27
B_30 FO	1300	0.7	0.7	0.7	-0.0005	4.5	0.6
P_32 FO	1600	0.7	0.7	0.7	-0.0005	5	0.6

Table 5 DEM input parameters with fixed values.

Assumed Parameters	Notation	Value
Contact plasticity	λ	0.9
Loading and Unloading/Reloading exponent	n	1.5
Adhesion exponent	x	5
Particle Poisson Ratio	ν	0.25
Particle Shear Modulus (GPa)	G	5.00E+06
Tangential Stiffness Multiplier	K_{tm}	0.286

Table 6 Material type and shaft rotational velocity configurations for the simulations and the experiments.

Notation	**Materials**	**Shaft Rotational Velocity**
Wet 110 RPM	P_32 – B_30	110 RPM
Dry 110 RPM	P_5 – W_6	110 RPM

An experimentally validated DEM study of powder mixing in a paddle blade mixer

Stefan Pantaleev [a], Slavina Yordanova [b], Alvaro Janda[c], Michele Marigo[d], Jin Y. Ooi[a]

Corresponding author:
Stefan Pantaleev
e-mail: s.pantaleev@ed.ac.uk
tel: 131 650 5790

[a]Institute of Infrastructure and Environment, School of Engineering, University of Edinburgh, Edinburgh, EH9 3JY, Scotland, UK

[b]Arup Group Ltd, Scotstoun House, South Queensferry, Edinburgh, EH30 9SE, Scotland, UK

[c] Particle Analytics Ltd, Alrick Building, Max Born Crescent, The King's Buildings , Edinburgh, EH9 3BF, UK

[d]Johnson Matthey Technology Centre, PO Box 1, Belasis Avenue, Billingham TS23 1LB, UK

Abstract

An investigation on the predictive capabilities of Discrete Element Method simulations of a powder mixing process in a laboratory scale paddle blade mixer is presented. The visco-elasto-plastic frictional adhesive DEM contact model of Thakur et al (2014) was used to represent the cohesive behaviour of an aluminosilicate powder in which the model parameters were determined using experimental flow energy measurements from the FT4 powder rheometer. DEM simulations of the mixing process using the contact model parameters were evaluated against the experimental measurements of the mixing rate. The results demonstrated that whilst the DEM model is capable of reproducing the FT4 flow energy of the powder to an excellent agreement, the simulations of the mixing process produced a qualitative agreement on the trend of the mixing rate in the experiments for both dry and wet powders. The mixing was under-predicted in the simulations, suggesting that flow energy measurements alone may not be sufficient for the optimization of a DEM model of powder mixing.

Keywords

Solid mixing, cohesive powder, numerical modelling, model calibration, discrete element method, DEM.

1. Introduction

Particulate materials are important in a wide range of industries including the pharmaceutical, chemical, metallurgical, food and others. Within these industrial mixing and blending of materials are some of the most demanding unit operations. Successful manufacturing of a variety of products is heavily dependent on the efficiency of this process, because the final product quality is inherently dependent on the quality of the obtained mixture. Inefficient mixing resulting in a non-homogenous product (typical detrimental effects can include segregation, particle breakage, unwanted agglomeration) can lead to products that might not meet the required quality in terms of chemical composition, colour, texture, flavour, reactivity, or particle size.

A variety of solid mixers are available in industry; these can be divided into two categories: mixers with rotating vessels (rotating drum, double cone blender, V-blenders, octagonal blender) and mixers with fixed vessels and rotating components (ribbon blender, paddle blender, plough mixer, double paddle mixer). Mixers can also be grouped depending on the predominant mixing mechanism that is driving the material such as convection, dispersion and shear [1].

A large amount of experimental and modelling work has been carried out on the mixing of powders in a variety of mixers, but the scientific understanding of the process remains limited. As a consequence the design and selection of appropriate mixing equipment is not straight forward and the common problems related to scale up and operation of mixing processes remain unsolved.

The experimental and numerical tools for the study of mixing in particulate systems are briefly reviewed below and the current developments have been reported extensively in the literature [e.g. 2]. Non-invasive experimental techniques such as positron emission tomography (PET) [3], positron emission particle tracking (PEPT) [4-8], X-ray tomography [9,10] and magnetic resonance imaging (MRI)[11,12] have been applied to look at the material flow, mixing and segregation within a variety of mixing unit operations. Although these techniques can give insightful information regarding the material behaviour within a particular system, they are costly and relatively difficult to access. A cheaper and easily accessible technique is to look at the material flow by optical imaging and post processing methods such particle image velocimetry [12–14]. However, these are limited to a 2D field of views or applied only at the free surface boundaries, which makes it challenging to apply to a plough or paddle type mixer.

Particulate material mixing and segregation in blenders have also been extensively studied numerically using the discrete element method (DEM). Various blender designs and the effect of operating variables (e.g. fill level, operating speed, and material type) have been investigated [15–17]. The motion of individual particles can be tracked in DEM simulations and therefore insight can be obtained into the mechanisms governing particles flow in a variety of mixing processes. The obtained information can then be used to inform the design, selection and operation of powder mixing equipment, reducing the need for pilot studies and speeding up the design optimization process.

Although DEM has been widely used to study a variety of processes, the experimental quantitative validation of the simulation results is rarely reported in the literature [18]. Furthermore, the appropriate methodology to determine DEM input parameters for a given application is often unclear [19]. This is especially true in the case of fine powders which are abundant in industry. Additionally, the computational cost to model a large number of particles of small sizes that constitute fine powders poses a significant challenge for the DEM modelling of these materials.

Often in the literature, the values of the DEM parameters are optimized with a global fitting between DEM simulation and an actual small scale experiment [20]. Extensive work has also been carried out to develop a multi-level parametric sensitivity method to understand the impact of the DEM input parameters on the bulk responses for a given simple system [19], [21]. The proposed approach provides a systematic method that can be used to show the importance of specific input parameters for a given system and then potentially facilitates their selection. Moreover particle scale methodologies have been developed to scale-up particles in a DEM model to capture a material bulk response similar to systems comprised of much smaller particles [22,23]. Considering these recent developments, DEM has become a promising simulation method for fine powders.

DEM simulations of the mixing of non-cohesive bulk solids have demonstrated a measure of quantitative accuracy when appropriate values of the model parameters were used [24]. Therefore, it would be of interest to determine if a quantitatively accurate model for cohesive powder mixing can be produced when its input parameters are appropriately optimized..

This study evaluates the predictive capabilities of a visco-elasto-plastic frictional adhesive DEM model [25] for the simulation of aluminosilicate powder mixing in a laboratory scale mixer. The mixer of choice was the MLH12 (WAM Group) paddle blade mixer, which is a laboratory scale mixer with a capacity of 12 litres. The FT4 powder rheometer was used to characterize the mechanical properties of the powder at a wide range of moisture contents. The test was replicated in DEM simulations and the contact model parameters were optimized to reproduce the experimental total flow energy measurements in the FT4 rheometer. A simple Plackett-Burman design of experiments was used to produce a set of simulations with systematically varied parameter values and a linear response model was fitted to the simulated total flow energy. The response model was then used to determine the input parameters, which produced the closest match to the experimental flow energy measurements. DEM simulations of the mixing process were performed using the optimized model parameters and the mixing rate in the simulations was calculated from the statistical distribution of particle concentrations. Finally, the simulation results were compared against experimental measurements of the mixing rate to assess the predictive capability of the DEM model.

2. Physical and mechanical properties of the test material

Synthetic zeolite powder was used as the test material for this study. It is a fine aluminosilicate powder representative of cohesive powders with challenging behaviour in industrial mixing applications.

The particle size distribution of the powder (Table 1) was measured using a Malvern Mastersizer 2000

particle size analyser [26]. Measurements were made using both a dry and wet dispersal and using two levels of ultrasonication power for the wet dispersal. The mean particle size of the powder (D50) was higher under wet dispersal conditions, demonstrating the ability of the particles to form stable agglomerates even in a water suspension. The mean particle size decreased with the increase in ultrasonication power due to the breakup of these agglomerates by the ultrasonic waves passing through the suspension. A Scanning Electron Microscopy (SEM) image of a powder sample (Figure 1) shows the tendency of the particles to agglomerate together due to van der Waals and liquid bridge type forces. On the bulk scale the powder was also observed to form stable agglomerates of millimeters in size, especially at higher moisture contents. Moreover, the non-spherical nature of the individual particles is evident from the SEM images suggesting that particle interlocking might have a significant effect on the bulk strength and flowability of the material.

The physical and mechanical properties of the zeolite powder were determined at several moisture contents in order to capture the wide range of its flow behaviour and to encompass a variety of operational conditions, found in industrial powder mixing applications. Batches of pink or blue coloured powder with different moisture contents were prepared. The powders were coloured, because the subsequent mixing experiments relied on colour measurement to quantify the rate of mixing. The highest moisture content powders of each colour were prepared by adding distilled water and dye to the powder and mixed to homogeneity in the MLH12 mixer. Powders at lower levels of moisture content were made by oven drying the high moisture content powders at 200^0C. A halogen moisture balance was used to determine the total moisture content of all batches, making three measurements for each. The instrument uses a halogen lamp to heat a sample to 110^0C and measure the change in its mass. The moisture content is then calculated from Eq. 1.

$$w_t = M_w/M_t \quad (1)$$

where M_w is the mass of water and M_t is the total mass of the sample.

Additionally, the bulk density of the powders was determined by filling the 160 ml glass cylinder of the FT4 powder rheometer with powder and measuring its mass. The resultant materials and their properties are listed in Table 2 and plotted in Fig. 2. The notation for each powder consists of a letter and a number. The letter indicates the colour of the powder – P for pink, B for blue and W for white (no dye added), while the number indicates the moisture content of the powder to the nearest integer.

Figure 2 shows the bulk density as a function of the moisture content of the different tested materials. The addition of a chemical dye to the powder could alter the chemical and mechanical properties of the particles and hence, the bulk properties of the material as a whole. It could, for example, affect the van der Waals forces and therefore particle agglomeration. Therefore only the properties of powders of the same colour can be rigorously compared. The effect of moisture content on the bulk density was assessed for the pink coloured powders as shown by the dashed line in Figure 2. The bulk density initially decreases with increasing moisture content resulting in an increase in porosity caused by the formation of liquid bridges between the particles which keep them slightly apart. As moisture content increases towards saturation, the bulk density reaches a minimum before increasing again due to the mass of the added water and a reduction of porosity with the disappearance of liquid bridging between particles.

The FT4 powder rheometer is increasingly used for characterization of powder flowability both in academia and industry [27]. It can measure some of the mechanical properties traditionally employed for the evaluation of powder flow behaviour, such as shear strength, compressibility and permeability. Furthermore, a common methodology for characterizing powder flowability with this instrument is the measurement of flow energy, which is the energy needed to drive an impeller blade through a bed of powder. The flow energy has been reported to correlate well with traditional flowability characterization techniques [27,28]. Using this methodology, the powder flowability is characterized in a dynamic flow

regime and under free surface conditions [28]. This is in contrast with the traditional methodologies which characterize the flowability in a quasi-static regime. Powder mixing in paddle-blade mixers, which is the process targeted in the current study, also occurs under dynamic flow and free surface conditions. This apparent correspondence between the flow conditions in the characterization experiment and the process under investigation suggests that the flow energy could be a relevant measurement of powder flowability for this study.

The Basic Flow Energy (BFE) test of the FT4 Powder rheometer, used for the determination of the flow energy, is described in full detail elsewhere [28]. In this test an impeller blade moves through a bed of powder. The movement of the impeller is defined by the helix velocity of the blade termed the blade tip speed. The incremental flow energy as the blade ploughs through an increment depth dz is calculated from the translational and rotational work of the blade using Eq. 2.

$$E_f = \left(F + \frac{T}{R\tan(\alpha)}\right) dz \quad (2)$$

where F and T are the instantaneous vertical force on the bottom of the vessel and the instantaneous torque on the shaft of the blade respectively, R is the radius of the impeller and α is the helix angle of the blade path.

The cumulative flow energy required for the blade to penetrate the sample to a depth z is then:

$$E_c = \int_0^z \left(F + \frac{T}{R\tan(\alpha)}\right) dz \quad (3)$$

and the total flow energy at the end of the test E_T is the cumulative energy at the maximum penetration depth of 70 mm.

While the evolution of the cumulative energy with depth can be obtained from the test, only the total flow energy is commonly used to characterize the powder flowability. In general, higher total flow energy corresponds to lower flowability and vice versa.

All test powders were characterized using the standard BFE test procedure proposed by Freeman [28] in which the 48 mm impeller blade was used. Initially a conditioning cycle was performed in which the blade slowly moved upwards clockwise through the sample at a helix angle of 5° and a blade tip speed of 60mm/s to create a reproducible loose packing state .The glass cylinder containing the sample was then split at the top to level off excess material, which resulted in a cylindrical powder bed, 80mm high and 50mm in diameter. Finally the impeller was driven anti-clockwise from the top to the bottom of the bed at a given blade tip speed to measure the flow energy.

The full set of measurements consisted of 11 test runs on the same sample at different blade tip speeds. According to the standard procedure, the first 8 test runs were performed at a blade tip speed of 100mm/s and a further three were performed at 70, 40 and 10 mm/s respectively. The previously described conditioning cycle was performed before each run to erase the stress history effect of the previous run. The results of the total flow energy as a function of the blade tip speed are shown in Figure 3. The measurements were repeated three times for each test condition, i.e. material and blade tip speed, and the average value and coefficient of variation was computed. An average value of the coefficient of variation for each test set is indicated in square brackets and demonstrates the good repeatability of the measurements.

The total flow energy measurements for the pink powders clearly differentiate between the two moisture content extremes (powders P_5 and P_32). The results for these two powders show that an increase in moisture content leads to an increase in flow energy, which could be explained by higher inter-particle adhesion due to liquid bridging. The results for the intermediate moisture content powders (P_14 and P_19) do not follow this trend however, so the relationship between moisture content and flow energy for the powder appears to be more complex when the full range of moisture contents is considered.

It is interesting to note that at low moisture contents (powders P_5 and W_6), the total flow energy increases markedly when the blade tip speed decreases. The trend is similar at intermediate moisture contents (powders P_14 and P_19) although it is less pronounced. This behaviour has been observed before [27,28], but an adequate explanation has not been proposed. It is worth noting that the wettest powders (P_32 and B_30) behave differently from the rest, showing an initial decrease in flow energy between the 70mm/s and 100 mm/s tests. A potential explanation for this difference in behaviour could be the method of preparation described before, in which the lower moisture content powders were made by oven drying and could therefore have altered mechanical properties.

3. Modelling methodology

The discrete element method (DEM) has been shown to be a powerful numerical method for modelling granular materials. DEM which was initially proposed by Cundall and Strack in 1979 [29] uses discrete particles that are allowed to overlap to mimic the particle contact deformation. The particles interact through contact forces that are calculated based on the magnitude of the overlap or interpenetration distance. Based on Newton's second law of motion, the position and velocity of the particles is calculated by integrating the total force on each particle with respect to time. The discrete representation of the material makes this method suitable for modelling particulate solids and processes where large discontinuous deformations take place in the material.

One of the crucial aspects for the successful application of DEM is to formulate contact force models capable of reproducing the mechanical behaviour of the real material. In the case of cohesive powders, this becomes very challenging since adhesive forces can have different physical origins including liquid bridges, electrostatic and van der Waals forces. Several DEM contact models have been proposed in literature to model the different types of adhesive forces between individual particles [30–34] and have been shown to be able to reproduce the behaviour of these forces. However they require the DEM particles to be of the size of the real powder particles. This approach becomes impractical because of the prohibitive computational time required to simulate the huge number of particles in an industrial system. For instance, a small powder specimen of $1cm^3$ can contain more than 10^9 micro-sized powder particles and one second of the simulation would take several years on a 12-core workstation. Furthermore, these adhesive contact models are only valid for the very simple cases of 2D disks or 3D spheres whereas in reality, the powder particles have complex shapes and the surfaces present asperities that render these models unsuitable for modelling real powders accurately in the current state of the art of DEM simulations.

In this study, the behavior of cohesive powders was modelled by means of a visco-elasto-plastic frictional adhesive contact model recently proposed by Thakur et al. [25]. The contact model does not attempt to model the source of each adhesive force precisely. Instead it is based on modelling the experimentally observed phenomena that when two particles or agglomerates are pressed together, they undergo elastic and plastic deformations, and that the pull-off (adhesive) strength increases with an increase of the plastic contact area. The target is therefore to use this phenomenological based model to capture the macroscopic mechanical behaviour observed in typical bulk characterization experiments. The model has been shown to be capable of providing good quantitative predictions of the behaviour of cohesive materials under different loading conditions including compression and shear failure [23,35].

The contact model comprises of a hysteretic spring for the normal force to capture the effect of the plastic deformation on the contact surface of the particles during compression. The loading and unloading/reloading branches of the hysteretic spring are defined by the stiffness parameters k_1, k_2 respectively and an exponent n that allows for non-linearity in the contact stiffness. The contact model also has a load dependent adhesive branch that captures the increase of the adhesive pull-off force with the increase of the contact surface due to plastic deformation. This branch is defined by the adhesive stiffness parameter k_{adh} and the exponent x that takes into account the non-linear reduction of the attractive force when two particles are separating [36]. The maximum adhesive normal force is defined by $\mathrm{f_{min}} = \frac{3}{2}\pi\Delta\gamma a$ where $\Delta\gamma$ represents an adhesion surface energy that is an input parameter of the simulation and a is the contact patch radius. Note that this limiting force has a similar form to that found in JKR [37] and DMT [38] theory for adhesive contacts. Finally, a constant pull-off force f_o is also included to mimic any van der Waals type adhesive forces. A schematic representation of the hysteretic spring normal force as a function of the contact normal overlap is shown in Figure 4.

The total normal contact force f_n is calculated as the sum of the hysteretic spring force f_{hys} and the normal viscous damping force f_{nd}:

$$f_n = f_{hys} + f_{nd} \quad (4)$$

The hysteretic spring force is mathematically expressed by:

$$f_{hys} = \begin{cases} f_0 + k_1\delta^n & if\ k_2\left(\delta^n - \delta_p^n\right) \geq k_1\delta^n \\ f_0 + k_2\left(\delta^n - \delta_n^p\right) & if\ k_1\delta^n > k_2\left(\delta^n - \delta_p^n\right) > -k_{adh}\delta^n \\ f_0 - k_{adh}\delta^n & if - k_{adh}\delta^n \geq k_2\left(\delta^n - \delta_p^n\right) \end{cases} \quad (5)$$

The normal damping force f_{nd} is computed as:

$$f_{nd} = \beta_n v_n \quad (6)$$

where v_n is the magnitude of the relative normal velocity of the pair of particles in contact and β_n is the dashpot coefficient calculated as:

$$\beta_n = \sqrt{\frac{4m^* k_1}{1 + \left(\frac{\pi}{\ln e}\right)^2}} \quad (7)$$

with the coefficient of restitution e, the equivalent mass of the particle m^* defined as $m_i m_j/(m_i + m_j)$ where $m_{i,}$ *and* m_j are the masses of the two particles in contact.

Similar to the normal force, the total tangential force f_t is the sum of the tangential spring force f_{ts} and the tangential viscous damping force f_{td}:

$$f_t = f_{ts} + f_{td} \quad (8)$$

The tangential spring force is computed in an incremental way as:

$$f_{ts} = f_{ts(n-1)} + \Delta f_{ts} \quad (9)$$

where $f_{ts(n-1)}$ is the tangential force spring force in the previous time-step and Δf_{ts} is the increment of the tangential force given by:

$$\Delta f_{ts} = -K_{tm} k_1 \delta_t \quad (10)$$

where K_{tm} is the tangential stiffness factor and δ_t is the increment of the tangential overlap. The tangential damping force f_{td} is defined by the tangential dashpot coefficient β_t and the relative tangential velocity as:

$$f_{td} = -\beta_t v_t \quad (11)$$

The tangential dashpot coefficient is expressed:

$$\beta_t = \sqrt{\frac{4m^* K_{tm} k_1}{1 + \left(\frac{\pi}{\ln e}\right)^2}} \quad (12)$$

The limiting tangential friction f_{ct} is calculated using the Coulomb friction criterion including the additive terms f_0 and $k_{adh}\delta^x$:

$$f_{ct} \leq \mu(f_n + k_{adh}\delta^x - f_0) \quad (13)$$

where f_n is the contact normal spring force and μ is the friction coefficient.

In the current investigation, an exponent $n = 3/2$ was used for the loading and unloading/reloading branches of the contact model. In this case, it is worth to note that the loading branch becomes equivalent to the standard Hertz theory. Therefore, a similar approach based on the equivalent Young's modulus E^* and the equivalent radius of the particles involved in each contact R^* has been followed to calculate the value of the loading stiffness parameter k_1:

$$k_1 = \frac{4}{3}\sqrt{r^*}E^* \quad (14)$$

where E^* is defined as $1/E^* = (1-\nu_i)/E_i + (1-\nu_j)/E_j$ and $r^* = r_i r_j/(r_i + r_j)$ with $E_{i,j}$, , $\nu_{I,j}$ and $r_{i,j}$ being the Young's modulus, Poisson ratio and radius of each particle in contact. Moreover, the Young modulus of the particles is calculated as $E_{i,j} = 2G_{i,j}(1 + \nu_{i,j})$ where $G_{i,j}$ is the shear modulus of the particles.

The unloading/reloading stiffness is expressed as a function of the loading stiffness k_1 with a contact plasticity parameter λ_p as follows:

$$k_2 = \frac{k_1}{1 - \lambda_p} \quad (15)$$

Note that the contact becomes purely elastic when $\lambda_p = 0$ with contact plasticity approaching rigid-plastic as the value of λ_p tends to one.

4. DEM representation of the physical system

In DEM, the bulk material is represented by discrete spherical or multi-spherical particles. The shape and size of these particles affects the mechanical behaviour of the model and their representation is an important aspect of DEM simulations.

The non-spherical shape of the powder particles can be seen in the SEM images in Figure 1. Mechanical interlocking of non-spherical particles could be a significant source of bulk shear strength of a granular material and therefore can affect its flowability. Hartl and Ooi [39] have shown that the geometric interlocking from non-spherical particle interaction has a significant effect on the bulk internal friction of a granular material and should be introduced in DEM simulations to capture the bulk shear strength of the material. The same study demonstrated that the exact shape of the particles does not need to be replicated and a two sphere paired particle with an aspect ratio larger than one can provide a satisfactory quantitative prediction. Bharadvaj et al. [40] studied the effect of particle aspect ratio on the simulated flow energy in the FT4 powder rheometer using paired particles of various aspect ratios. The authors established that introducing a particle aspect ratio of 1.25 caused a significant increase in the predicted flow energy but increasing the aspect ratio further up to 2 did not make any further difference. Therefore the non-spherical paired particle with an aspect ratio of 1.25 shown in Figure 5 was used in the simulations.

As discussed before, bulk materials consist of very large numbers of particles per unit volume and simulating industrial processes using the physical particle size becomes extremely computationally expensive in DEM simulations. This is especially true for powders which have a mean particle size in the micro scale. Some level of particle upscaling is therefore needed to make DEM simulations practical. In this study, the particle size was upscaled two orders of magnitude to achieve practical computational times. Studies have shown that the contact-model, outlined above, is capable of quantitatively capturing the bulk mechanical behaviour of powders at similar levels of particle upscaling as long as the scaling laws are applied correctly [22,23,25]. Concerning the particle size distribution, the study by Bharadvaj et al. [40] suggests that it has no significant effect on the simulated flow energy in the FT4 rheometer at this level of particle upscaling. Therefore, mono-dispersed particles were adopted in the simulations presented in this paper. This decision can be further justified by the narrow particle size distribution of the zeolite powder.

The Basic Flowability Energy test of the FT4 powder rheometer was replicated in EDEM, which is a widely used commercial DEM code, previously verified against a set of benchmark tests by Chung and Ooi [41].

The contact model described in section 3 was used for the particle-particle interaction in order to capture the elasto-plasticity and stress dependent cohesive strength of the zeolite powder. The powder particles were not observed to adhere to the surface of the glass vessel or the blade of the instrument during the tests, despite their small mass. This suggests that the adhesion forces between the particle and these surfaces are negligible. Therefore, the purely elastic non-adhesive Hertz-Mindlin contact model with a tangential frictional slider [42] was used for the particle-geometry interaction.

The DEM material parameters used in the simulations are given in Table 3. Experimentally measured values were directly assigned for the parameters of the vessel and the blade [43]. However, assigning such values to the particle material is less meaningful due to the adopted mesoscopic modelling approach. This will be explained in more detail in section 5.

One parameter of special significance is the particle shear modulus. It is the determining parameter with respect to the overall stiffness of the system and hence the critical time-step for numerical stability [44]. A higher particle shear modulus leads to a lower critical time-step and longer computational times. The particle shear modulus was therefore chosen low enough to produce practical computational times but high enough to avoid excessive normal particle overlaps. From a physical point of view, the adopted low

value is not unreasonable considering that each particle in the simulation represents a powder agglomerate, which is quite soft in reality.

The standard test procedure of the BFE test, described in section 2, was reproduced in the simulations. The particles were generated using a random particle factory in EDEM and were allowed to fall and settle into the vessel under gravity, to mimic the experimental filling procedure as close as possible. The system was kept at rest until the total kinetic energy reached values below 10^{-5} J to ensure static conditions were attained.

As Bharadwaj et al. [40] has established that the conditioning cycle of the test has no effect on the flow energy in DEM simulation, the conditioning cycle was omitted in this study to reduce the required computational time. After filling, the splitting of the sample was achieved by accelerating the upper cylinder in the horizontal direction to a velocity of 0.05 m/s in 1 second and then reversing the motion. In the final step the blade was moved into the bed at a 100mm/s blade tip speed and a helix angle of 5°, which correspond to the highest blade tip speed test. Images of the simulation during the different stages of the test are shown in Figure 6.

The instantaneous vertical force and torque on the shaft of the blade were exported from the simulations with a sampling frequency of 20 Hz, which corresponds to the sampling frequency of the physical experiments. The evolution of the cumulative flow energy with penetration depth was then calculated from the instantaneous measurements using Eq. 2 and 3. An example of the simulation results can be seen in Figure 7.

The importance of selecting an appropriate value for the time-step in DEM simulation has been discussed before [44]. The effect of the time-step on the simulation results was explored by running identical simulations with the values of $0.2\times T_R$ and $0.05\times T_R$, where T_R is the Rayleigh time-step value calculated from Eq. 16.

$$T_R = \left(\frac{\pi r}{0.163\nu + 0.8766}\right)\sqrt{\frac{\rho}{G}} \quad (16)$$

where r is the radius of the particles, ν is the Poisson ratio, ρ is the particle solid density and G is the shear modulus.
The results are plotted in Figure 7 and show that the size of the time-step has no effect on the flow energy within this range of values. Therefore a value of $0.2\times T_r$ was chosen for all simulations, to minimize the required computational time.

5. Determination of the DEM contact model parameters

The determination of appropriate values of the DEM contact model parameters is essential in order to get accurate quantitative predictions of the behaviour of the material in a physical process. Two broad approaches can be found in the literature. The first one consists of determining the properties of the individual particles that are related to the parameters of the DEM contact model [45,46]. This approach usually requires time-consuming and expensive experimental techniques which make it not feasible for industrial cases. Moreover, even if the properties of the individual particles can be measured, the predictions obtained by means of the DEM simulations may not be in good agreement with the experiments because the DEM particle is often a drastic simplification of the real particle. The second approach consists of determining the value of the DEM contact model parameters so that the simulations are able to reproduce the mechanical response of the material observed in selected bulk experiments [45,47–49]. For this approach, it is of vital importance that the bulk experiments and responses obtained

from them are representative of the loading regimes that the material experiences in the process under investigation.

In this study, the second approach based on matching the experimental and numerical responses from a bulk test was followed. As discussed in section 2 the FT4 rheometer has been chosen as a suitable test for characterising the rheological behaviour of the powders [28]. Furthermore, its total flow energy measurement is correlated well with the flowability of bulk materials, which is expected to be an important property with respect to powder mixing. Thus, the determination of the model parameters is based on reproducing the total flow energy of the powder material in the FT4 test at a tip speed of 100 mm/s. This is the highest tip speed test that can be performed with the FT4 rheometer and was chosen as the most representative of the loading regime that the material experiences during the mixing process, where blade velocities are even higher.

The determination of the values of DEM contact model parameters is usually achieved by trial and error. However, this approach becomes very time consuming since many different combinations of the values of the contact model parameters need to be tested until the DEM simulation matches the experimental response selected for parameter optimization. Moreover, this process would need to be repeated from scratch for materials with different values of the bulk response.

An alternative approach is to take advantage of Design of Experiments (DoE) [21,50] to reduce the number of simulations that need to be conducted. The results from the simulations in a DoE can be used to establish a response function that relates the values of the DEM model parameter with the bulk responses.

In this investigation a Plackett-Burman design of experiments [51] was selected to speed-up the determination of the contact model parameters. This kind of design of experiments is suitable for screening of parameters and determining principal effects of the different parameters on the bulk response. Its main advantage is that the number of points needed is low and as a consequence the number of simulations to be run is reasonable. Nevertheless, this kind of DoE does not provide information on any interaction effects between the parameters or any non-linear effects in the responses.

The Plackett-Burman design was applied for the DEM model parameters listed in Table 4a. For each contact model parameter low and high values were defined so that a spectrum of total flow energies can be reproduced. In the case of the particle-cylinder static friction $\mu_{sp\text{-}g}$ and particle-blade static friction $\mu_{sp\text{-}b}$, their values were always lower than or equal to the particle-particle static friction $\mu_{sp\text{-}p}$. This was achieved by defining the particle-cylinder relative static friction $\chi = \mu_{sp-g}/\mu_{sp-p}$ and particle-blade relative static friction $\psi = \mu_{sp-b}/\mu_{sp-p}$ that was constrained to a high value equal to one.

The resulting design consisted of a set of 12 different simulations with the combinations of the high and low values specified for the DEM parameters. Simulation of the FT4 basic flowability energy test was run for each of these combinations. From each simulation, the total flow energy was calculated from the force and torque on the blade geometry as described in Eq. 2 and Eq. 3.

In order to establish an empirical correlation between the values of the DEM contact model parameters and the total flow energy E_t, the data obtained from the simulations of the DoE were fitted by the following linear response model:

$$E_t = c_0 + c_1 e + c_2 \mu_{sp-p} + c_3 \chi + c_4 \psi + c_5 f_0 + c_6 \Delta\gamma + c_7 \rho_s \quad (17)$$

where the c_n are the coefficients to be determined by fitting the simulation data.

The goodness of fit of Eq. 17 was evaluated by plotting the values of total flow energy measured in the simulations as a function of the values of the total flow energy predicted by the linear response model (Figure 8). The results show that the linear model is able to capture the overall trend of the total flow energy within the explored range of values of the DEM contact model parameters. Nevertheless, they also show some discrepancies, especially for low values of the total flow energy where the model predictions are not so accurate. This fact could be due to the simplicity of the linear model which is not able to capture non-linear effects of the contact model parameters or interactions between them. A potential improvement of the predictions could be achieved by means of a more sophisticated model including quadratic and interaction terms. For this purpose, a three level DoE such as Box-Behnken or Central Composite Designs would be needed [50]. This would imply a larger number of simulations and is out of the scope of the current investigation.

The linear response model fitted to the results of the DoE was used to optimize the contact model parameters in order to reproduce the experimental total flow energy of the test materials. This range of materials includes both low and high moisture contents in the powders (see section 2). The optimization was conducted by means of the function *fmincon* of Matlab® [52]. The objective function *f* to minimize during the optimization process was defined as the absolute value of the relative error between the experimental total flow energy E_t^{exp} and the value predicted by the linear response model E_t^{LM} obtained in section 5:

$$f = \left| \frac{E_t^{exp} - E_t^{LM}}{E_t^{exp}} \right| \quad (18)$$

The optimization of the parameters was conducted separately for each of the powder materials. In all cases the final value of the objective function was lower than 0.03, which corresponds to a relative error lower than ±3%. The values obtained for the DEM contact model parameters for each tested material are shown in Table 4b.

In order to check the results obtained from the optimization using the linear model, the values of the contact model parameters were used to simulate the FT4 BFE test. For each simulation the evolution of the cumulative flow energy E_c with the penetration depth was computed (see Eq. 2 and 3) and compared with their corresponding experimental curves. The numerical and experimental curves for the four different materials are shown in Figure 9. In the case of the powders with high moisture content (B_30 and P_32), the experimental and numerical curves are in good agreement. However, larger discrepancies are observed for the powders with low moisture content (P_5 and W_6). This is attributed to the capability of the linear response model to reproduce the relationship between the DEM contact model parameters and the total flow energy in the simulations. As discussed before, the accuracy of the linear model is biased towards high values of the total flow energy observed in powders B_30 and P_32 and as a consequence, the results of the optimization for these cases are in agreement with the experimental values. However the predictions of the linear model show significant discrepancies for low values of total flow energy and as a result, the simulated curves obtained with the optimized parameters for P_5 and W_6 deviate significantly from the experimental ones. As stated previously, this problem could be solved by augmenting the DoE so that a more complex response model could be used to reproduce more accurately the relationship of the DEM contact model parameters and the total flow energy.

A further optimization of the parameters was conducted for the powders in order to get closer agreement between the numerical and experimental flow energy curves. This was performed by further tuning the parameter estimates obtained from the optimization of the linear model. The results of this further optimization of parameters are shown in Figure 10 and Table 4c. An excellent agreement between the

numerical and experimental curves can be observed for all powders. These further optimized values of the DEM contact model parameters will be used in the next section for simulating the mixing process with the aim of evaluating the predictive capabilities of the DEM simulations against mixing experiments.

The model parameters, not included in the design of experiments, were assigned the fixed values shown in Table 5. The value adopted for the particle shear modulus was discussed in the previous section. The contact plasticity was set to $\lambda = 0.9$ to take into account the high plasticity of the powder material. In the case of the tangential stiffness multiplier, its value was set to 2/7 as suggested in previous studies in the literature for a hysteretic spring contact model [53]. The exponent n for the loading and unloading/reloading branches was set to 3/2 and the exponent of the adhesion branch was set to $x = 5$ to include non-linearity of the load dependent adhesion branch as observed in experimental AFM measurement for silica particles [36]. Finally, the rolling friction coefficient for all contacts was set to the low value of 0.01, because the rolling resistance of the particles was accounted for in the simulations by the use of the non-spherical paired particles of aspect ratio 1.25 [40].

6. Assessing the predictive capabilities of the optimized DEM models for powder mixing

6.1 Mixing simulations

DEM simulations of powder mixing in the MLH12 [54] laboratory scale paddle blade mixer were performed. The mixer consists of a cylindrical vessel with a rotating shaft, passing through its centre. The vessel is 220 mm in diameter, 350 mm long and with a capacity of approximately 12 litres. The geometry of the mixer was replicated in the simulations. The shaft and vessel of the mixer are entirely made of stainless steel and were assigned the relevant material properties (shear modulus, Poisson's ratio and density) as listed in Table 3.

The mixing of the lowest and the highest moisture content powders was studied to provide the two extreme cases for the comparison between simulations and experiments. The test configurations are listed in Table 6.

The powder material was represented with the same DEM particle shape and size used in the previous simulation of the FT4 powder rheometer (see section 4) in order to remain consistent with the conducted optimization of the contact model parameters. The further optimized contact model parameters listed in Table 5 were used. However, the contact parameters between two types of powders in each simulation have not been measured. A simple approach of using the averaged optimized parameter values for the contact between particles representing different powders was adopted in this study.

The initial state of the mixing simulations was a completely segregated lateral fill (see figure 11a) which replicated the experimental conditions. This was achieved by generating 600 grams of particles representing each of the two materials using the random rainfall method. The resultant level of filling was approximately 12% and 25% for the simulations with high and low moisture content powders respectively. The experimental mixing process was replicated in the simulations. The experiments included stopping the mixer for sampling at specific time intervals and this was also included in the simulations. At each stop in the simulation the system was kept at rest until the total kinetic energy of the particles was lower than 10^{-5} J. Images of the simulations at different stages can be seen in Figure 11.
The mixing rates in the simulations were calculated to compare against the experimental measurements. The mixing rate was characterized by the temporal evolution of the homogeneity of the mix. The mix homogeneity at a given time can be quantified in DEM simulations using a variety of statistical methods [55]. One such method, which has been successfully used before, is the calculation of the relative standard deviation of particle concentrations in a number of samples within the mixer volume[17,56].

This simple but effective approach was adopted in the present study. The relative standard deviation (RSD) of the concentration of particles of one of the powder materials in the samples was calculated using Eq. 19:

$$\mathrm{RSD} = \frac{\sigma}{\bar{x}}, \qquad \sigma = \sqrt{\sum_{i=1}^{n} \frac{(\bar{x} - x_i)^2}{n-1}} \quad (19)$$

where x_i is the concentration of particles of one of the power materials in sample i, $\bar{x}$ is the mean concentration over all samples and n is the total number of samples. A value of RSD equal to 1 corresponds to a completely segregated state and a value close to 0 to a perfectly random mix. To avoid the disproportional effect of samples with a small number of particles, the average number of particles in each sample was computed and only those containing more particles than the average were included in the calculation [16].

The sampling procedure was implemented by discretizing the volume of the mixer using the lattice shown in Figure 12. In the experiments, the sampling was done at the surface of the powder bed only. This procedure was mimicked in the simulations by exporting the particle coordinates and detecting the particle with the largest positive y-coordinate in each cell during each stop. In the case where there were particles resting on top of the mixer shaft, those particles were ignored for the detection. The particles which were at a given depth below the maximum detected y-coordinate were then included in the sample for the calculation of the RSD values. A depth of 20 mm was used as an estimate of the sampling depth in the experiment. This procedure ensured that the state of the mix was evaluated on the surface of the powder bed in both the simulations and the experiments.
Using a lattice with a small number of samples can lead to an underestimation of the RSD values and therefore the effect of the lattice density was explored. The 28 by 28 lattice (Figure 12) was found to be sufficiently dense as increasing the number of samples further did not affect the results.

6.2 Mixing experiments

Mixing experiments corresponding to the test configurations in Table 6 were performed in order to provide experimental data for the validation of the DEM model. A completely segregated lateral fill was created in the MLH12 laboratory mixer, by adding 600 grams each of two powders of different colours. This resulted in a level of fill of approximately 16% and 20% for the high and low moisture content experiments respectively.

Colour measurement has been used in a number of studies for the evaluation of different mixers and mixing conditions [57–59]. Barling et.al. (2014) successfully used colour measurement to study different technologies and process conditions for mixing of lactose powders (white colour) with iron oxide tracer (red colour) in order to identify their effect on the mixing behaviour and mixture quality.

In this study, the performance of the mixing process was characterized by measuring the colour of powder samples taken from eight different locations in the mixer (see figure 13). To this end, the mixer was periodically stopped and material was scooped only from the surface of the settled powder bed to minimize disturbance to the mixture. For the sampling points in the region of the shaft of the mixer, the samples were taken from the surface underneath the shaft and not from the powder resting on top of it. The material was scooped to a depth of approximately 20 mm to provide a large enough sample for colour measurement and the sample was then returned to the same location after the measurement.

The bulk colour of each sample was analysed using the Konica Minolta Chroma Meter colorimeter [60].

The colour was characterized in the CIELAB colour space in terms of a lightness channel L* and two colour channels – a* and b*. The compound colour of each sample was quantified by the chroma, calculated from Eq. 20.

$$C^* = \sqrt{(a^{*2} + b^{*2})} \quad (20)$$

The homogeneity of the mix was quantified by the relative standard deviation of the chroma measurement over the eight sampling points, calculated from Eq. 21. This allowed the experimental and simulation results to be compared against the same measure.

$$\mathrm{RSD} = \frac{\sigma}{\overline{C^*}}, \qquad \sigma = \sqrt{\sum_{i=1}^{n} \frac{(\overline{C^*} - C_i^*)^2}{n}} \quad (21)$$

where C^* is the chroma value defined in Equation 20, C_i^* is the chroma value in sample i, $\overline{C}^*$ is the average chroma value and n is the number of sampling points.

The L* measurements, which indicate lightness, were found to be nearly constant for all samples and were not used in the study.

6.3 Comparison between simulations and experiments

Here the simulations are compared against experimental measurements to assess the accuracy of the model. Only limited information is available from the experiments and therefore the validation process was based only on the rate of mixing, which is often the parameter of interest in industrial mixing applications. As discussed before, the relative standard deviation (RSD) of particle concentrations in the simulations and chroma measurements in the experiments were used to characterize the homogeneity of the mixture at a given time. The temporal evolution of the RSD can then be used as an indication of the mixing rate.

A comparison between the experimental and simulation results for the high and the low moisture content powders can be seen in figure 14 and figure 15 respectively. Despite the optimization, the DEM simulations overpredicted the experimental RSD values (i.e. underpredicted the degree of mixing). However, the agreement between the simulation and the experiments improves when examining only the results for the sampling points away from the end boundaries of the mixer (points 3 to 6 in Figure 13) with the corresponding region in the simulations as shown in Figure 16. The results for these cases are shown in figures 17 and 18. Notably, the DEM modelling appears to give a satisfactory prediction of the trend for the RSD for both moisture content extremes. However significant quantitative differences still exist in the RSD values from simulation and experiment which are further explored with the following explanations.

Firstly, the relationship between the chroma of a sample and the concentration of the two coloured powders in it may not be directly comparable. Indeed, previous studies have shown that this relationship can be complex and non-linear [68]. Therefore the direct quantitative comparison of the two RSD values as presented above becomes questionable. This issue could be addressed if an experimental calibration of the chroma measurements with respect to the concentration of the two coloured powders in a sample is carried out.

Secondly, the adopted large DEM particle size could have an effect on the RSD calculation in the simulations. Examining equation 19 it is clear that the value of the RSD is dependent both on the number

of cells in the lattice used for the calculation and the concentration of particle types in each cell. Statistically, a small number of cells leads to an underestimation of the RSD value, so a sufficiently dense lattice is needed [55]. The result is a limited number of DEM particles in each cell, which reduces the resolution of the calculated particle concentration. Therefore the direct quantitative comparison of the RSD measurements requires both a sufficiently dense mesh and small enough particle size. This has been confirmed by a previous study of a similar mixing process which established that both the lattice density and the particle size have an effect on the RSD in the simulation [17].

Thirdly, the observed discrepancies could stem from the adopted simple approach of using the averaged values of the optimized contact model parameters for the two coloured powders to model the contact between particles representing each powder. An alternative may have been to determine the parameters for this contact by optimizing their values using the flow energy of a mixture of the two powders. A potential challenge in this case would be to capture the flow energy of mixtures with a range of ratios of the two powders using a single set of parameter values. This would be important since the powder mixture is not uniform in time and space within the mixer.

Lastly it is possible that the FT4 basic flow energy is not a sufficient response for the optimization of a DEM model for powder mixing and that the model needs to be calibrated against different or additional experimental measurements to fully capture the mechanics of mixing.

The larger discrepancy of the results when the ends of the mixer are included could be explained by an enhanced boundary effect due to the DEM particle size. In the following section (6.4) we present further analysis of the simulation results to explore this hypothesis.

The homogeneity of the mix was evaluated only at the free surface in both the simulations and the experiments. Therefore there is the question of how representative the free surface is of the entire mixer volume. The simulation results can be used to give an indication of this. In figures 19 and 20 we show the effect of the sampling depth on the RSD. We limit the investigation to the central part of the mixer only, where the simulations provide a better agreement with the experiments. The depth of 20 mm is representative of the depth of the sampling in the experiments and the sampling depth of 110 mm means the entire bed is sampled underneath each cell. The experimental results have been added to the graphs for comparison.

The results show that the homogeneity of the mix was lower on the surface than it was for the full depth and suggest that the state at the free surface is not representative of the full volume of the bed at least for the simulations presented here. However, it is also possible that the differences arise from the increased number of particles in the now taller cells of the lattice in the simulations as discussed before. To improve the confidence in the model validation, more sophisticated experimental techniques such as positron emission tomography (PET) [3], positron emission particle tracking (PEPT) [4-8], X-ray tomography [9, 10] or magnetic resonance imaging (MRI)[11, 12] should be used as these provide information about the internal flow of the powder during mixing.

6.4 Further analysis of the mixing performance

In this section we employ the spatial and temporal coarse-graining method [62] to analyze the performance of the mixer on the basis of the DEM simulations. This method allows the calculation of local macroscopic variables (e.g. stress, solid fraction) from the discrete particle data in DEM simulations. The analysis was performed using the commercial software developed by Particle Analytics Limited [63].

Using this coarse graining technique, it is possible to examine the evolution of mixing by directly

visualizing the relative concentration of particles of one type in the simulations. Figure 21 shows the particle concentration at the end of mixing at different positions along the axis of the mixer. The cut planes are normal to the shaft axis and are located at the centerlines of the blades. The values of 1 and 0 correspond to zones fully saturated with opposite particle types and a value of 0.5 corresponds to an ideal mix of the two types. It is also possible to spatially average the results over all planes normal to the shaft axis. This reduces the results to a single value at each point on the shaft axis. Plotting these values against time leads to the 2D plot in Figure 22 that shows the evolution of the particle concentration with time along the shaft axial direction of the mixer.

It can be seen from Figure 22 that initially the particles are completely segregated in the axial direction except for a small mixed region in the center of the mixer where the two powder beds interface. As time progresses the mixed zone spreads axially from the center to the ends of the mixer but never reaches the mixer end-walls. Instead there are clearly visible dead zones where mixing has not occurred for both the wet and dry mixing simulations. These are also visible in Figure 21 on the planes at the ends of the mixer. Whilst dead zones were observed in the experiments, they were not to the extent seen in the simulations and, as discussed before, this could be the cause of the quantitative discrepancy between the simulation and experimental results when the entire mixer volume is considered. The over-prediction of these dead zones could be the result of the particle size used in the simulations.

To investigate the cause of the different efficiency of mixing at high and low moisture contents we analysed the dynamics of the system in terms of the kinetic stress σ_k tensor as derived by Goldhirsch [64]:

$$\sigma_k = \sum_{i=1}^{N} m_i V_i^{'} V_i^{'} W(r - r_i) \quad (23)$$

where m_i is the particle mass, W is a Gaussian coarse-graining function, r and r_i are the coordinates of the point of calculation and the particle center of mass respectively. V_i' is the particle velocity fluctuation given by $V_i^{'} = V - V_i$ where V_i is the individual particle velocity and V is the coarse-grained mean particle velocity at the point of calculation. In order to characterize the strength of the kinetic stress, we use the kinetic pressure P_k calculated as follows:

$$P_k = \frac{tr(\sigma_k)}{3} \quad (24)$$

where $tr(\sigma_k)$ is the trace of the kinetic stress tensor.

From Eq. 23 and 24, it is clear that the kinetic pressure can be used to characterize the particle velocity fluctuations which determine the granular temperature of the system[65]. In the literature, this metric has been previously shown to be highly correlated with the performance of solids mixing [14,66–68]

The time averaged kinetic pressure distribution along the shaft axis of the mixer is shown in Figure 23. The wet mixing simulation has significantly higher values of the kinetic pressure, suggesting that it is in higher dynamic regime than the dry mixing one. This could be the explanation of the higher mixing rate both predicted and observed for the wet powders. The higher kinetic pressure during wet mixing could be explained by the lower level of fill, because a shallower powder bed poses less resistance and provides more space for particle movement in the mixer volume.

Figure 24 shows the time-averaged kinetic pressure results at the locations of the mixer paddles for both the wet and dry mixing simulations. It can be seen that the values are similar for the central four blades

but are significantly lower for the two blades at the axial ends of the mixer. This suggests that these two blades are less effective and their performance could be improved by changing their geometry. The low efficiency of these blades could also explain the predicted dead zones at the ends of the mixer.

7 Conclusions

The predictive capabilities of a visco-elasto-plastic frictional adhesive DEM contact model for simulating the mixing process of zeolite powder with different moisture contents were assessed in this study. To this end, a methodology for the optimization of the DEM model parameters against experimental flow energy measurements from the FT4 powder rheometer was used. The methodology takes advantage of a statistical design of experiments approach in order to reduce the number of simulations required for the optimization. The powder mixing in the MLH12 paddle blade mixer at two extremes of moisture content was simulated and compared to experimental measurements of the homogeneity of the mix in order to validate the model. The following conclusions can be drawn from the work.

The measured flow energy of the zeolite powder increases markedly between the two moisture content extremes, suggesting that the contribution of inter-particle adhesive forces to the shear resistance of the powder is significant. However, the increase in flow energy is not continuous at intermediate moisture contents and overall the relationship between moisture content and flow energy appears to be complex for this powder.

The DEM simulations using the final optimized contact model parameters were able to reproduce the measured flow energies for low and high moisture contents with an excellent agreement both in terms of the total flow energy and the evolution of the cumulative energy with time.

With regards to the optimization methodology of the model parameters, the results show that whilst a simple Plackett-Burman Design of Experiments with a linear response model is able to reproduce the total flow energy measurements in FT4, some discrepancies did exist for low values of the total flow energy which suggests a more complex response model, which captures the non-linear terms and the interaction between the model parameters, may be needed. It can be expected that a non-linear response model produced with a higher order DoE would result in a more accurate optimization.

Using the optimized DEM model parameters, the simulations of the mixing process showed a good agreement of the evolution of mixing over time with the experiments but significantly overpredicted the RSD values i.e. predicted a poorer rate of mixing than the experiments. The prediction of mixing rate improved significantly when considering only the central region of the mixer. The poorer prediction for the regions adjacent to the mixer ends can be attributed to the large DEM particle size used or the fact that the DEM model was not optimized against an experimental response involving a powder-steel interaction and therefore may not capture adequately the stress and flow regimes near the mixer end walls. An additional source of error could be the use of the averaged contact model parameters of each coloured powder to model the contact between particles of the two different powders. In a future investigation it might be interesting to explore other alternatives such as the optimization of these parameter values using the flow energy of a mixture of the two powders. The effect of the large DEM particle size on the calculation of the RSD in the simulations could also be a source of error.

It is also plausible that the total flow energy measurement from FT4 rheometer is not sufficient as a single response for the optimization of the DEM model parameters. Additional powder characterization measurements to better calibrate the model optimization process should improve the predictive capabilities of the DEM model.

The quantitative discrepancies between the simulations and the experiments could also be caused by a non-linear relationship between the colour of the samples and the concentration of each powder in them. Therefore, establishing this relationship experimentally is vital if colorimetry is to be used for the

validation of DEM models in powder mixing.

In addition, the simulation results suggest that the mixing state at the free surface of the powder bed is not representative of the entire volume of the powder bed and therefore the adopted strategy of sampling at the superficial region only may be inadequate. More advanced non-invasive experimental techniques should be used to provide information about the internal flow of the powder during mixing.

Acknowledgements

The financial support of Johnson Matthey Plc is gratefully acknowledged.

Funding sources

This research did not receive any specific grant from funding agencies in the public, commercial, or not-for-profit sectors.

References

[1] N. Harnby, M.F. Edwards, A.W. Nienow, Mixing in the process industries, second ed., Oxford, 2001.

[2] A.-N. Huang, H.-P. Kuo, Developments in the tools for the investigation of mixing in particulate systems – A review, Adv. Powder Technol. 25 (2014) 163–173. doi:10.1016/j.apt.2013.10.007.

[3] E. Barrett, The study of pharmaceutical powder mixing through improved flow property characterization and tomographic imaging of blend content uniformity, Birmingham University, 2011.

[4] S.Y. Lim, J.F. Davidson, R.N. Forster, D.J. Parker, D.M. Scott, J.P.K. Seville, Avalanching of granular material in a horizontal slowly rotating cylinder: PEPT studies, Powder Technol. 138 (2003) 25–30. doi:10.1016/j.powtec.2003.08.038.

[5] H.P. Kuo, P.C. Knight, D.J. Parker, J.P.K. Seville, Solids circulation and axial dispersion of cohesionless particles in a V-mixer, Powder Technol. 152 (2005) 133–140. doi:10.1016/j.powtec.2004.12.003.

[6] P.M. Portillo, A.U. Vanarase, A. Ingram, J.K. Seville, M.G. Ierapetritou, F.J. Muzzio, Investigation of the effect of impeller rotation rate, powder flow rate, and cohesion on powder flow behavior in a continuous blender using PEPT, Chem. Eng. Sci. 65 (2010) 5658–5668. doi:10.1016/j.ces.2010.06.036.

[7] B.F.C. Laurent, P.W. Cleary, Comparative study by PEPT and DEM for flow and mixing in a ploughshare mixer, Powder Technol. 228 (2012) 171–186. doi:10.1016/j.powtec.2012.05.013.

[8] M. Marigo, M. Davies, T. Leadbeater, D.L. Cairns, a. Ingram, E.H. Stitt, Application of positron emission particle tracking (PEPT) to validate a discrete element method (DEM) model of granular flow and mixing in the Turbula mixer, Int. J. Pharm. 446 (2013) 46–58. doi:10.1016/j.ijpharm.2013.01.030.

[9] C.-Y. Yang, X.-Y. Fu, Development and validation of a material-labeling method for powder process characterization using X-ray computed tomography, Powder Technol. 146 (2004) 10–19. doi:10.1016/j.powtec.2004.06.011.

[10] R. Liu, X. Yin, H. Li, Q. Shao, P. York, Y. He, T. Xiao, J. Zhang, Visualization and quantitative profiling of mixing and segregation of granules using synchrotron radiation X-ray microtomography and three dimensional reconstruction, Int. J. Pharm. 445 (2013) 125–133. doi:10.1016/j.ijpharm.2013.02.010.

[11] N. Sommier, P. Porion, P. Evesque, B. Leclerc, P. Tchoreloff, G. Couarraze, Magnetic resonance imaging investigation of the mixing-segregation process in a pharmaceutical blender, Int. J. Pharm.

222 (2001) 243–258. doi:10.1016/S0378-5173(01)00718-9.
[12] C. Wightman, F.J. Muzzio, J. Wilder, A quantitative image analysis method for characterizing mixtures of granular materials, Powder Technol. 89 (1996) 165–176. doi:10.1016/S0032-5910(96)03178-6.
[13] X. Liu, C. Zhang, J. Zhan, Quantitative comparison of image analysis methods for particle mixing in rotary drums, Powder Technol. 282 (2014) 32–36. doi:10.1016/j.powtec.2014.08.076.
[14] S.L. Conway, A. Lekhal, J.G. Khinast, B.J. Glasser, Granular flow and segregation in a four-bladed mixer, Chem. Eng. Sci. 60 (2005) 7091–7107. doi:10.1016/j.ces.2005.03.008.
[15] M. Lemieux, G. Léonard, J. Doucet, L. a. Leclaire, F. Viens, J. Chaouki, F. Bertrand, Large-scale numerical investigation of solids mixing in a V-blender using the discrete element method, Powder Technol. 181 (2008) 205–216. doi:10.1016/j.powtec.2006.12.009.
[16] P.W. Cleary, M.D. Sinnott, Assessing mixing characteristics of particle-mixing and granulation devices, Particuology. 6 (2008) 419–444. doi:10.1016/j.partic.2008.07.014.
[17] M. Alian, F. Ein-Mozaffari, S.R. Upreti, Analysis of the mixing of solid particles in a plowshare mixer via discrete element method (DEM), Powder Technol. 274 (2015) 77–87. doi:10.1016/j.powtec.2015.01.012.
[18] Y.C. Chung, J.Y. Ooi, A study of influence of gravity on bulk behaviour of particulate solid, Particuology. 6 (2008) 467–474. doi:10.1016/j.partic.2008.07.017.
[19] Z. Yan, S.K. Wilkinson, E.H. Stitt, M. Marigo, Discrete element modelling (DEM) input parameters: understanding their impact on model predictions using statistical analysis, Comput. Part. Mech. (2015). doi:10.1007/s40571-015-0056-5.
[20] M.W. Johnstone, Calibration of DEM models for granular materials using bulk physical tests The University of Edinburgh, (2010).
[21] M.M. Z. Yan*, S.K. Wilkinson, S.A. Turnbull, E.H. Stitt, Parametric evaluation for powder flowability using a Freeman rheometer: a discrete element method study, in: Crossroads Part. Sci. Technol., 2015.
[22] S.C. Thakur, J.Y. Ooi, H. Ahmadian, Scaling of discrete element model parameters for cohesionless and cohesive solid, Powder Technol. (2015). doi:10.1016/j.powtec.2015.05.051.
[23] A. Janda, J.Y. Ooi, DEM modelling of cone penetration and unconfined compression in cohesive solids, Powder Technol. (2015). doi:10.1016/j.powtec.2015.05.034.
[24] R.L. Stewart, J. Bridgwater, Y.C. Zhou, A.B. Yu, Simulated and measured ow of granules in a bladed mixer — a detailed comparison, 56 (2001) 5457–5471.
[25] S.C. Thakur, J.P. Morrissey, J. Sun, J.F. Chen, J.Y. Ooi, Micromechanical analysis of cohesive granular materials using the discrete element method with an adhesive elasto-plastic contact model, Granul. Matter. 16 (2014) 383–400. doi:10.1007/s10035-014-0506-4.
[26] Malvern Instruments, Malvern.com, (2015). http://www.malvern.com/en/products/product-range/mastersizer-range/mastersizer-2000/ (accessed April 10, 2015).
[27] M. Leturia, M. Benali, S. Lagarde, I. Ronga, K. Saleh, Characterization of flow properties of cohesive powders: A comparative study of traditional and new testing methods, Powder Technol. 253 (2014) 406–423. doi:10.1016/j.powtec.2013.11.045.
[28] R. Freeman, Measuring the flow properties of consolidated, conditioned and aerated powders - A comparative study using a powder rheometer and a rotational shear cell, Powder Technol. 174 (2007) 25–33. doi:10.1016/j.powtec.2006.10.016.
[29] P.A. Cundall, O.D.L. Strack, A discrete numerical model for granular assemblies, Géotechnique. 29 (1979) 47–65. doi:10.1680/geot.1979.29.1.47.
[30] J. Tomas, Assessment of Mechanical Properties of Cohesive Particulate Solids. Part 1: Particle Contact Constitutive Model, Part. Sci. Technol. 19 (2001) 95–110. doi:10.1080/02726350152772056.
[31] V. Richefeu, M.S. El Youssoufi, R. Peyroux, F. Radjaï, A model of capillary cohesion for numerical simulations of 3D polydisperse granular media, Int. J. Numer. Anal. Methods Geomech. 32 (2008) 1365–1383. doi:10.1002/nag.674.

[32] Y. Muguruma, T. Tanaka, Y. Tsuji, Numerical simulation of particulate flow with liquid bridge between particles (simulation of centrifugal tumbling granulator), Powder Technol. 109 (2000) 49–57. doi:10.1016/S0032-5910(99)00226-0.
[33] F. Soulié, F. Cherblanc, M.S. El Youssoufi, C. Saix, Influence of liquid bridges on the mechanical behaviour of polydisperse granular materials, Int. J. Numer. Anal. Methods Geomech. 30 (2006) 213–228. doi:10.1002/nag.476.
[34] T. Gröger, U. Tüzün, D.M. Heyes, Modelling and measuring of cohesion in wet granular materials, Powder Technol. 133 (2003) 203–215. doi:10.1016/S0032-5910(03)00093-7.
[35] S.C. Thakur, H. Ahmadian, J. Sun, J.Y. Ooi, An experimental and numerical study of packing, compression, and caking behaviour of detergent powders, Particuology. 12 (2014) 2–12. doi:10.1016/j.partic.2013.06.009.
[36] R. Jones, H.M. Pollock, D. Geldart, a. Verlinden, Inter-particle forces in cohesive powders studied by AFM: Effects of relative humidity, particle size and wall adhesion, Powder Technol. 132 (2003) 196–210. doi:10.1016/S0032-5910(03)00072-X.
[37] K.L. Johnson, K. Kendall, A.D. Roberts, Surface Energy and the Contact of Elastic Solids, Proc. R. Soc. A Math. Phys. Eng. Sci. 324 (1971) 301–313. doi:10.1098/rspa.1971.0141.
[38] B.V. Derjaguin, V.M. Muller, Y.P. Toporov, Effect of contact deformations on the adhesion of particles, Prog. Surf. Sci. 45 (1994) 131–143. doi:10.1016/0079-6816(94)90044-2.
[39] J. Härtl, J.Y. Ooi, Numerical investigation of particle shape and particle friction on limiting bulk friction in direct shear tests and comparison with experiments, Powder Technol. 212 (2011) 231–239. doi:10.1016/j.powtec.2011.05.022.
[40] R. Bharadwaj, W.R. Ketterhagen, B.C. Hancock, Discrete element simulation study of a Freeman powder rheometer, Chem. Eng. Sci. 65 (2010) 5747–5756. doi:10.1016/j.ces.2010.04.002.
[41] Y.C. Chung, J.Y. Ooi, Benchmark tests for verifying discrete element modelling codes at particle impact level, Granul. Matter. 13 (2011) 643–656. doi:10.1007/s10035-011-0277-0.
[42] DEM Solutions, EDEM 2.6 Theory Reference Guide, Edinburgh, 2014. http://www.dem-solutions.com/forum/viewtopic.php?f=17&t=653&sid=19b09cd9bcfb2d3c91734e34c2ca128c.
[43] E.Z. Grigoriev, I.S., Meilikhov, Handbook of physical quantities, CRC Press, LLC, 1997.
[44] O. Sullivan, D. Jonathan, Selecting a suitable time step for discrete element simulations that use the central difference time integration scheme, Eng. Comput. 21 (2004) 2–4.
[45] C. González-Montellano, Á. Ramírez, E. Gallego, F. Ayuga, Validation and experimental calibration of 3D discrete element models for the simulation of the discharge flow in silos, Chem. Eng. Sci. 66 (2011) 5116–5126. http://linkinghub.elsevier.com/retrieve/pii/S0009250911004696.
[46] F. Alonso-Marroquín, Á. Ramírez-Gómez, C. González-Montellano, N. Balaam, D.A.H. Hanaor, E.A. Flores-Johnson, Y. Gan, S. Chen, L. Shen, Experimental and numerical determination of mechanical properties of polygonal wood particles and their flow analysis in silos, Granul. Matter. 15 (2013) 811–826. doi:10.1007/s10035-013-0443-7.
[47] M. Marigo, E.H. Stitt, Discrete Element Method (DEM) for Industrial Applications: Comments on Calibration and Validation for the Modelling of Cylindrical Pellets, KONA Powder Part. J. 32 (2015) 236–252. doi:10.14356/kona.2015016.
[48] M.W. Johnstone, Calibration of DEM models for granular materials using bulk physical tests The University of Edinburgh, (2010).
[49] C.J. Coetzee, D.N.J. Els, Calibration of discrete element parameters and the modelling of silo discharge and bucket filling, Comput. Electron. Agric. 65 (2009) 198–212. http://linkinghub.elsevier.com/retrieve/pii/S0168169908002184.
[50] J.P.C. Kleijnen, Design and analysis of simulation experiments, Springer, Verlag, 2008.
[51] J.P. Plackett, R. L., Burman, The Design of Optimum Multifactorial Experiments, Biometrika. 33 (1946) 305–325.
[52] Matlab, version 8.3.0 (R2014a), (2014).
[53] O.R. Walton, Viscosity, granular-temperature, and stress calculations for shearing assemblies of inelastic, frictional disks, J. Rheol. (N. Y. N. Y). 30 (1986) 949. doi:10.1122/1.549893.

[54] WAM Group, A laboratory mixer, (2015). http://pdf.directindustry.com/pdf/wamgroup-spa/laboratory-mixer-mlh-12-brochure/29492-172485.html.
[55] Z. Gu, J.J.J. Chen, A probabilistic analysis of some selected mixing indices, Chem. Eng. Res. Des. 93 (2015) 293–303. doi:10.1016/j.cherd.2014.04.014.
[56] L. Pezo, A. Jovanović, M. Pezo, R. Čolović, B. Lončar, Modified screw conveyor-mixers – Discrete element modeling approach, Adv. Powder Technol. (2015). doi:10.1016/j.apt.2015.07.016.
[57] M. Satoh, T. Yoshida, T. Yanagida, T. Iwasaki, H. Kimura, Evaluation of the mixing process based on a disintegrating rate model of the powder agglomerates, Adv. Powder Technol. 9 (1998) 377–390. doi:10.1016/S0921-8831(08)60567-1.
[58] T. Iwasaki, M. Satoh, Characterization of powder mixers based on mechanical energy using soft dye granules, Adv. Powder Technol. 13 (2002) 395–409. doi:10.1163/156855202320536034.
[59] D. Barling, D. a V Morton, K. Hapgood, Pharmaceutical dry powder blending and scale-up: Maintaining equivalent mixing conditions using a coloured tracer powder, Powder Technol. 270 (2014) 461–469. doi:10.1016/j.powtec.2014.04.069.
[60] Konica-Minolta, Konica-Minolta, (2015). http://www.konicaminolta.eu/en/measuring-instruments/products/colour-measurement/chroma-meters/cr-400-410/introduction.html.
[61] J. Matsuda, Y., Shiromoto, S., Takeda, Y., Hayashi, S.-I., Okada, Mixing of Pharmaceutical Powders examined by Use of Colored Particles: Discussions on Coloration Difference, Chem. Pharm. Bull. 22 (1975) 2803–2811.
[62] C. Labra, J.Y. Ooi, J. Sun, Spatial and temporal coarse-graining for DEM analysis, in: AIP Conf. Proc., 2013: pp. 1258–1261. doi:10.1063/1.4812167.
[63] Particle Analytics, (2016). http://particle-analytics.com/ (accessed June 21, 2016).
[64] I. Goldhirsch, Stress, stress asymmetry and couple stress: From discrete particles to continuous fields, Granul. Matter. 12 (2010) 239–252. doi:10.1007/s10035-010-0181-z.
[65] I. Goldhirsch, Introduction to granular temperature, Powder Technol. 182 (2008) 130–136. doi:10.1016/j.powtec.2007.12.002.
[66] J.M. Ottino, D. V Khakhar, Mixing and segregation of granular materials, Annu. Rev. Fluid Mech. 32 (2000) 55–91.
[67] B. Remy, J.G. Khinast, B.J. Glasser, Discrete element simulation of free flowing grains in a four-bladed mixer, AIChE J. 55 (2009) 2035–2048. doi:10.1002/aic.11876.
[68] B. Remy, J.G. Khinast, B.J. Glasser, Polydisperse granular flows in a bladed mixer: Experiments and simulations of cohesionless spheres, Chem. Eng. Sci. 66 (2011) 1811–1824. doi:10.1016/j.ces.2010.12.022.

Figure captions

Figure 1 Scanning Electron Microscopy image of a virgin zeolite powder sample at x3000 magnification.

Figure 2 Bulk density as a function of moisture content for all zeolite powders. The error bars correspond to the coefficient of variation of the measurements. The dashed line represents the trend for the pink samples as explained in the main text.

Figure 3 FT4 Powder rheometer BFE test measurements: Total Flow Energy vs. Blade Tip Speed.

Figure 4 Normal contact force – normal overlap relationship of the elasto-plastic frictional adhesive contact model [25].

Figure 5 Size and shape of the DEM particles used in the simulations.

Figure 6 DEM simulation of the FT4 powder rheometer (cut through centre of the blade).

Tables

Table 1 Particle size distribution of zeolite 4A powder

D10 (µm)	D50 (µm)	D90 (µm)	Dispersal	Ultrasonication power	Relative Error
1.7	3.5	6.2	Wet	85 %	2 %
2	4.1	7.3	Wet	0 %	2 %
1.1	2.9	5.5	Dry	2 %	2 %

Table 2 Moisture content and bulk density measurements of the zeolite powders. The values correspond to the arithmetic average of the measurements for each material.

Notation	Moisture Content (%)	Bulk Density (kg/m3)
P_32	32.4	612
P_19	19.2	489
P_14	13.7	455
P_5	4.5	566
B_30	30.2	530
W_6	6.3	380

Table 3 Shear moduli, Poisson's ratios and solid densities used in the simulations.

Zeolite			
Poisson ratio	v	0.25	
Shear modulus	G	5.00E+06	Pa
Solid density	ρ	Variable	kg/m3
Stainless steel			
Poisson ratio	v	0.3	
Shear modulus	G	7.30E+10	Pa
Solid density	ρ	7800	kg/m3
Borosilicate glass			
Poisson ratio	v	0.3	
Shear modulus	G	2.40E+07	Pa
Solid density	ρ	2500	kg/m3

Table 4 Values of the DEM contact model parameters explored in the optimization phase.

a)

DoE Parameters	Notation	Low	High
Restitution coefficient	e	0.2	0.6
Particle-Particle Static Friction	μ_{sp-p}	0.1	0.7
Particle - Cylinder Relative Static Friction	$\chi = \mu_{sp-g}/\mu_{sp-p}$	0.1	1
Particle - Blade Relative Static Friction	$\psi = \mu_{sp-b}/\mu_{sp-p}$	0.1	1
Const. Pull-off force (N)	f_0	-1E-2	-1E-05
Surface Energy (J/m2)	$\Delta\gamma$	0.01	5
Particle solid density (kg/m3)	ρ_s	600	1400

b)

Linear Response Model Optimization							
Notation	**ρ_s**	**μ_{sp-p}**	**χ**	**ψ**	***f_0***	**$\Delta\gamma$**	**e**
W_6 LM	600	0.24	0.08	0.11	-0.0045	2.68	0.35
P_5 LM	600	0.35	0.17	0.19	-0.005	2.56	0.39
B_30 LM	1400	0.7	0.7	0.7	-0.008	1.4	0.6
P_32 LM	1400	0.7	0.7	0.7	-0.01	0.01	0.6

c)

Further Optimization							
Notation	**ρ_s**	**μ_{sp-p}**	**χ**	**Ψ**	***f_0***	**$\Delta\gamma$**	**e**
W_6 FO	600	0.3	0.3	0.4	-1.0E-05	0.01	0.4
P_5 FO	600	0.69	0.69	0.25	-0.0005	2.06	0.27
B_30 FO	1300	0.7	0.7	0.7	-0.0005	4.5	0.6
P_32 FO	1600	0.7	0.7	0.7	-0.0005	5	0.6

Table 5 DEM input parameters with fixed values.

Assumed Parameters	Notation	Value
Contact plasticity	λ	0.9
Loading and Unloading/Reloading exponent	n	1.5
Adhesion exponent	x	5
Tangential Stiffness Multiplier	K_{tm}	0.286
Particle Poisson Ratio	ν	0.25
Particle Shear Modulus (GPa)	G	5.00E+06
Coefficient of rolling friction	μ_r	0.01

Table 6 Material type and shaft rotational velocity configurations for the simulations and the experiments.

Notation	Materials	Shaft Rotational Velocity
Wet 110 RPM	P_32 – B_30	110 RPM
Dry 110 RPM	P_5 – W_6	110 RPM

Figure 1

Click here to download high resolution image

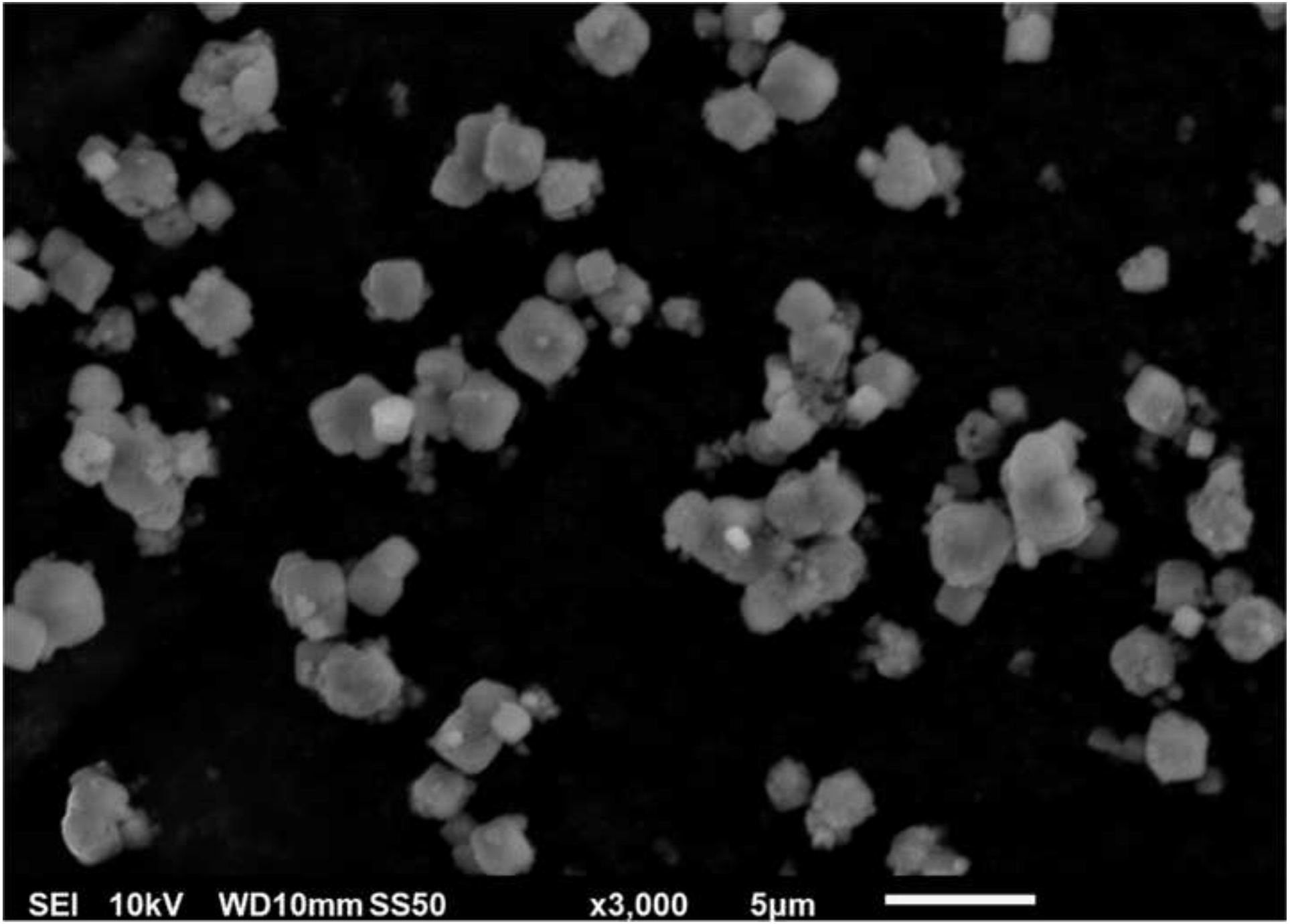

Figure 2

Click here to download high resolution image

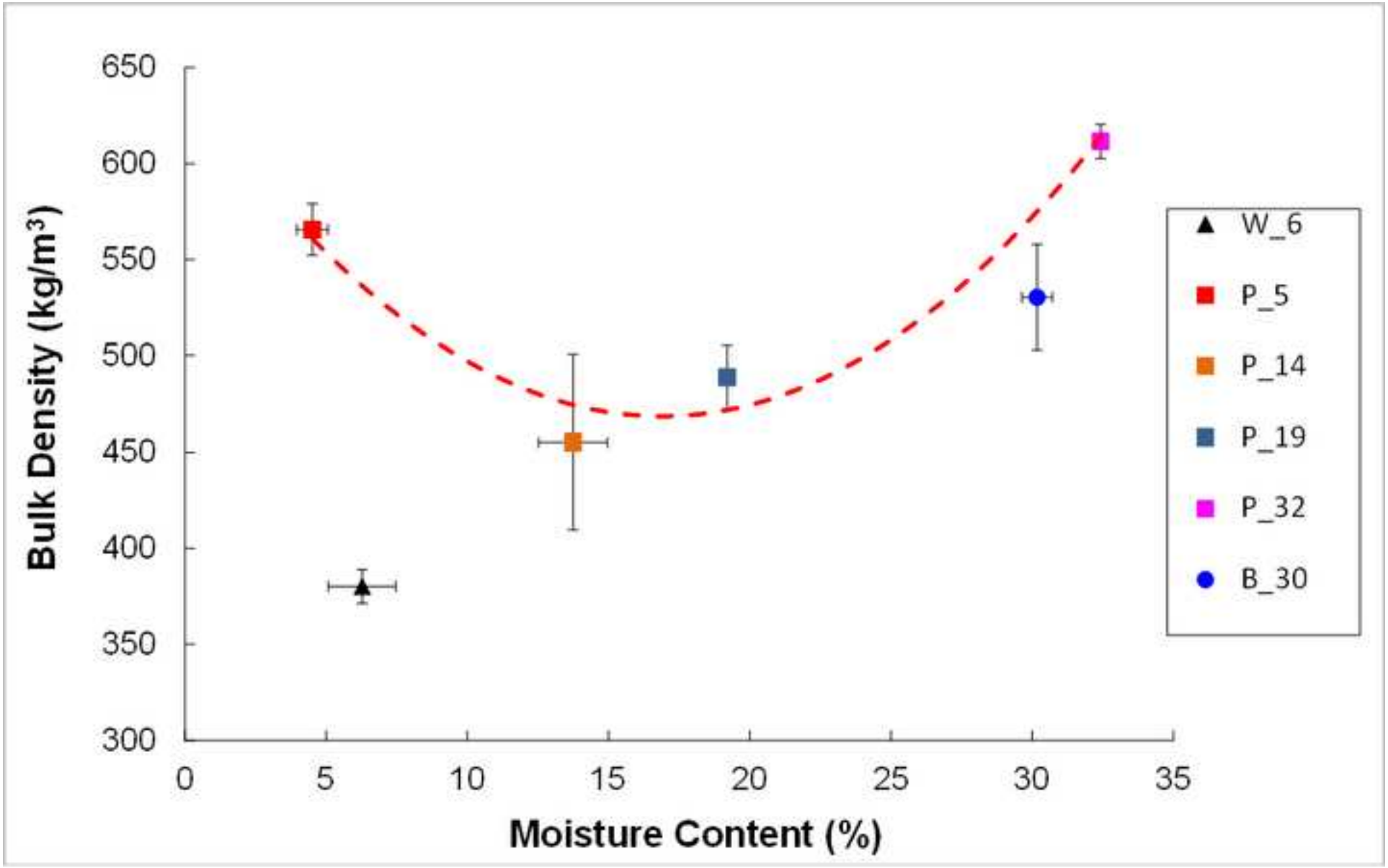

Figure 3

Click here to download high resolution image

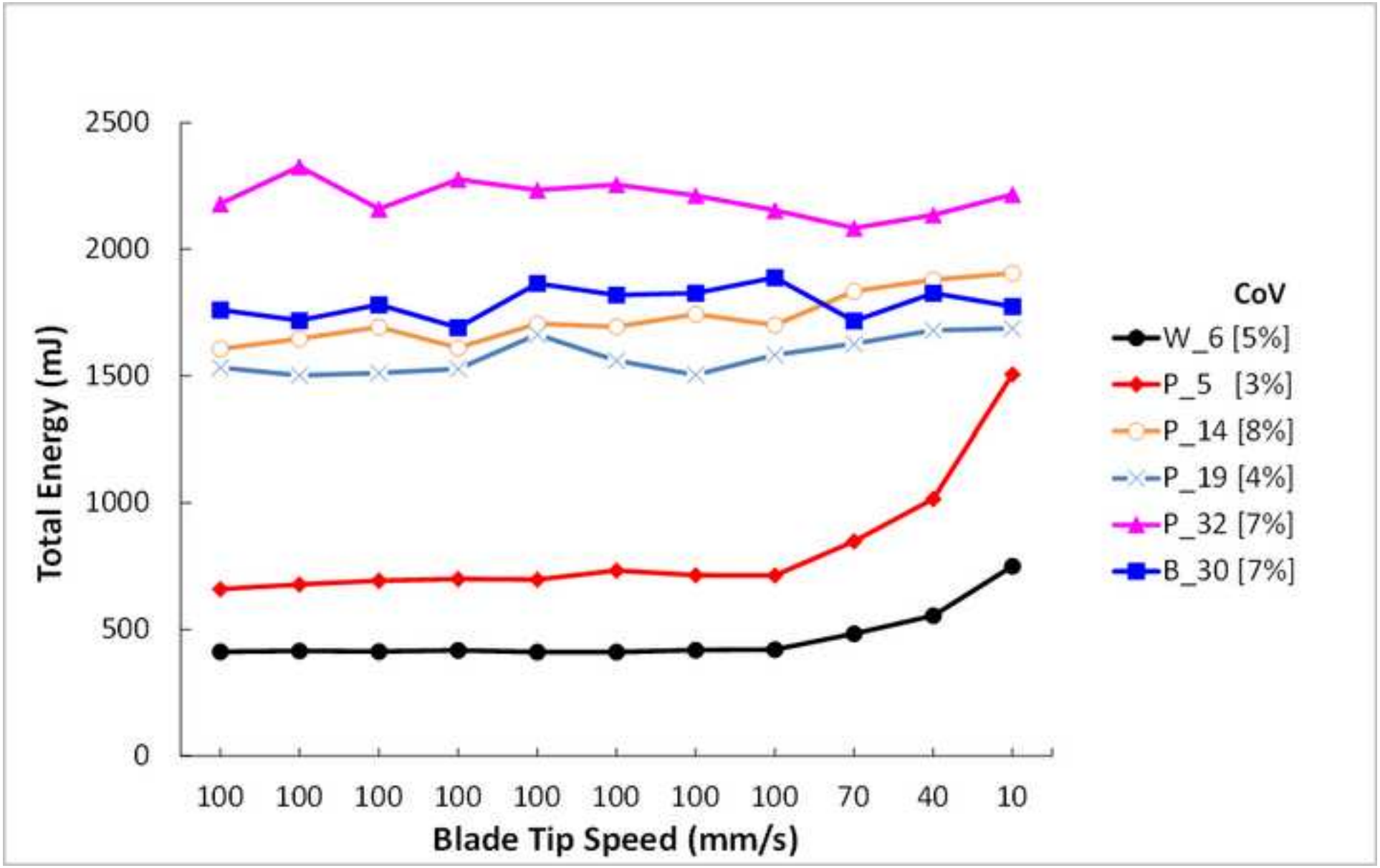

Figure 4

Click here to download high resolution image

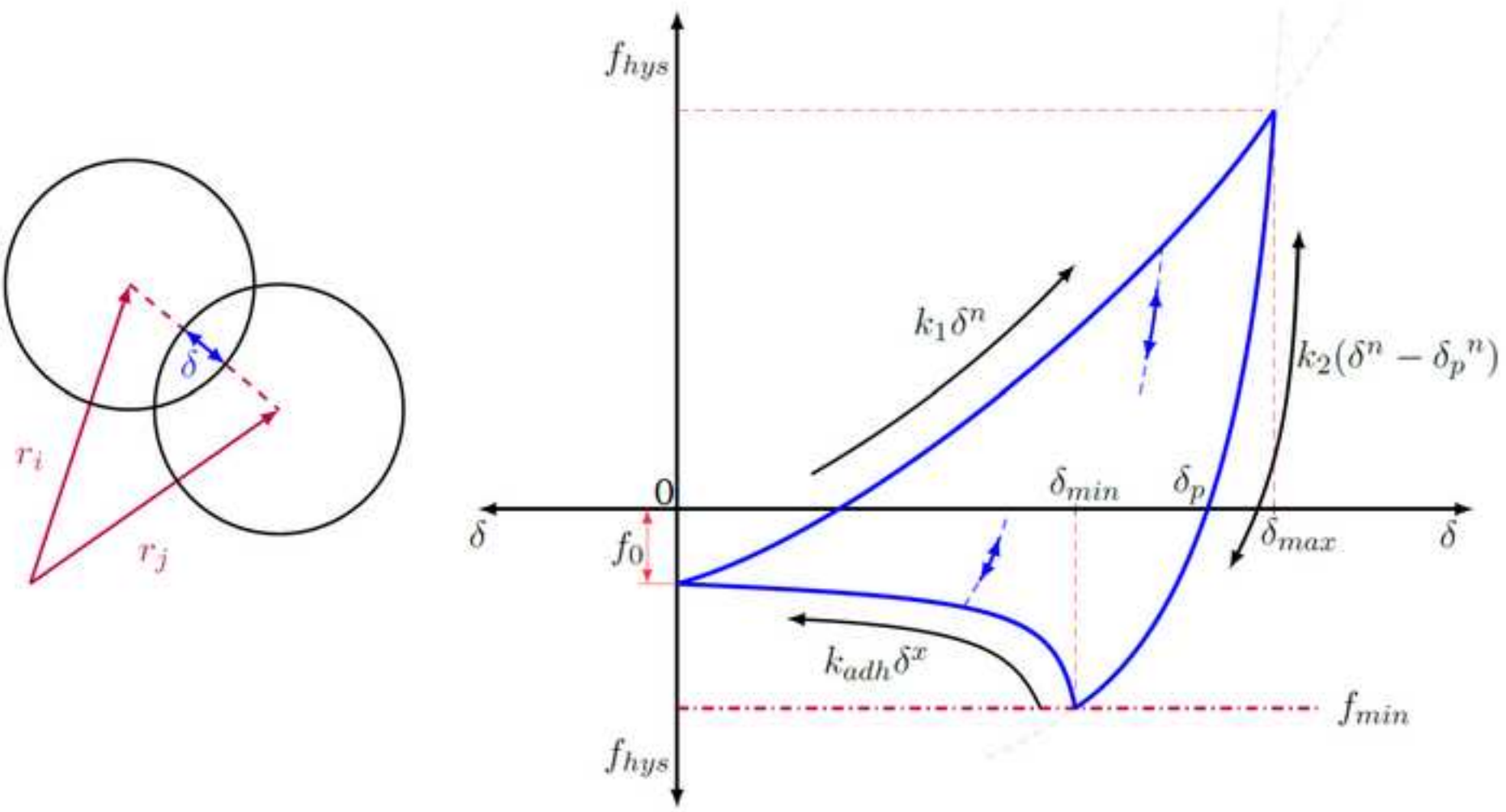

Figure 5

Click here to download high resolution image

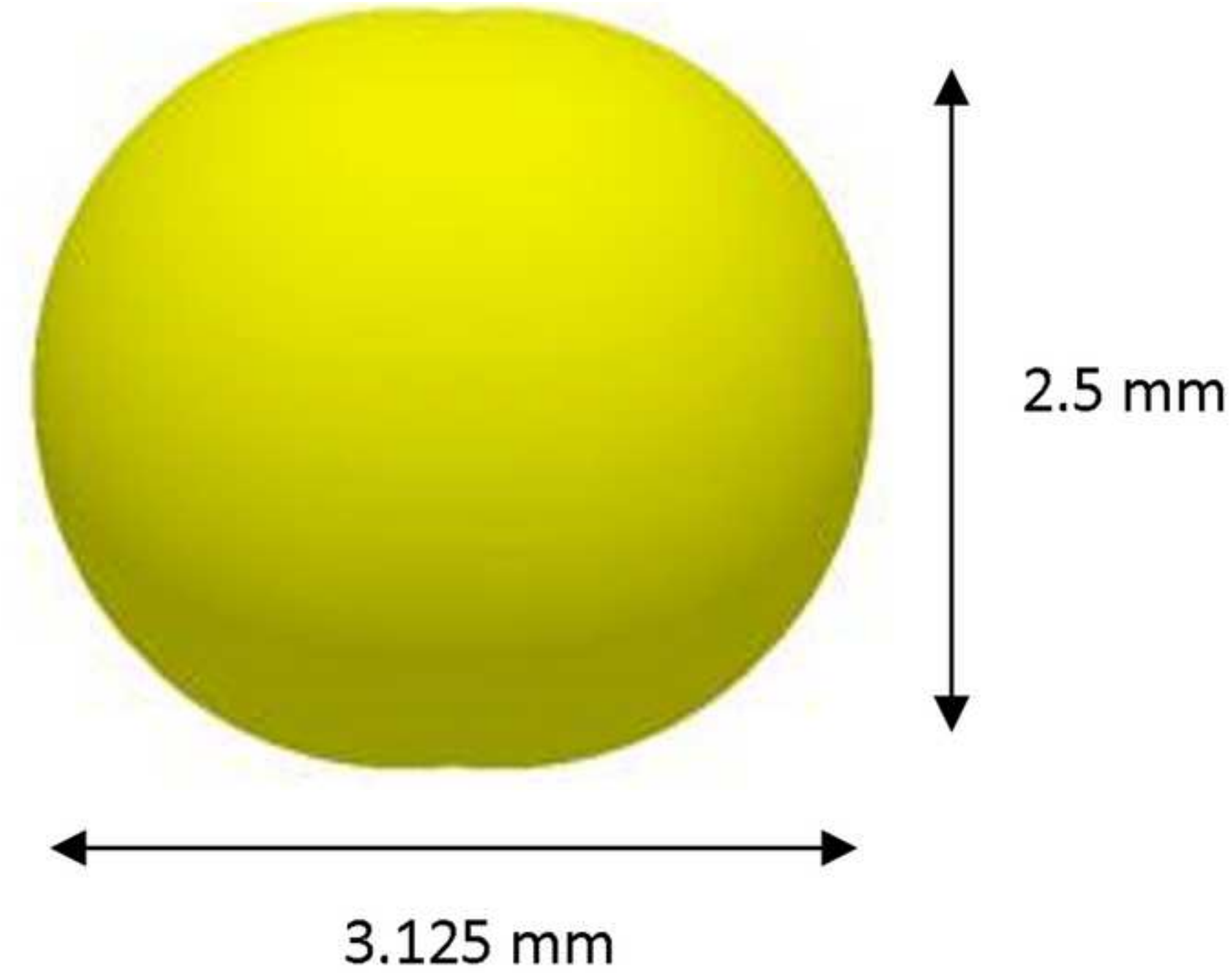

Figure 6

Click here to download high resolution image

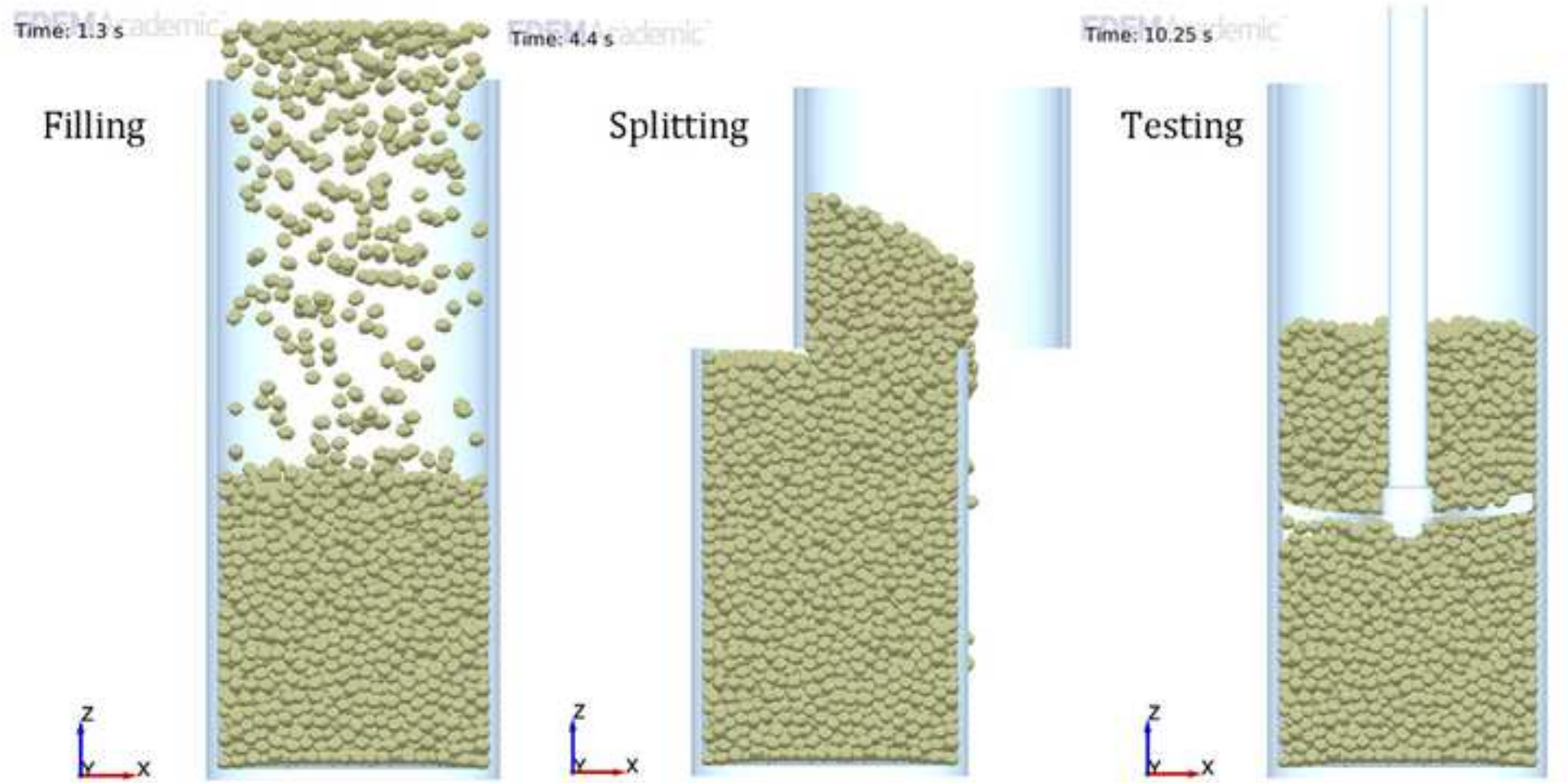

Figure 7

Click here to download high resolution image

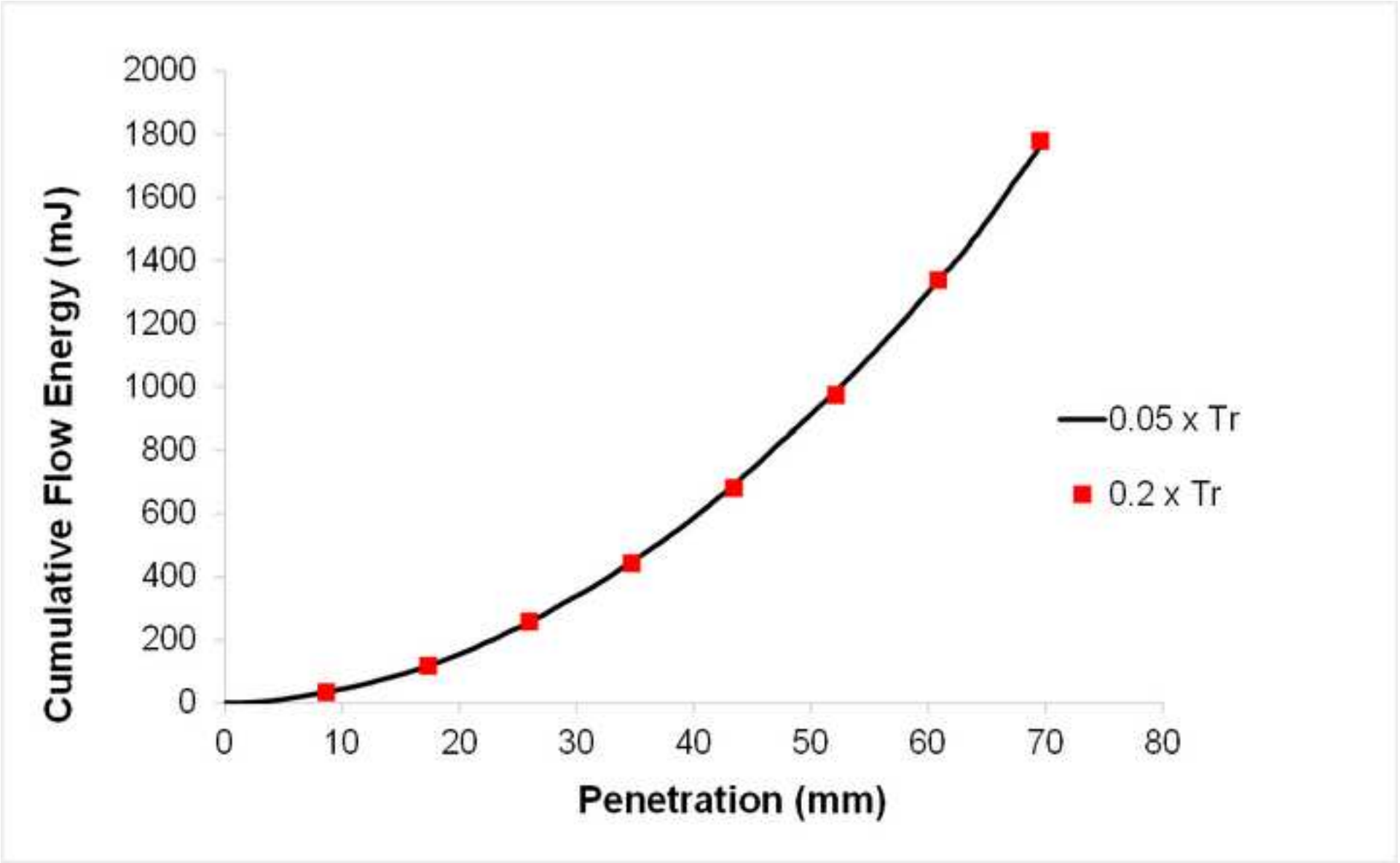

Figure 8

Click here to download high resolution image

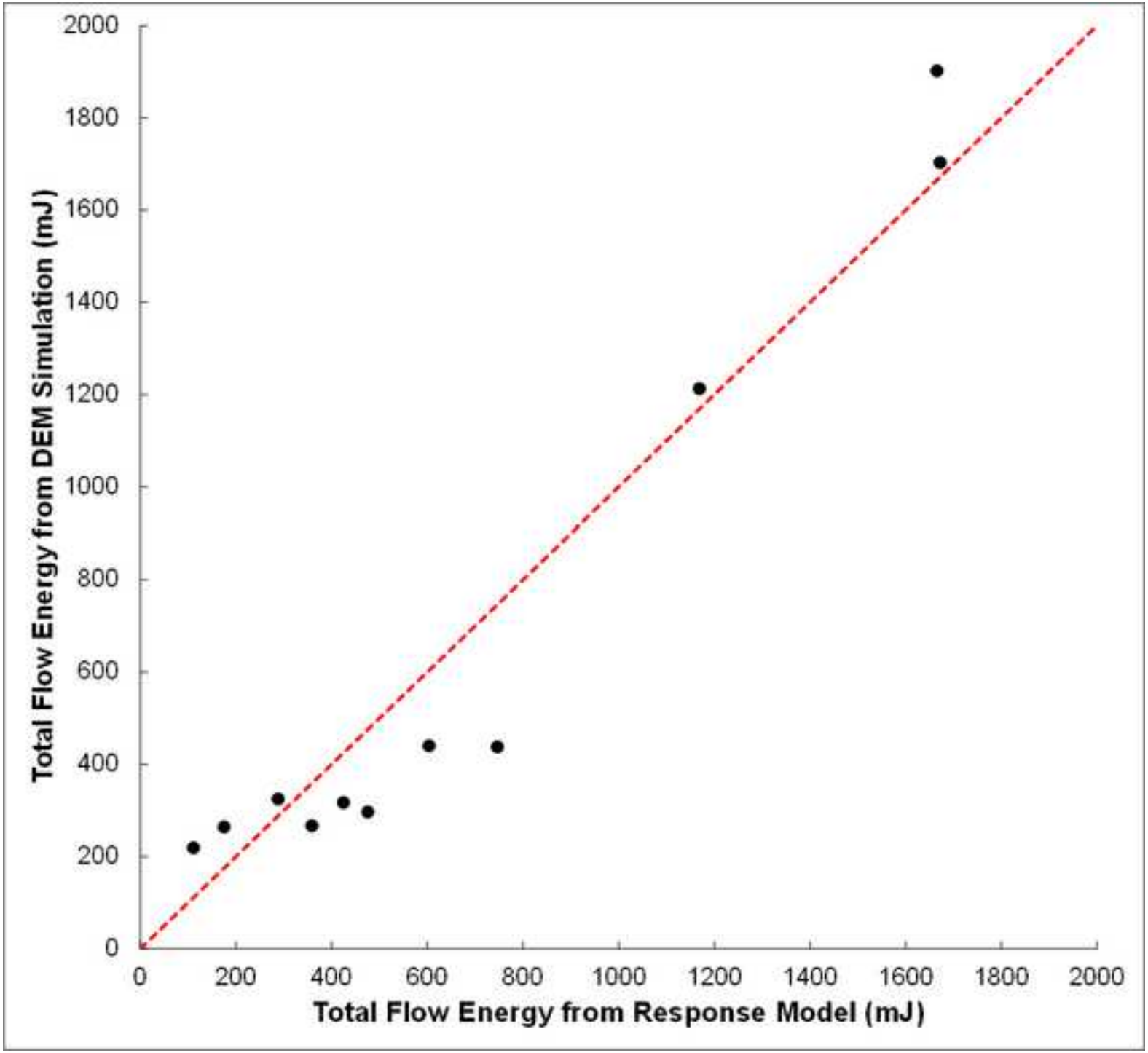

Figure 9

Click here to download high resolution image

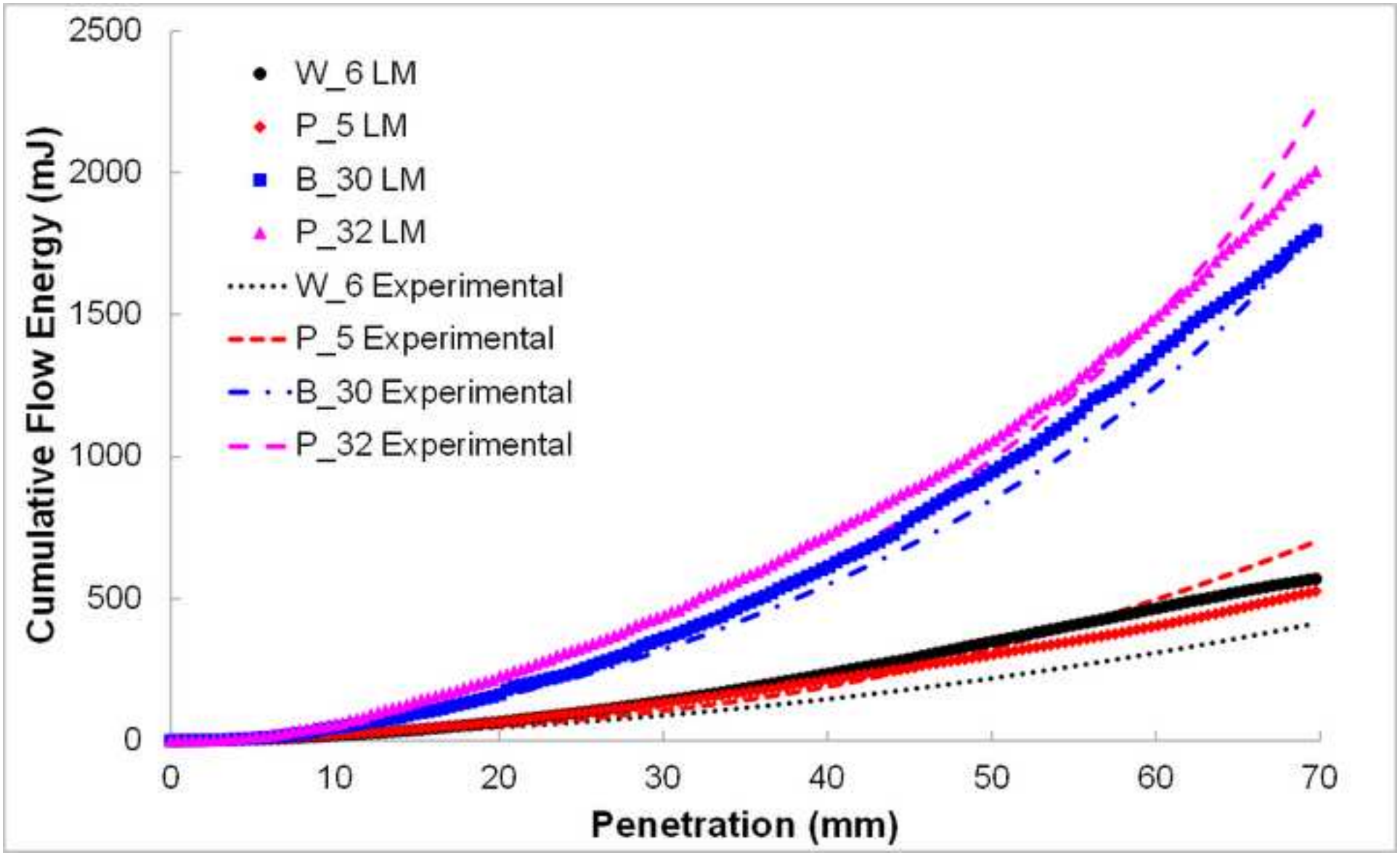

Figure 10

Click here to download high resolution image

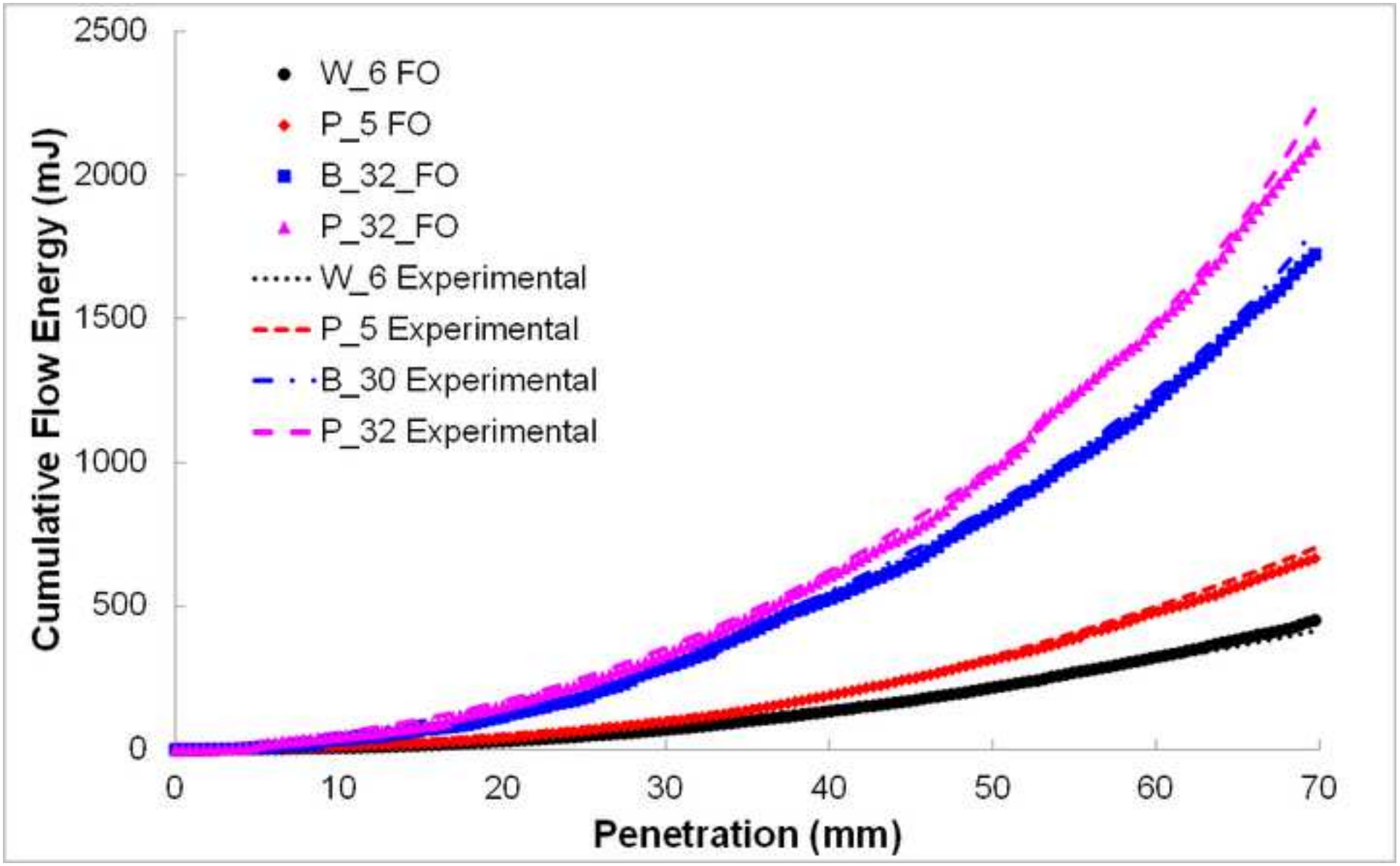

Figure 11
Click here to download high resolution image

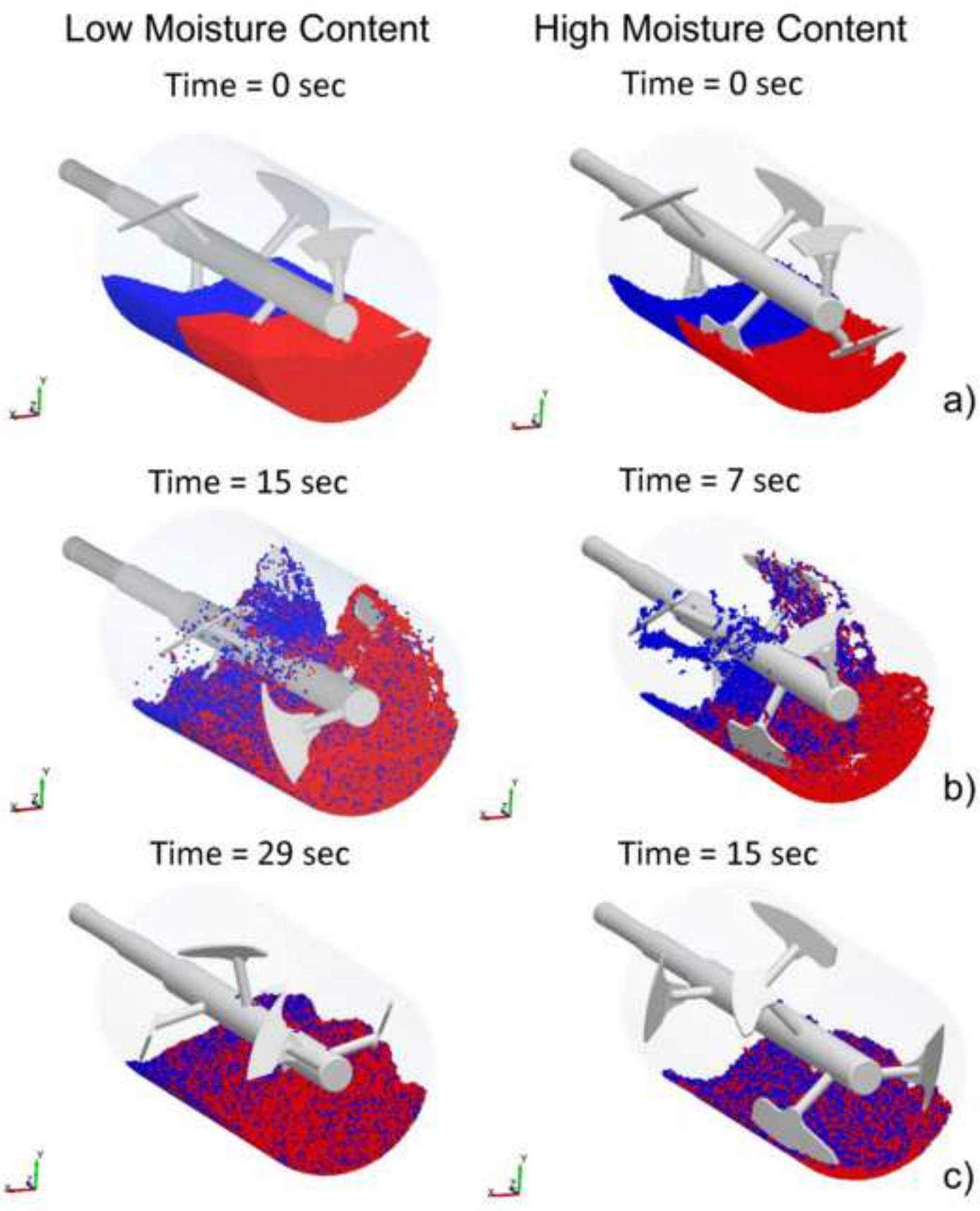

Figure 12

Click here to download high resolution image

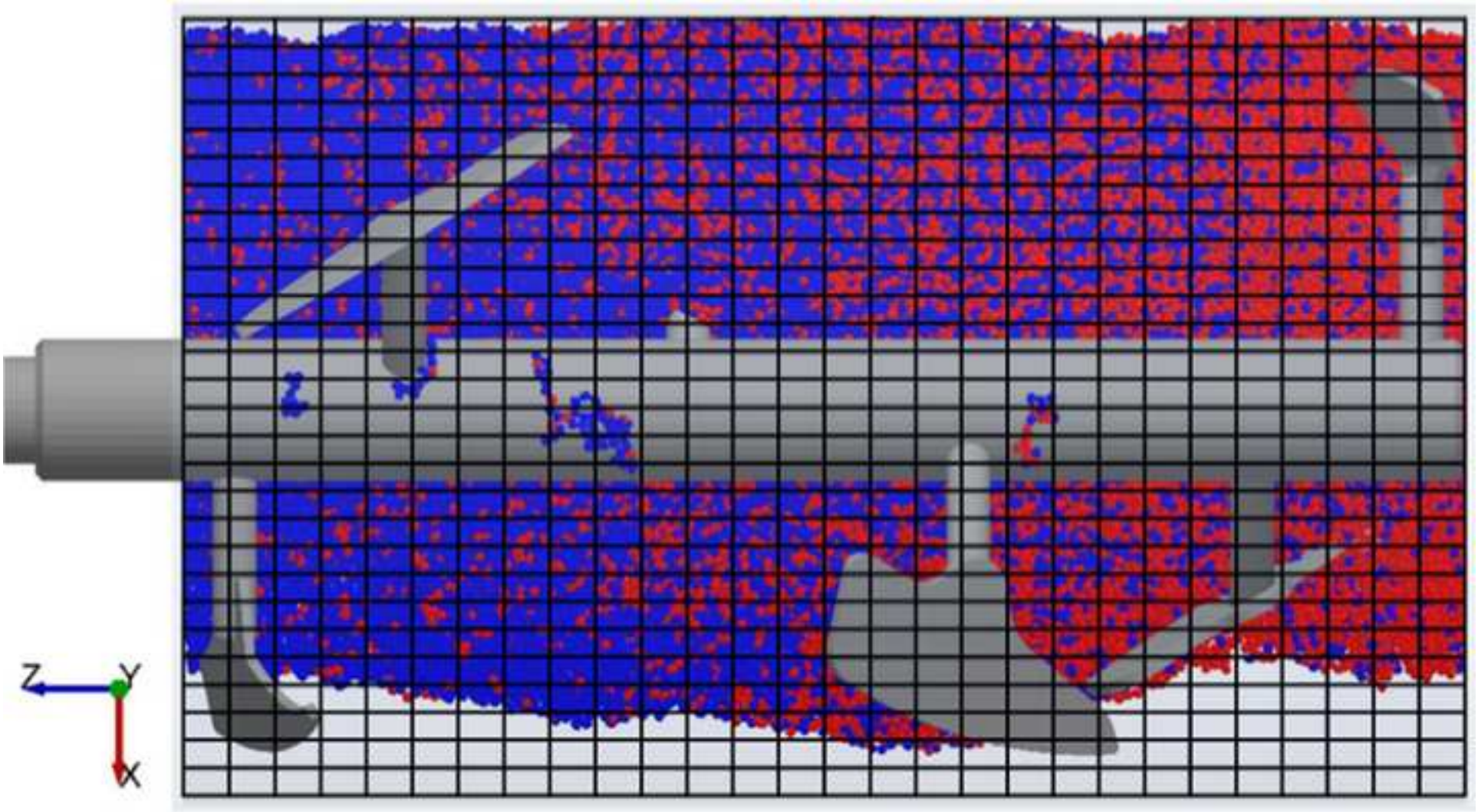

Figure 13

Click here to download high resolution image

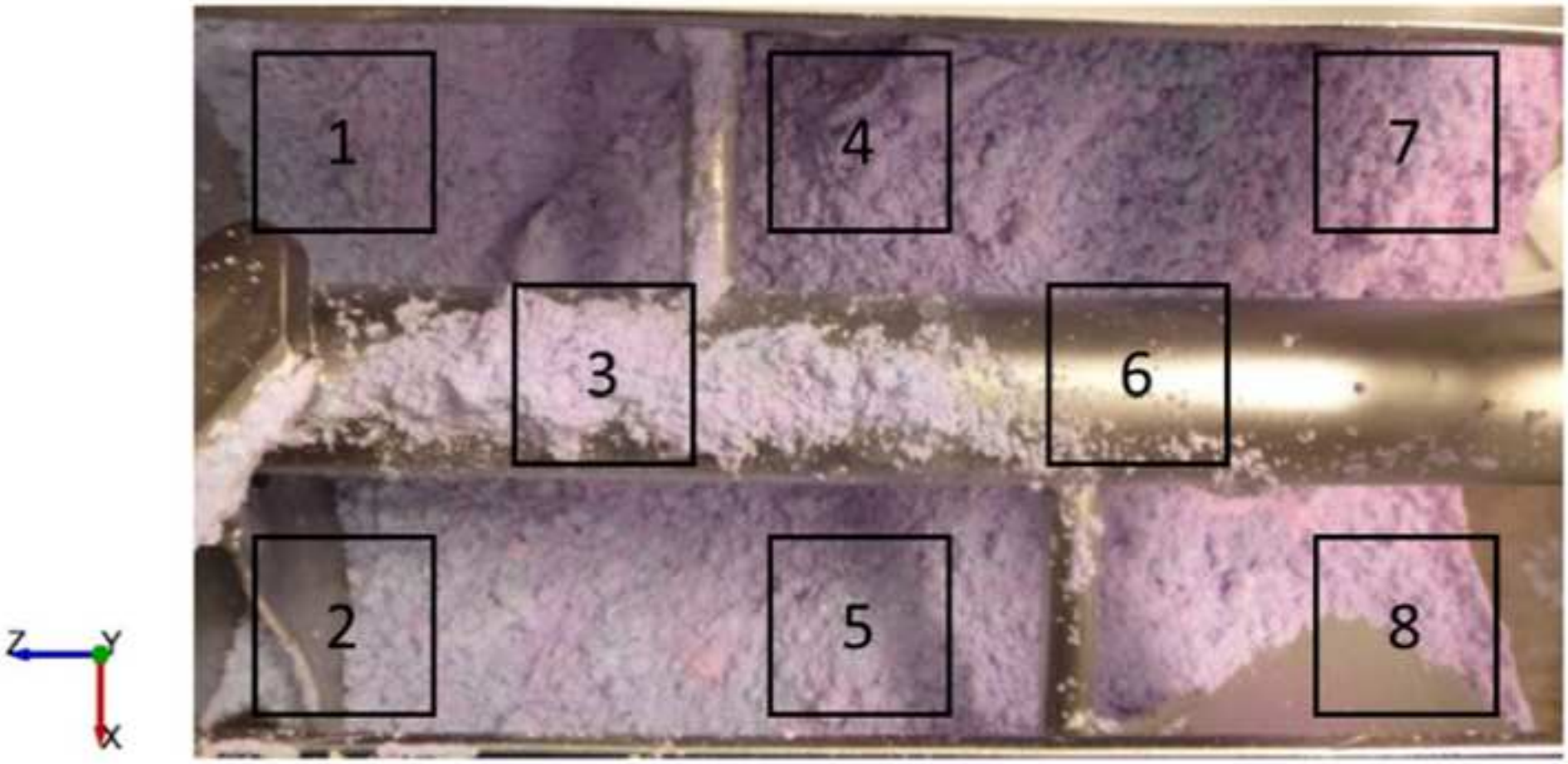

Figure 14

Click here to download high resolution image

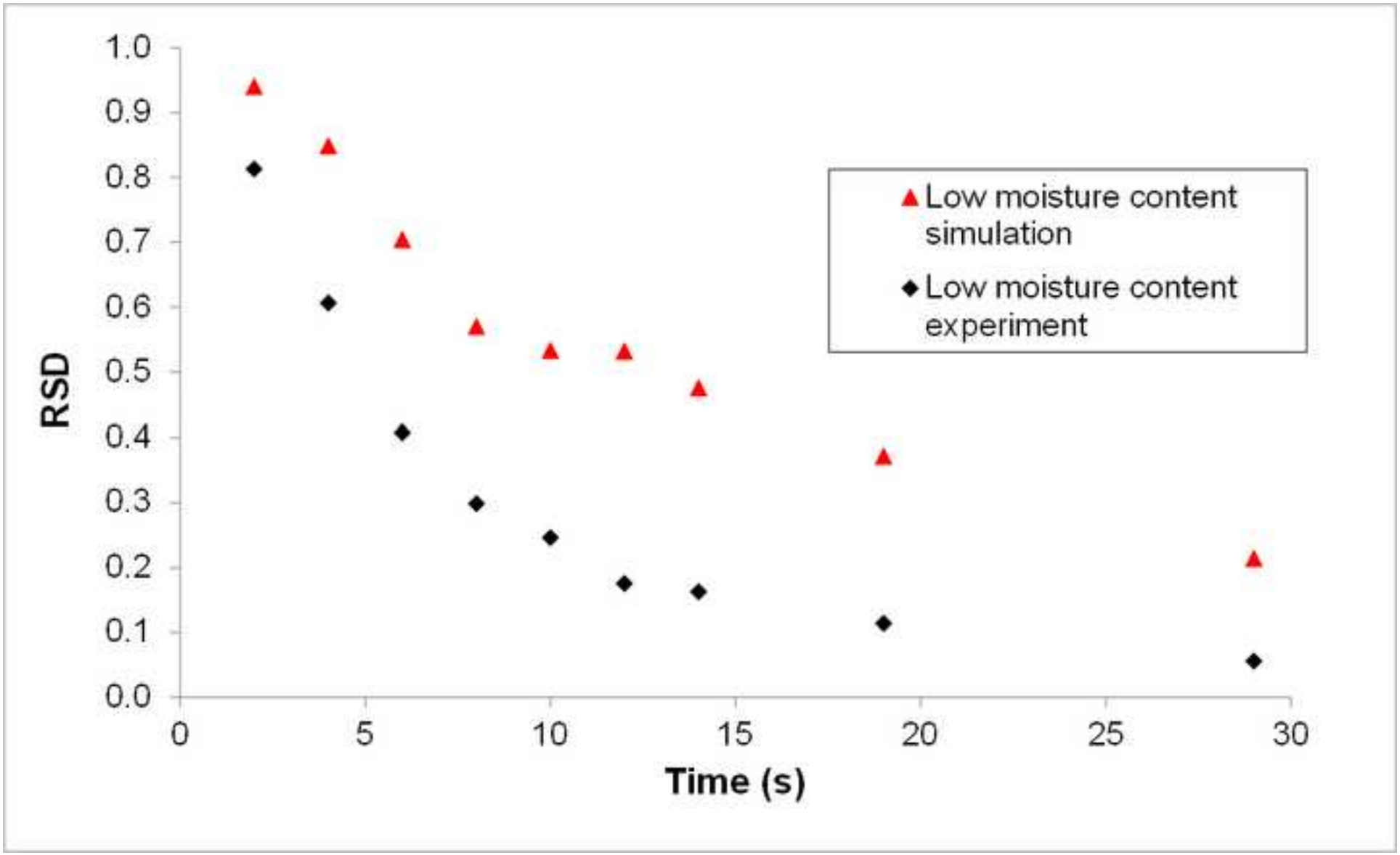

Figure 15

Click here to download high resolution image

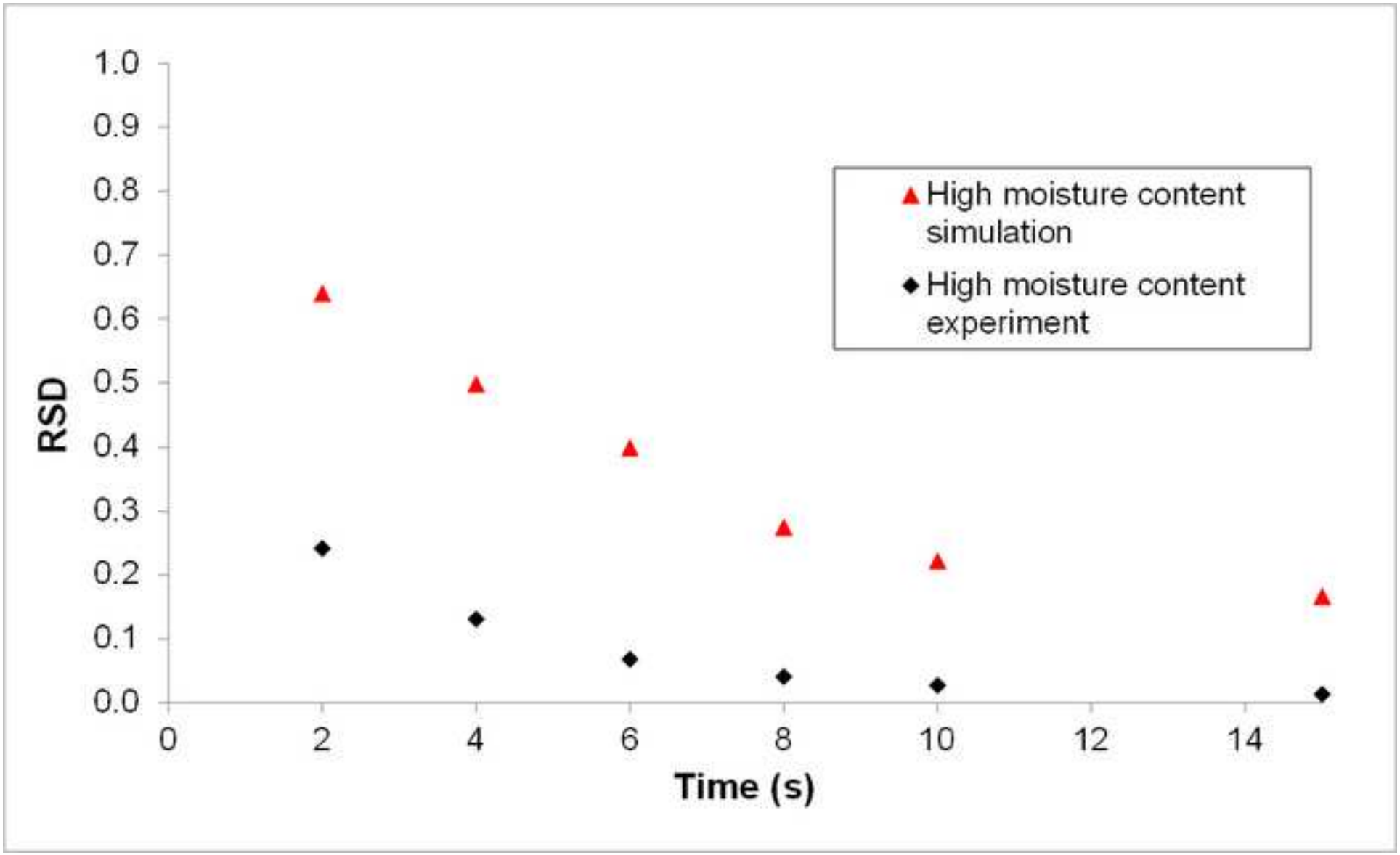

Figure 16

Click here to download high resolution image

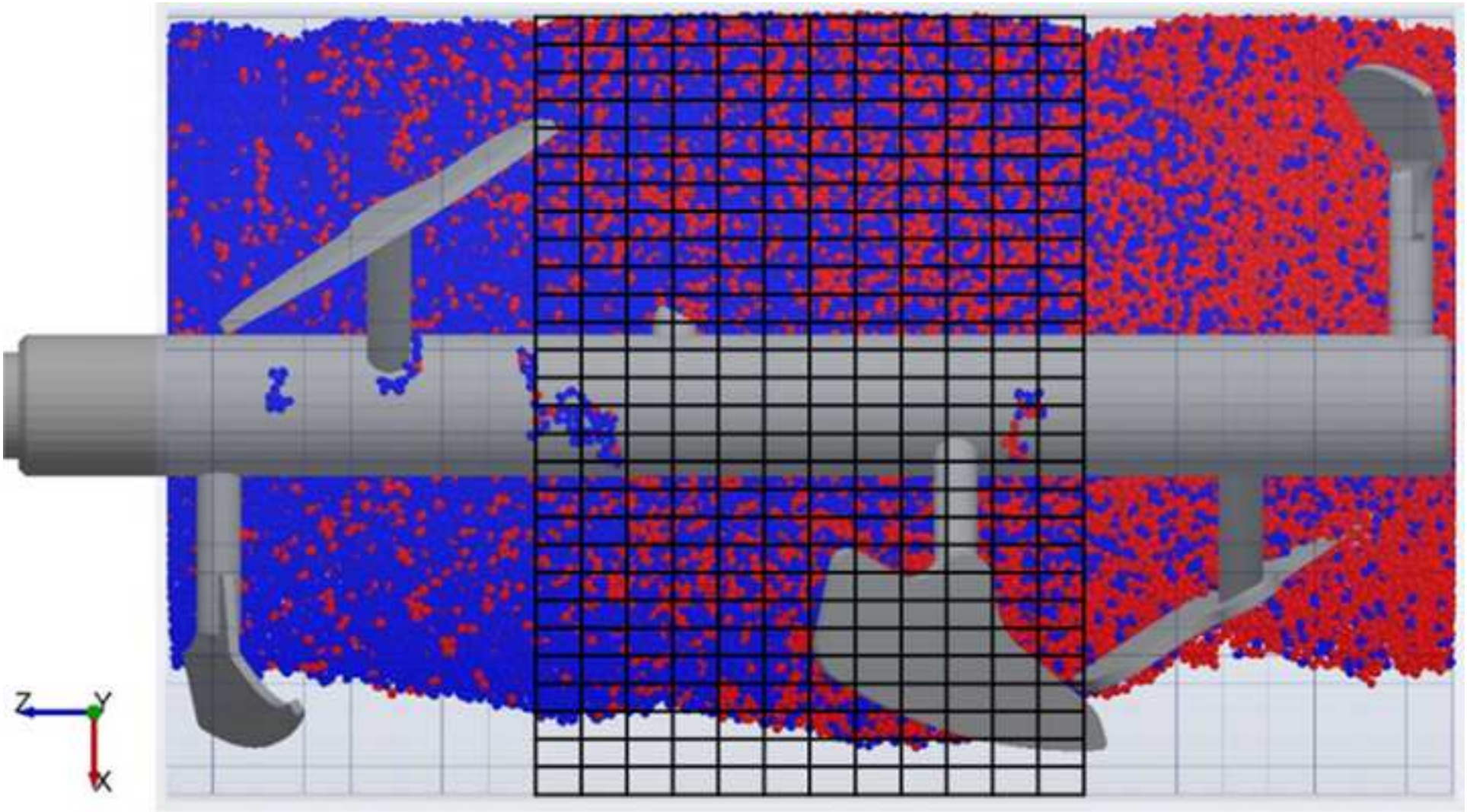

Figure 17
Click here to download high resolution image

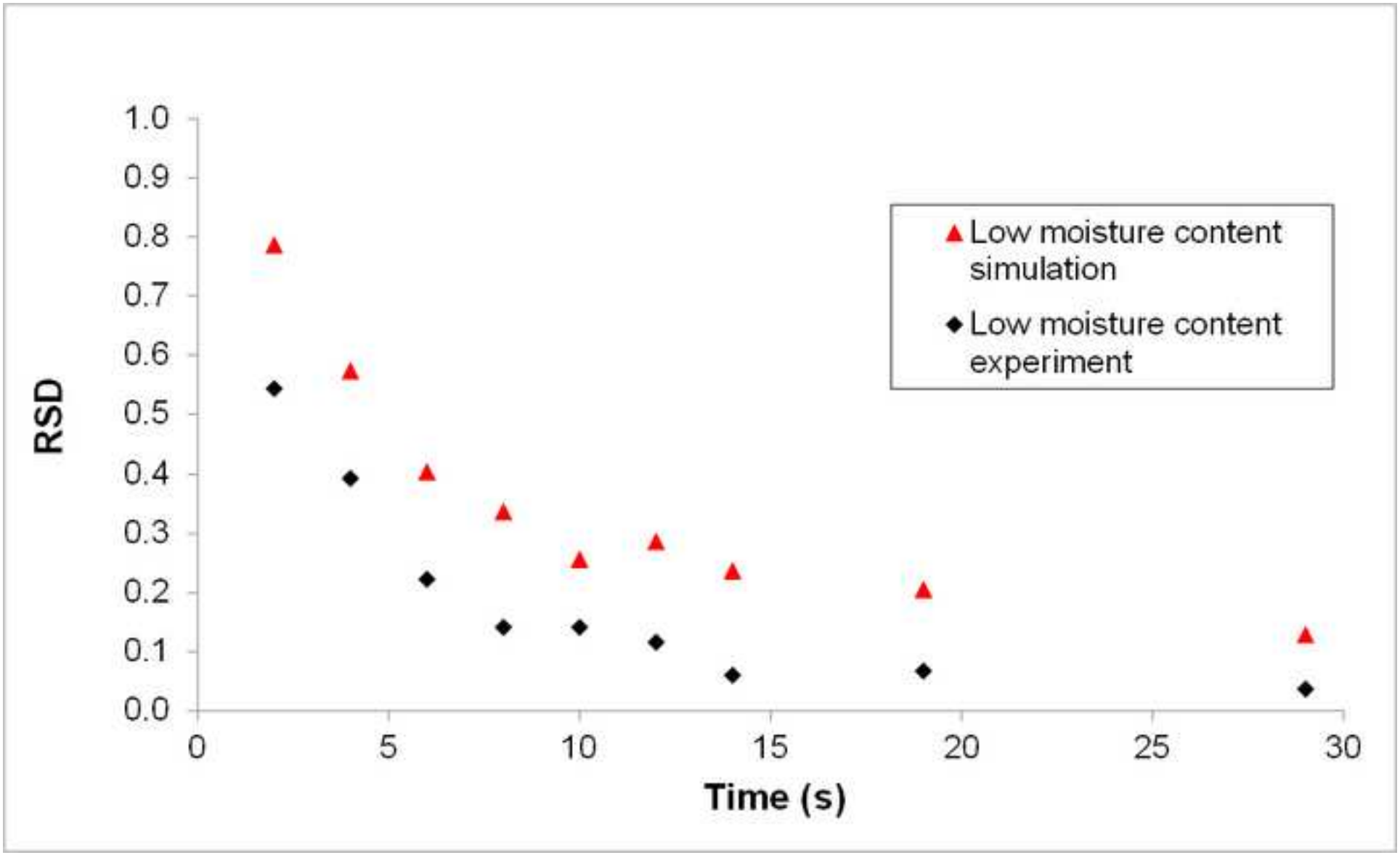

Figure 18

Click here to download high resolution image

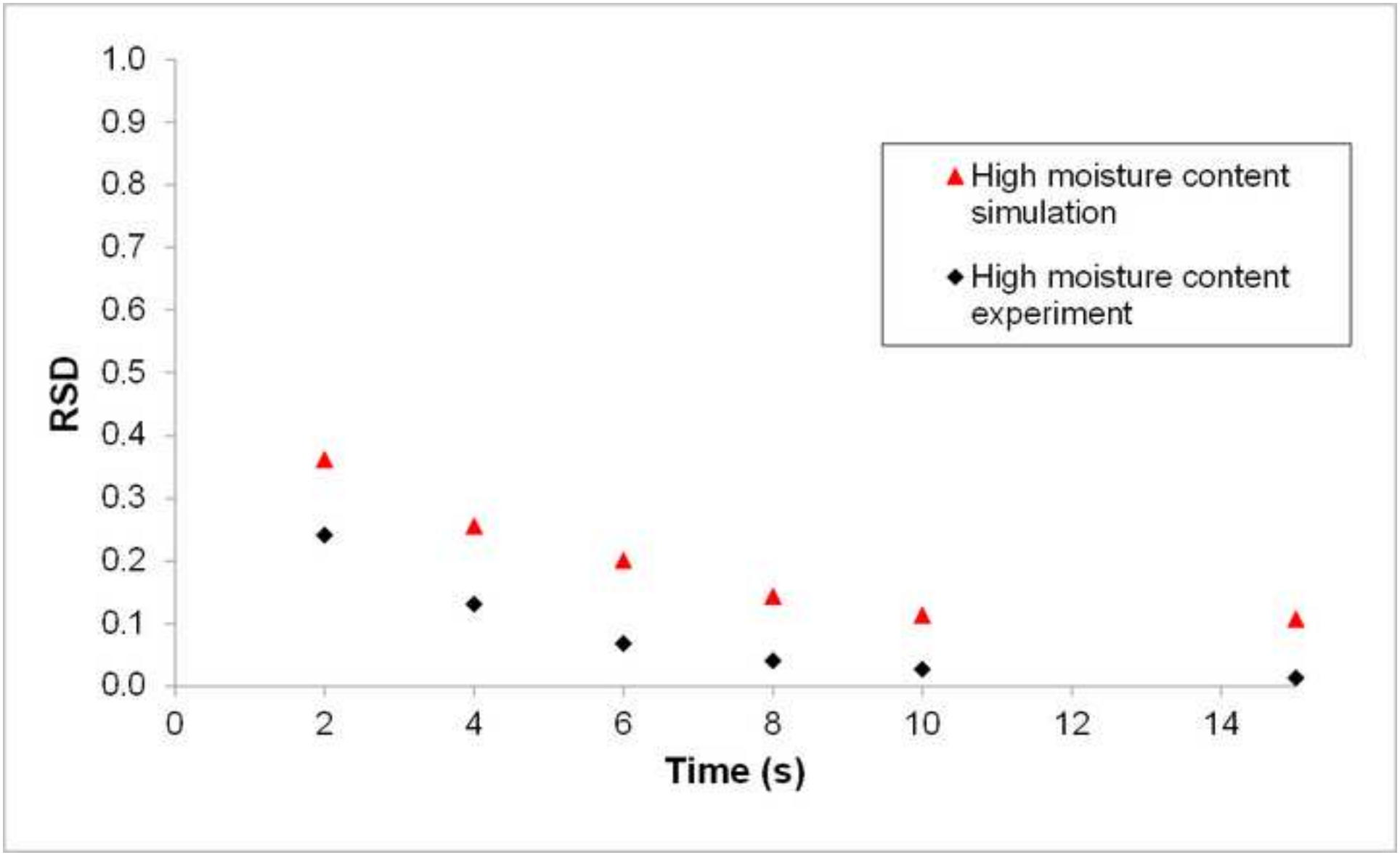

Figure 19

Click here to download high resolution image

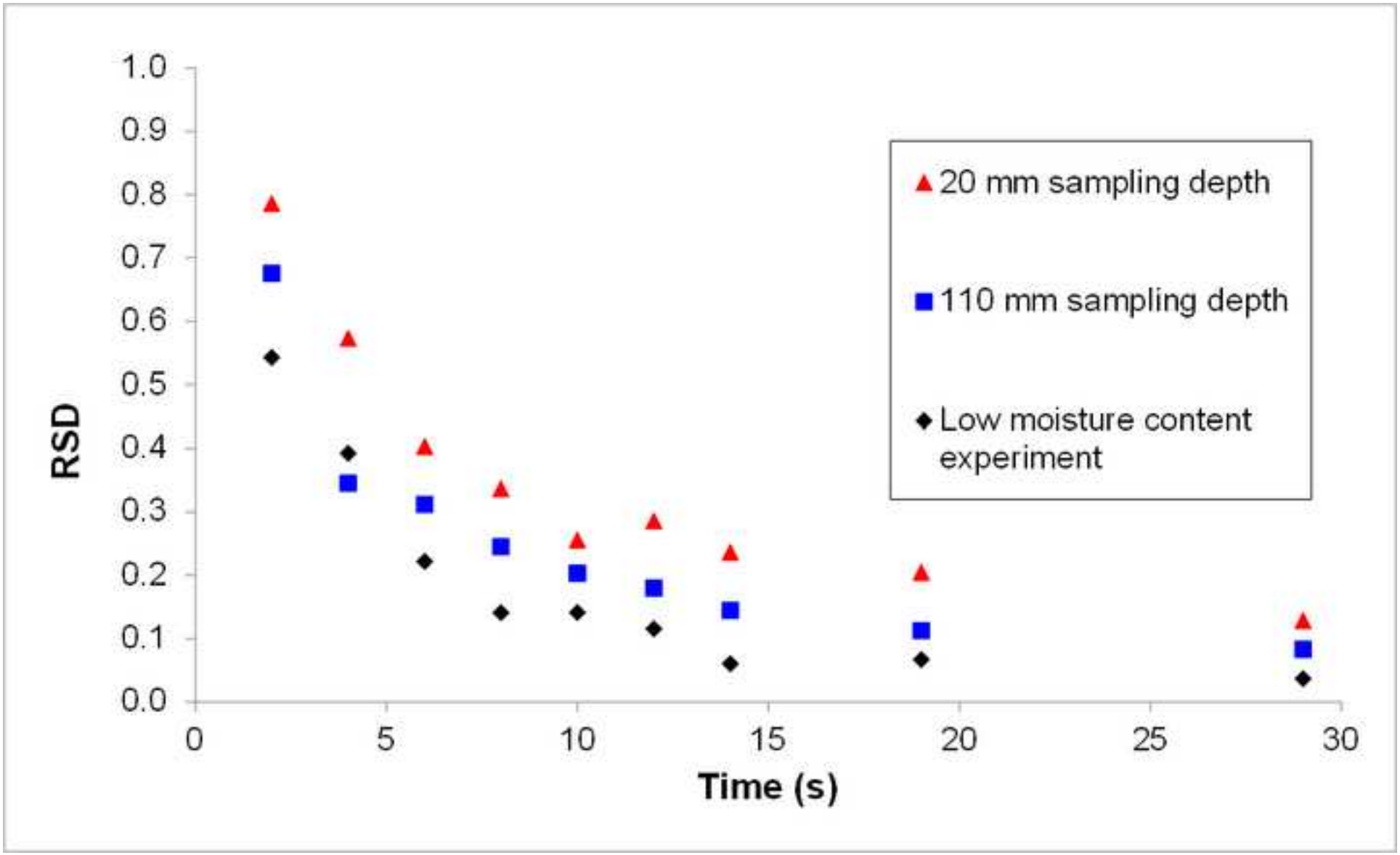

Figure 20
Click here to download high resolution image

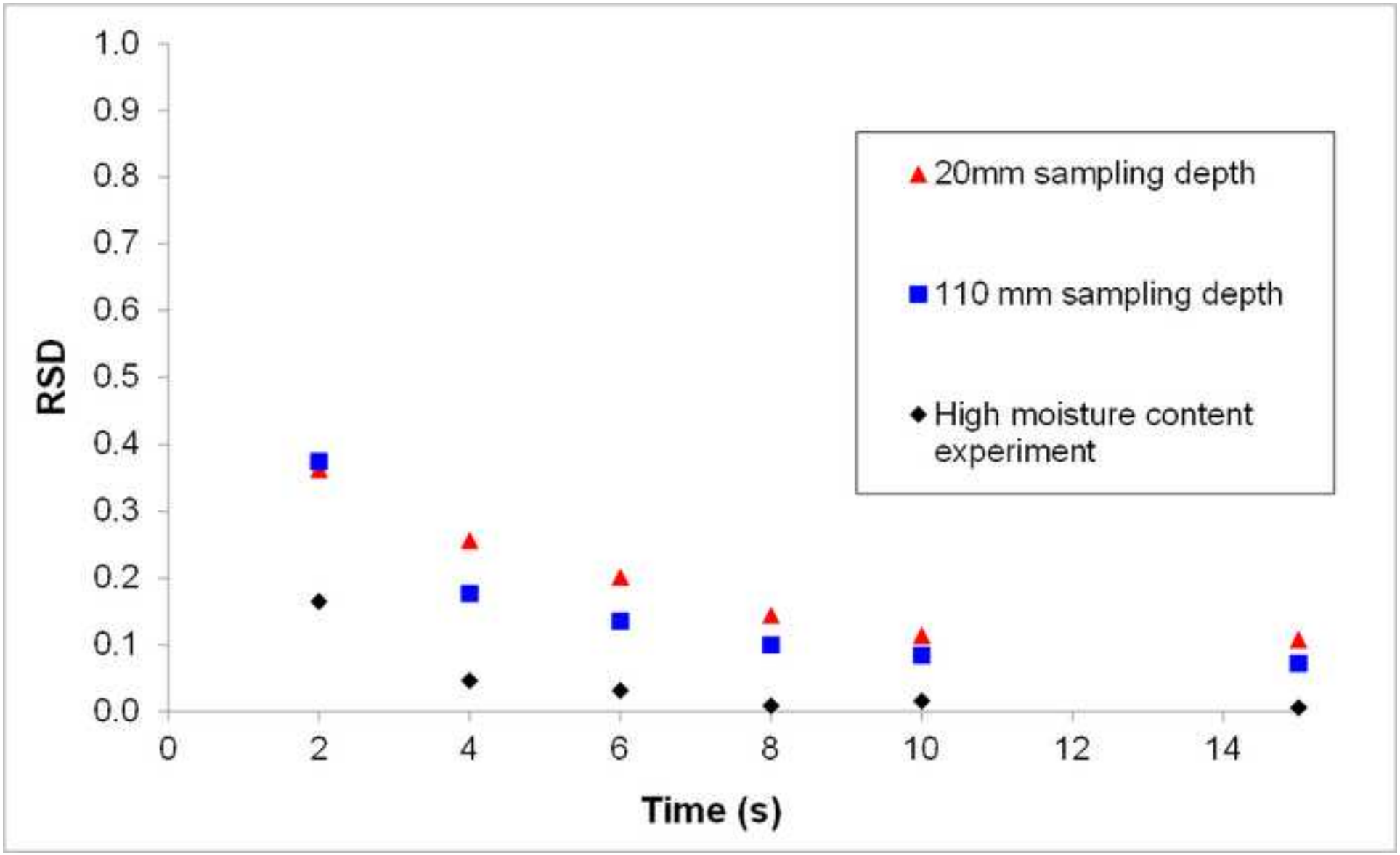

Figure 21
Click here to download high resolution image

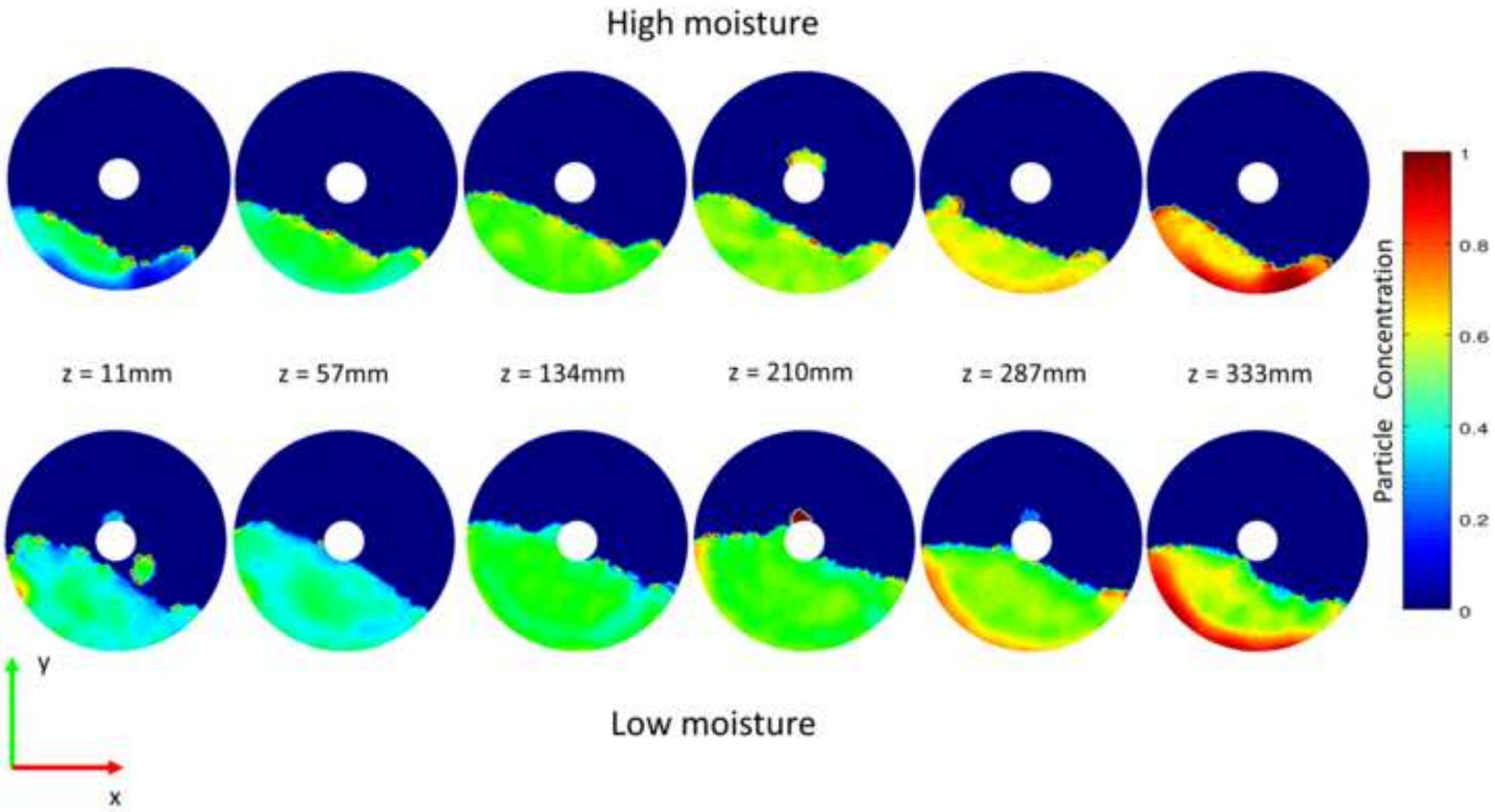

Figure 22

Click here to download high resolution image

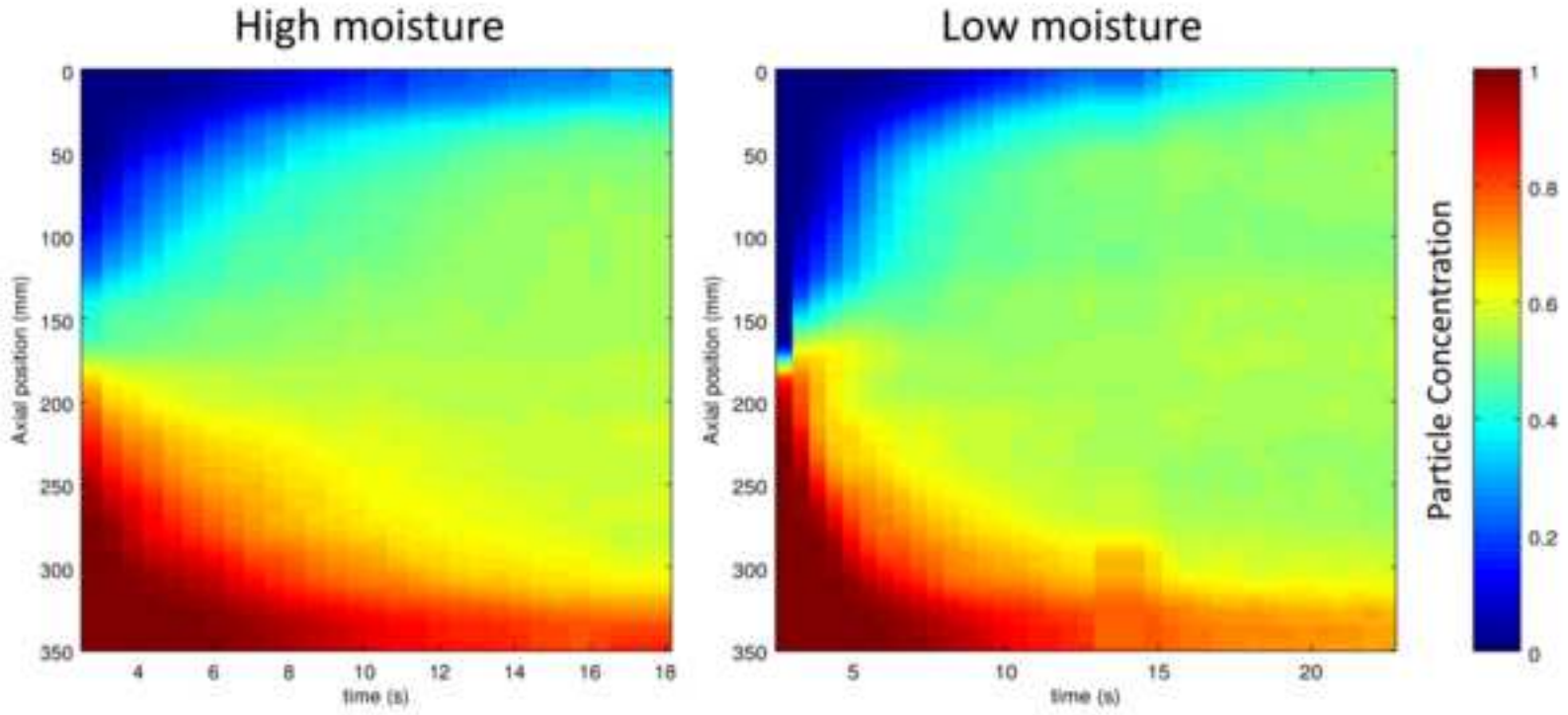

Figure 23
Click here to download high resolution image

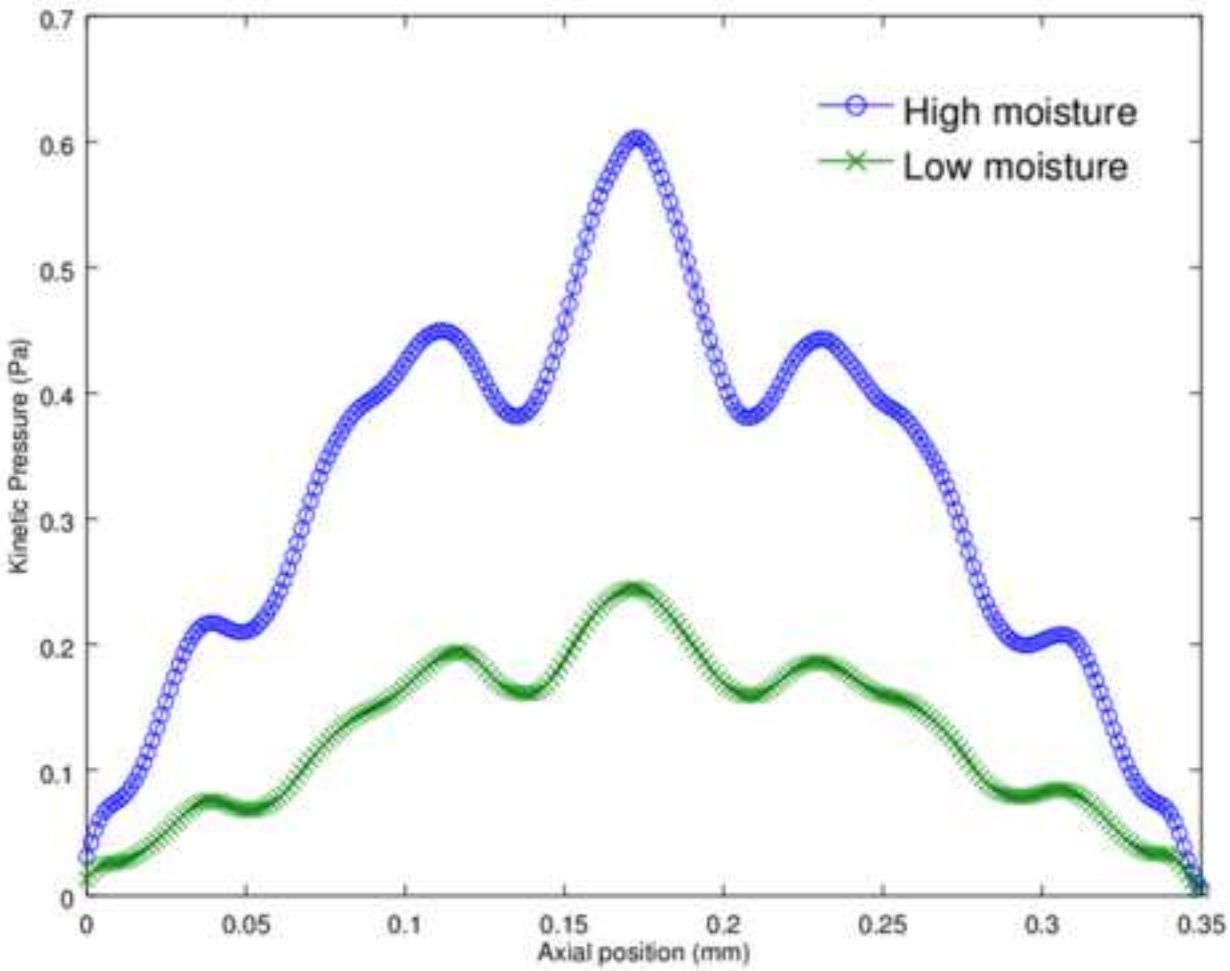

Figure 24

Click here to download high resolution image

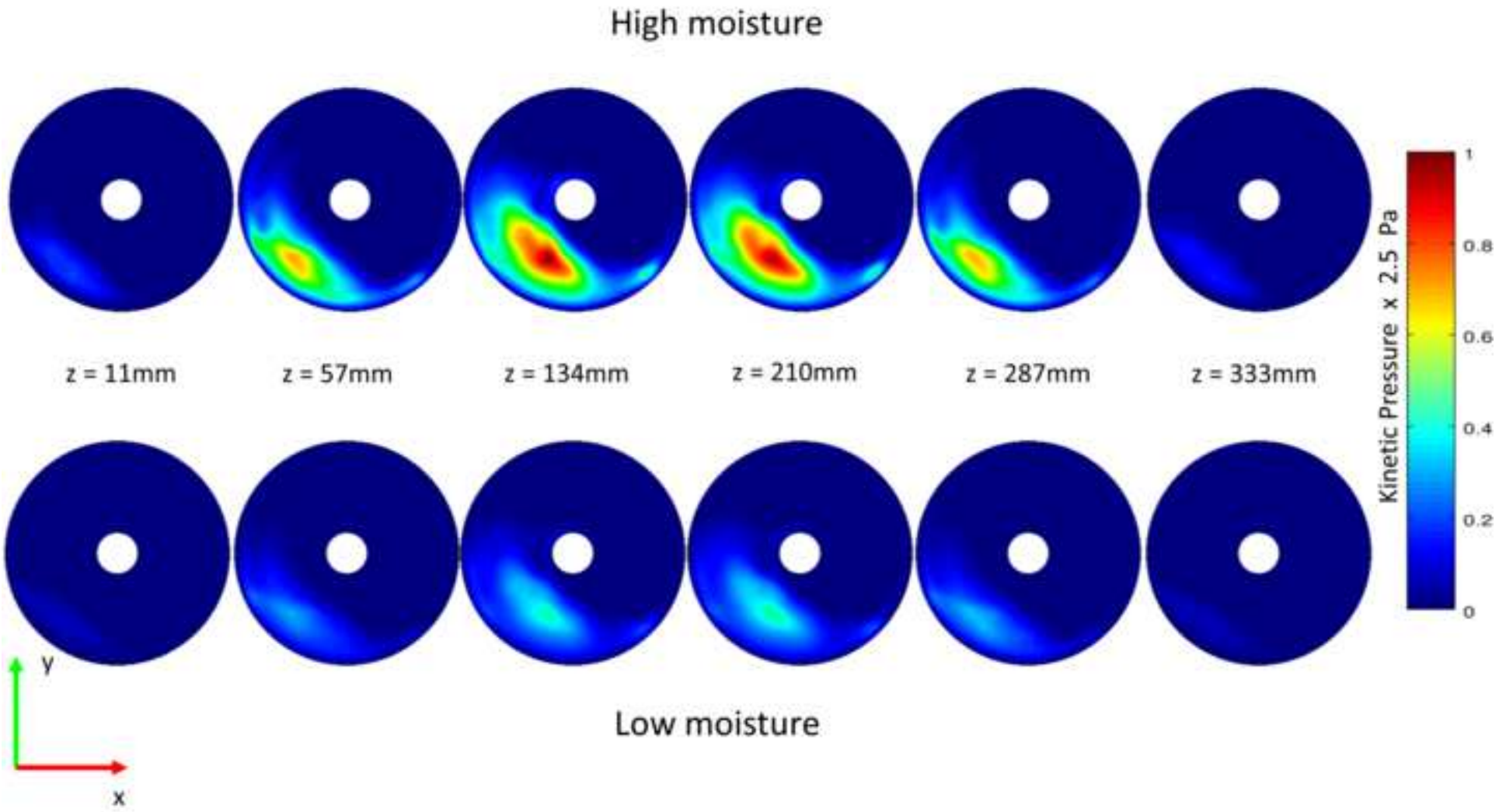

***Highlights (for review)**

- The validity of a DEM model for powder mixing in a paddle blade mixer is assessed.
- An elasto-plastic adhesive contact model is used to model aluminosilicate powder.
- Model parameters are determined using flow energy measurements from the FT4 rheometer.
- The optimized model reproduces the flow energy measurements to an excellent agreement.
- The model predicts the measured mixing rate qualitatively for wet and dry powders.